TriDurLE

National Center for Transportation Infrastructure Durability & Life-Extension

Project ID: 2020-WSU-01

Final Research Report

Test Methods and Bond Performance Characterization of Shotcrete-Concrete Interface

By

Haifang Wen, Ph.D., P.E.
Associate Professor

Pizhong Qiao, Ph.D., P.E.
Former Professor

Ayumi Manawadu, Ph.D.
Scholarly Assistant Professor

Washington State University,
Department of Civil and Environmental Engineering
Sloan Hall, Room 101
Pullman, WA 99164-2910

Prepared for

National Center for Transportation Infrastructure Durability & Life-Extension
(TriDurLE)

August 2022

TECHNICAL REPORT STANDARD TITLE PAGE

1. REPORT NO.	2. GOVERNMENT ACCESSION NO.	3. RECIPIENT'S CATALOG NO.

4. TITLE AND SUBTITLE	5. REPORT DATE
Test Methods and Bond Performance Characterization of Shotcrete-Concrete Interface	August 2022
	6. PERFORMING ORGANIZATION CODE
7. AUTHOR(S)	8. PERFORMING ORGANIZATION REPORT NO.
Haifang Wen, Pizhong Qiao and Ayumi Manawadu	
9. PERFORMING ORGANIZATION NAME AND ADDRESS	10. WORK UNIT NO.
Washington State University Department of Civil and Environmental Engineering Pullman, WA 99164-2910	11. CONTRACT OR GRANT NO.
12. SPONSORING AGENCY NAME AND ADDRESS	13. TYPE OF REPORT AND PERIOD COVERED
National Center for Transportation Infrastructure Durability & Life-Extension	Final Report
	14. SPONSORING AGENCY CODE

15. SUPPLEMENTARY NOTES
This study was conducted in cooperation with the U.S. Department of Transportation, Federal Highway Administration.

16. ABSTRACT

Shotcrete is becoming popular for vertical and overhead applications where conventional formwork and repairs are difficult and costly. However, the substrate and the shotcrete overlay interface can be vulnerable, and the bond properties in this region are not well understood. Furthermore, the interface bond could be adversely affected by long-term freeze-thaw weathering in northern states leading to debonding from the existing substrate and corrosion of rebars. Hence, characterization of the shotcrete-substrate interface bonds is critical for the performance evaluation of shotcrete construction. To this goal, this study evaluated the shotcrete-concrete interface bond using four representative substrate surface preparation methods: chipped, pressure-washed, sandblasted, and as-cast, under three different loading conditions: tensile, shear, and Mode-II fracture. The study also investigated the long-term freeze-thaw durability of these bonds and introduced a probabilistic damage model to predict their service lives. The estimated surface texture depth and bond behavior are also correlated using laser texture scans of the substrate. Results indicate that the chipped substrates led to the highest interface bond strength and mode-II fracture energy. Out of the remaining surfaces, pressure-washing produced an interface bond that is more tensile-resistant, whereas sandblasting led to an interface bond that is more shear-resistant. Therefore, it is recommended to consider the actual loading application on the shotcrete-concrete interface bond when choosing appropriate surface preparation and testing techniques. Recommendations were proposed to include in the shotcrete specifications. Specifically, a tensile bond strength of minimum 145 psi from a direct tensile bond strength test (e.g. ASTM C1583) is recommended for overhead shotcrete application and a shear bond strength of minimum 300 psi from a direct shear bond strength test (e.g. AASHTO T323) for slope stabilization with shotcrete. Substrates with minimum estimated surface texture depths of 0.294 mm or larger (based on ASTM E2157 or D8271) or ICRI CSP No. 4 or higher led to bond strengths greater than 145 psi as specified by ACI. However, the predicted service life of shotcrete-concrete interface bonds is significantly reduced in regions prone to a higher number of freeze-thaw cycles. Therefore, methods to improve the long-term durability of bond strength need to be further investigated.

17. KEY WORDS	18. DISTRIBUTION STATEMENT
Shotcrete, substrate to overlay, surface preparation, interface bonds	No restrictions.

19. SECURITY CLASSIF. (of this report)	20. SECURITY CLASSIF. (of this page)	21. NO. OF PAGES	22. PRICE
Unclassified	Unclassified		

DISCLAIMER

The contents of this report reflect the views of the authors, who are responsible for the facts and accuracy of the data presented herein. The contents do not necessarily reflect the official views or policies of the National Center for Transportation Infrastructure Durability & Life-Extension or the Federal Highway Administration. This report does not constitute a standard, specification, or regulation.

ACKNOWLEDGEMENT

The authors wish to thank the National Center for Transportation Infrastructure Durability & Life-Extension and Washington Department of Transportation for funding and support. Thanks also go to Micah Silberman from The Conco Construction Companies; Erik Christopherson of Superior Gunite; Jesse Espy from Pre-mix Inc.; Miles Pepper and Eric Barrow from the WSU engineering workshop; and Vishal Sonawane from WSU for their assistance during the test program.

TABLE OF CONTENTS

LIST OF TABLES

Page

LIST OF FIGURES

Page

EXECUTIVE SUMMARY

Shotcrete has become an attractive alternative for fascia and retaining walls in many states. It is most beneficial in vertical and overhead work where conventional formwork and repairs are difficult to make and costly. However, the life expectancy of structures can be compromised if the interface bond properties between shotcrete and the substrate are not well developed. In addition, long-term freeze-thaw weathering in northern states also degrades the bond strength of the interface and results in debonding from the existing substrate concrete structures and corrosion of rebars. Thus, proper shotcrete placement and its bond properties underneath concrete substrates are paramount to service performance and durability in shotcrete application.

The Phase I study showed that shotcrete is a viable and promising product in terms of performance when compared with cast-in-place (CIP) concrete, and if thoroughly investigated, it may replace CIP concrete and be suitable for infrastructure applications. The Phase II study demonstrated no significant difference in shotcrete's short-term and long-term performance before and after shooting, based on their comparisons and correlations of the mechanical properties and freeze-thaw (F/T) resistance. *Shooting* is an important step in the shotcrete application process. Shotcrete mixes that have not been *shot* with a nozzle are referred to as *"before shooting"* in this context. Instead, these mixes are placed similarly to conventional concrete. In contrast, *"after shooting"* describes shotcrete mixes that have been *shot* with a nozzle per ACI specifications by qualified nozzlemen. The first two phases focused on the individual performance of shotcrete as a material. This Phase III project aimed to develop test methods and specifications to address the debonding issues associated with the substrate and shotcrete overlays to assure the adequate bonding

and monolithic behavior of shotcrete construction. Such composite structures could be seen in wall fascia and slope stabilization, as well as in structure repair and rehabilitation. This report discusses the impact of substrate surface preparation, test techniques, surface roughness, and frost resistance on bond quality.

First, a comprehensive review of academic and industry knowledge on bi-layer cementitious bonds was conducted. Then, an experimental investigation was conducted to evaluate the influence of the substrate surface preparation technique on the performance of the shotcrete overlay-to-substrate interface bond. In addition, the frost damage resistance of the interface bond was analyzed using rapid F/T conditioning cycles, and a probabilistic damage model was used to predict the structure's service life.

(1) Literature review and industry survey: Based on the literature review and the industry survey, four types of substrate surface preparation techniques, namely, chipped, pressure-washed, sandblasted, and as-cast, were identified for this study. Two types of established test methods, shear and tensile bond strengths, were identified to characterize these surfaces. Additionally, a fracture mechanics-based test was designed and developed for the interface characterization of the structures. Freeze-thaw durability of the shotcrete-concrete interface bonds also was identified as an essential aspect.

(2) Short-term (without F/T cycles) tensile bond strength: The tensile bond strength values were correlated with the surface preparation technique. These techniques can be sorted from the largest to smallest interface tensile bond strengths as chipped, pressure-washed sandblasted, and as-cast (unprepared). For comparison purposes, the chipped, pressure-washed, and sandblasted specimens were reported to have 6.4, 5, and 2.7 times more resistance to tensile bond failure than the unprepared surfaces. The advisable limit

for a good bond mentioned in ACI 506-R16 is 145 psi (1 MPa) based on the pull-off direct tension test. Only the chipped and pressure-washed samples achieved this bond quality based on tensile bond strength. An estimated texture depth (ETD) of 0.294 mm is needed to achieve a good quality at the shotcrete overlay to substrate interface bond. Table1 indicates a summary of bond strengths (tensile and shear), and fracture energy for unconditioned samples (i.e., not subjected to freezing and thawing).

Table 1. Summary of bond strengths and fracture energy for unconditioned samples

Interface bond property	Chipped	Pressure-washed	Sandblasted	As-cast
Tensile strength (psi)	284	225	120	45
Shear strength (psi)	594	165	299	105
Mode-II fracture energy ($lb.ft/ft^2$)	368	82	253	54

(3) Short-term shear strength: The shear bond strength values are obtained using a guillotine-type direct shear test and have reported values in descending order as chipped, sandblasted, pressure-washed, and as-cast specimens. Specifically, as indicated in Table 1, the shear bond strength specimens with chipped, sandblasted, and pressure-washed surface preparation was 5.7, 2.9, and 1.6 times more resistant to shear bond failure than specimens with as-cast surfaces. In contrast to tensile bond strength, the sandblasted specimens recorded a superior shear bond strength compared to pressure-washed samples, likely due to the sensitivity of tensile bond strength to cleanliness by pressure-washing over sandblasting. ACI 546.3R-14 specifies that a direct shear bond strength of 300 psi or higher indicates a good bond strength. Therefore, only samples with chipped and sandblasting surface preparations can meet this requirement.

(4) Short-term fracture tests: Mode-II (in-plane shear) was used to characterize the bond fracture resistance of all four substrate preparation techniques. The chipped samples, as indicated in Table 1, reported the highest mode-II fracture energy with 368 lb.ft/ft^2 (498 J/m^2), followed by sandblasted and pressure-washed samples. Specifically, the fracture energies of specimens with chipped, sandblasted, and pressure-washed surface preparation were 6.81, 4.68, and 1.53 times more resistant to mode-II fracture failure than the unprepared surfaces.

(5) Comparison of test methods: The surface preparation technique greatly influenced the bond strength values. The data for the chipped samples shows the highest bond strengths and fracture energy of all test categories, while the as-cast specimens showed the lowest values. The shear bond strength to tensile bond strength ratios of chipped, pressure-washed, sandblasted, and as-cast samples are 2.09, 0.73, 2.49, and 2.35, respectively. In addition, the mode-II fracture energy correlates with the shear strength behavior across different surface preparation techniques.

(6) Long-term F/T durability of shotcrete-concrete interface bonds: Generally, the bond durability has decreased with the number of freeze-thaw cycles tested (0, 100, 200, and 300). Based on tensile bond strength, the chipped specimens indicated the highest durability, followed by pressure-washed, sandblasted, and as-cast samples. The tensile bond strength of these specimens after 300 cycles have reduced by 35.3%, 44.2%, 46.3%, and 96%, respectively, as given in Table 2 (i.e., tensile strength retained is 64.7%, 55.8%, 53.7%, and 4%). Freeze-thaw resistance evaluated using the mode-II fracture energy was still superior in the chipped specimens, followed by sandblasted, pressure-washed, and as-cast specimens. In both tensile and fracture tests, the as-cast interface bonds have reduced

their original strength by over 93%, indicating the importance of surface preparation in cold regions. The ASTM C666 mentions a reduction of dynamic modulus to be less than 40% at 300 freeze-thaw cycles (compared to unconditioned samples) to qualify an individual material as durable. Only chipped surface preparation satisfies this criterion. However, the dynamic modulus is a non-destructive test that indicates lower durability reductions than destructive tests used in this study.

Table 2. Value of bond property at 300 freeze-thaw cycles as a percentage of corresponding bond property of unconditioned samples

Bond property	Chipped	Pressure-washed	Sandblasted	As-cast
Tensile strength (%)	64.7	55.8	53.7	4
Mode-II fracture energy (%)	91.4	41.6	46.5	6.59

(7) Probabilistic damage model: A probabilistic damage model based on the Weibull distribution was used to predict the field service life of shotcrete-concrete interface bonds. Based on the model, it was found that the service life of shotcrete-concrete bonds in eastern Washington (e.g., Pullman) can be less than ten years, while a similar structure in western Washington can be up to 50 years, depending on the surface preparation methods.

Based on above findings, **it is recommended to include the following in the shotcrete specifications, if applicable:**

(a) A tensile bond strength of minimum 145 psi (in accordance with ASTM C1583 or similar tests) is needed when shotcrete is applied to overhead structure and a shear bond strength of minimum 300 psi (in accordance with AASHTO T323 or similar tests) for slope stabilization by shotcrete.

(b) Chipped surface preparation should be applied whenever possible. Otherwise, pressure washing can be applied for the overhead structure application of shotcrete and sandblasting for slope stabilization. It is recommended that after chipping or sandblasting, the substrate surface be washed. Unprepared substrate concrete surface is not recommended to use.

(c) A minimum estimated texture depth (ETD) of 0.294 mm of substrate concrete which can be determined using a laser texture scanner (ASTM E2157) or a digital concrete profile gauge (ASTM D8271) is needed to achieve a good quality of the shotecrete overlay to substrate interface bond. Alternatively, an International Concrete Repair Institute (ICRI)'s Concrete Surface Profile (CSP) No. 4 or higher can be specified as an alternative to ETD.

(d) Caution should be exercised when shotcrete is applied to a structure in regions subjected to frequent freeze-thaw cycles, due to concern on the long-term freeze-thaw durability of the interface bond. For such regions, shotcrete may need to be anchored to the substrate.

Note that the above recommendations are based on the assumptions that shotcrete is applied to a sound substrate concrete. In addition, based on the experimental program conducted in the Phase III study, suggestions are provided for future studies at the end of this report.

Chapter 1. INTRODUCTION

1.1 Background and problem statement

In many states, shotcrete has become an attractive alternative for fascia walls and soil nail retaining walls. Properly placed shotcrete is structurally sound, durable, and exhibits excellent bonding properties with the underlying substrates. Due to its rapid application process, shotcrete is beneficial used in vertical and overhead work where conventional formworks and repairs are difficult to make, costly, and often short-lived. However, the life expectancy of shotcrete structures may be reduced due to an inadequate bond development between shotcrete and the substrate, which could be due to numerous reasons, including lack of surface roughness, cleanliness, and soundness of the substrate surface at the time of shotcrete application. In addition, long-term freeze-thaw (F/T) weathering in northern states can degrade the bond strength of the interface and result in debonding from the existing structures and the corrosion of rebars. The mechanisms and characteristics of the bond between the existing substrate and overlay have been researched in past studies. However, the scope of existing guidance and specifications on testing methods and construction practices to ensure adequate long-term bond performance is limited. Moreover, practices for the surface preparation of the substrate in shotcreting and their effects on bond development are still inadequately guided and studied.

Very few guidelines and specifications are available for the application of shotcrete, primarily for bridge repair and building construction, such as ACI 506R-16 “Guide to Shotcrete” (ACI Committee 506-R, 2016), ACI 506.2-13 “Specification for Shotcrete” (ACI Committee 506, 2014), “Guide Specification for Structural Shotcrete Walls” (Morgan & Totten, 2014), and “Standard Specifications for Road, Bridge and Municipal

Construction" (WSDOT, 2022). These reference standards only briefly address some practical issues mainly related to shotcrete as an individual material. For example, the Washington Department of Transportation (WSDOT) specifications for shotcrete include the compressive strength (4000 psi), procedure for testing of cores, qualification of the nozzleman, application procedure to reduce rebound and increase compaction, and prewetting.

Although sprayed shotcrete is widely used as an overlay for structural repairs, guidelines to ensure adequate bond strength (for the interface bond between the shotcrete and the substrate) and acceptance criteria for harsh environments, particularly cold regions, are very limited. Cleanliness and roughness of substrate are widely known as essential factors. According to ACI 506R-16, removing all deteriorated, loose, and unsound materials from the substrate surface is imperative for proper interface bond development. The unique nature of the shotcrete process leads to an adequate bond if the substrate surface is prepared correctly and at saturated-surface-dry (SSD) conditions. ACI 506.4R-94 "Guide for the Evaluation of Shotcrete" (ACI Committee 506., 1994) provides the evaluation method (i.e., direct tension pull-off test) to determine the bond strength and the failure location of a composite substrate-to-overlay system.

The short-term (e.g., after shotcrete hardens) bond characteristics between the substrate and overlay have been widely researched in past decades. Most of the existing literature is based on the direct tension pull-off test, in which the failure primarily occurs in the overlay, followed by the interface failure and substrate failure (Seymour et al., 2010). The dominant reasons are the differential strength gains between layers and the combined effects of differential shrinkage and thermal strains. Julio et al. (2005) concluded that using

epoxy and curing compound on the substrate surface adversely affects the bond strength. This is because some bonding agents create “bond breakers” at the interface, leading to bond failure. Additional surface treatments (roughing and blasting) can enhance the local bond at the interface. Beaupre (1999) observed that the waiting duration between successive layers of shotcrete overlay (the period after shooting one layer until shooting the next layer of shotcrete in multilayer shotcreting) had no significant influence when good surface preparation was in place. Silica fume improved the bond strength, whereas fly ash, slag, or fibers portrayed no significant effect (Martin et al., 2015). The bond strength is found to be critically related to the tensile strength and homogeneity of the shotcrete mixture.

As demonstrated, the short-term bond strength of the shotcrete-to-substrate interface has gained more attention because rapid development of a solid bond to the substrate is vital for efficiency and safety (Bryne et al., 2014). However, despite the relatively large pool of practical knowledge related to shotcrete's early age bond strength, the long-term bond characteristics are still inadequately addressed. In addition, long-term bond deterioration is the rebars (Talbot et al., 1994; Tang et al., 2016). Therefore, there is a pressing need to investigate shotcrete's long-term, time-dependent bond performance under an aggressive environment. Moreover, potential methods to enhance long-term bond properties should be investigated. An investigation of this type may eventually recommend practice guidance and specifications to ensure a durable long-term bond and successful shotcrete applications.

The Phase I study showed that shotcrete is a viable and promising product when compared to the performance of cast-in-place (CIP) concrete. If thoroughly investigated, it

may even be able to replace CIP concrete in infrastructure applications. Based on the mechanical properties and freeze-thaw resistance, the Phase II study found no significant differences in shotcrete's short-term and long-term properties before and after shooting. In contrast to the Phase I and II studies, which considered the behavior of shotcrete as an individual material level, this Phase III study focused on the long-term durability of the shotcrete-concrete interface bonds. Nevertheless, other pending issues, including best construction practices, effects of mix design on short- and long-term bond performance, quality assurance (QA)/quality control (QC) criteria, and specifications, still warrant further investigations.

1.2 Research objectives

As a continuation of the Phase I and II studies which focused on shotcrete as an individual material, this Phase III project aimed to address the issues related to the shotcrete-concrete interface bonds in potential concrete repair applications. The following topics were investigated in-depth in the Phase III study. Note that in this study, the focus was on the bond between hardened concrete substrates and shotcrete overlays.

a) Influence of the substrate (i.e. hardened concrete in this study) surface preparation technique on the short-term performance of the shotcrete-concrete interface bond
b) Influence of the substrate surface preparation technique on the long-term performance of the shotcrete-concrete interface bond
c) Influence of the test method on the measured bond strengths of shotcrete-concrete interface
d) Development of a life-prediction method for the shotcrete-concrete interface bond and estimation of the service life

Chapter 2. LITERATURE REVIEW

The literature review summarizes a brief introduction to shotcrete, the past studies on characterizing the performance of cementitious bi-layer material interfaces, and shotcrete overlay to substrate interface bonds. In addition, test methods and long-term bond performance of cementitious bi-material interfaces were reviewed. An industry-focused survey summary on current shotcreting practices is also included.

2.1 Shotcrete

This section starts with a brief background of shotcrete in terms of its materials composition, and properties before and after shooting, based on literature review, and previous studies by Washington State University (WSU), followed by an elaboration on bond characteristics between shotcrete and substrate.

2.1.1 Introduction

Shotcrete is pneumatically sprayed concrete that is projected at a high velocity onto a receiving substrate surface. The unique application process allows the shotcrete to compact rapidly and simultaneously consolidate due to the impact force. There are two main shotcrete application methods: the dry-mix and wet-mix processes as indicated in Figure 2.1. The dry-mix process involves pumping water and other damp or dry constituents separately through two hoses to the nozzle head. Water is mixed with the constituents at the nozzle head, just as the two streams are sprayed onto the receiving surface. In contrast, the wet-mix process involves mixing all the constituents with water and then pumping them through the hose to the nozzle. In either case, the quality of the shotcrete is highly dependent upon the nozzleman's skill and experience.

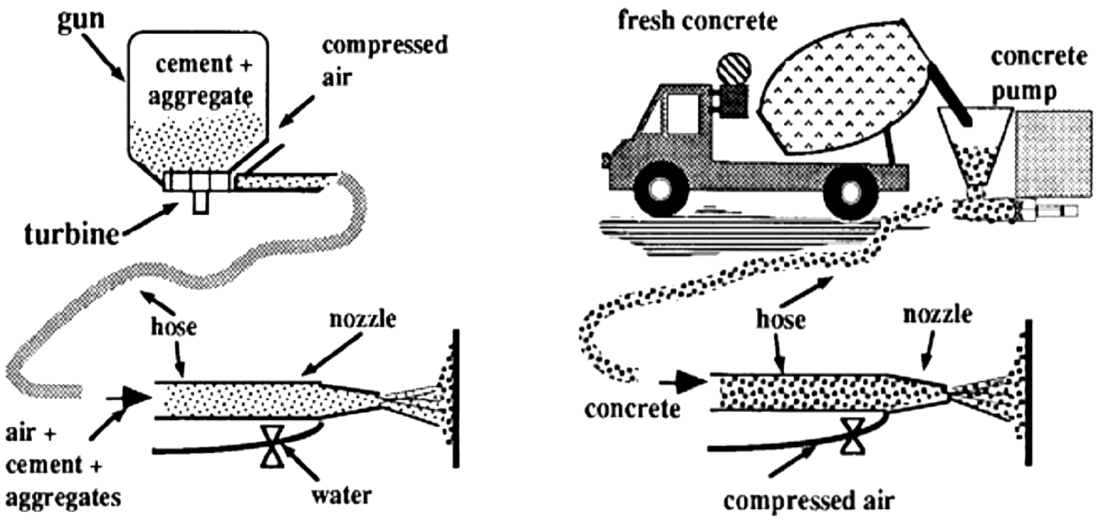

(a) (b)

Figure 2.1 Schematic of shotcrete production: (a) dry-mix process; and (b) wet-mix process (Beaupre, 1994)

The fresh and hardened properties of shotcrete are similar to those of conventional concrete, depending upon the specific mix design. The compressive strength of shotcrete ranges from 4,000 psi (27.5 MPa) to 10,000 psi (68.9 MPa) at 28 days in field construction (Zhang, 2014). Nevertheless, due to the impact force, shotcrete is subjected to significant air loss by the time it reaches the substrate surface. Hence, the air content of the fresh mix needs to be adjusted accordingly to ensure that an adequate air void system is created to improve long-term durability. Moreover, shotcrete mixes usually have a small norminal maximum aggregate size (NMAS) to improve pumpability and shootability. Therefore, shotcrete is further characterized by a higher paste content, which raises concerns about drying shrinkage cracking. In addition, the rebound of materials, especially aggregates, is caused due to ricochet following high impact force, which may lead to material loss and reduced strength.

Like conventional concrete, shotcrete mixes consist of Portland cement, aggregates, water, and admixtures, if needed. In addition, the mechanical properties of shotcrete can be significantly improved through supplementary cementitious materials (SCM, such as silica fume (SF), fly ash (FA), ground granulated blast-furnace slag (GGBFS), etc.), air-entraining admixture (AEA), water-reducing admixture, shrinkage-reducing admixture, set retarding admixture (retarder), accelerating admixtures (accelerator), and fibers.

The water/cement ratio of shotcrete depends on the application but generally varies from 0.3 to 0.6. The NMAS is usually 1/2 inch or 3/8 inches. The ACI Committee 506 (ACI Committee 506-R, 2016) has recommended grading limits for shotcrete to minimize drying shrinkage and rebound. Shotcrete produced with finer aggregates exhibits more significant drying shrinkage, whereas coarser aggregate leads to more rebound. Table **2**.**1** indicates typical grading limits for shotcrete.

Table 2.1 **Grading limits for the aggregates of shotcrete indicated as percent by mass passing individual sieves (ACI Committee 506-R, 2016)**

Sieve Size	**Grading No. 1**	**Grading No. 2**	**Grading No. 3**
3/4 in.	-	-	100
1/2 in.	-	100	80-95
3/8 in.	100	90-100	70-90
No. 4	95-100	70-85	50-70-
No. 8	80-100	50-70	35-55
No. 16	50-85	35-55	20-40
No. 30	25-60	20-35	10-30
No. 50	10-30	8-20	5-17-
No. 100	2-10	2-10	2-10

Due to the significant air loss during pumping and shooting, air-entraining admixtures (AEA) are vital to improving shotcrete's quality and freeze-thaw durability. Mainly, freeze-thaw durability depends on the air content and the void structure of the shotcrete or concrete mix. A fresh shotcrete batch of initial air content between 8% and20% could lead to in-place shotcrete with an air content between 3% and 6% (Talukdar & Heere, 2019).

2.1.2 Freeze-thaw durability

Concrete or shotcrete structures in cold climates are frequently subjected to cyclic freezing and thawing, resulting in accelerated material degradation. Frost damage reduces the strength and modulus of elasticity, leading to structural damage, durability issues, and loss of serviceability (Marzouk & Jiang, 1995). Frost damage occurs due to cracking from the expansion of saturated water while freezing (Hanjari et al., 2011). When the water inside the saturated capillary pores of porous media freezes, it expands by about 9%, building tensile stresses on the surrounding materials. A well-distributed air-void system helps release pressure build-up, leading to better freeze-thaw damage resistance. Note that the air content and spacing factor of air voids are important air-void characteristics regarding freeze-thaw durability. Air entraining admixtures help improve the air-void system by introducing entrained air.

Many studies have been conducted on the freeze-thaw durability of shotcrete (Beaupre, 1994; Jolin et al., 1997; Lamontagne et al., 1996; Mainali et al., 2015; Morgan, 1989; Talbot et al., 1994; Wang et al., 2018; Zhou & Qiao, 2019). Freeze-thaw durability of shotcrete is typically measured using the relative dynamic modulus of elasticity in accordance with ASTM C666 (ASTM International, 2008). Also, ASTM C231 (ASTM

International, 2010a) and ASTM C 457 (ASTM International, 2010b) are suitable methods for measuring the air content of fresh shotcrete and the air-void characteristics of hardened shotcrete, respectively. Figure 2.2 indicates the freeze-thaw performance of air-entrained shotcrete as opposed to ordinary shotcrete measured in terms of relative dynamic modulus (Chen et al., 2014). Other testing methods that could be used to investigate the pore structure of shotcrete include X-ray diffraction, acoustic emissions (AE), thermogravimetry-differential scanning calorimetry (TGA-DSC), scanning electron microscopy (SEM), and X-ray computed tomography.

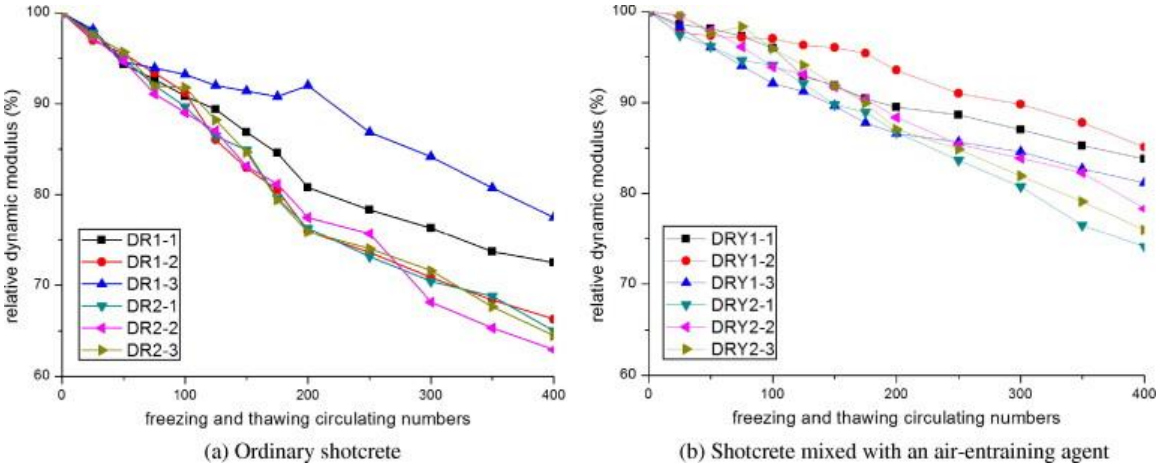

Figure 2.2 Change in relative dynamic modulus of shotcrete with and without air-entrainment admixtures during freeze-thaw cycles (Chen et al., 2014)

2.2 Overlay-to-substrate bond interfaces

Section 2.1 of this report focused on the properties and performance of shotcrete as an individual material. However, when shotcrete is applied to existing structures (concrete, hard rock, slopes, rebar, etc.), the quality of the bond interface determines the integrity of the entire composite system. For instance, due to mismatches in elastic material properties, thermal coefficients, and shrinkage, differential deformations can occur in the substrate and overlay. Therefore, the shotcrete-to-substrate interface bond is subjected to additional

stress; hence, it is typically the weakest link in the system. Premature failure of the interface bond affects the integrity of the entire structure. Therefore, Section 2.2 focuses entirely on the overlay-to-substrate interface bond.

2.2.1 Failure modes in overlay-to-substrate composite systems

The three main components of a bi-layer composite system with no adhesive layer (e.g., shotcrete-concrete composite system) are the substrate, overlay, and overlay-to-substrate interface bond. When such systems are subjected to external loads, failure may occur in any of those regions, as shown in Figure 2.3. In cohesive failure, cracks occur outside the interface zone, either entirely in the overlay (Figure 2.3 (b)) or in the substrate (Figure 2.3 (c)), indicating that the interface bond is stronger than the individual layers of the composite system. Conversely, adhesive failure (Figure 2.3 (a)) occurs at the interface, indicating that the bond between the two layers is weaker than the strength of each material layer. In contrast, mixed-mode failure combines adhesive and cohesive failure modes attributed to the development of secondary stresses and local strength variations along the bond plane (López-Carreño et al., 2017). The failure mode is influenced by the strength of components of the bi-layer system (adhesive and cohesive) and the test specimen geometry. Therefore, understanding the inherent characteristics of various test methods helps better analyze the experimental results.

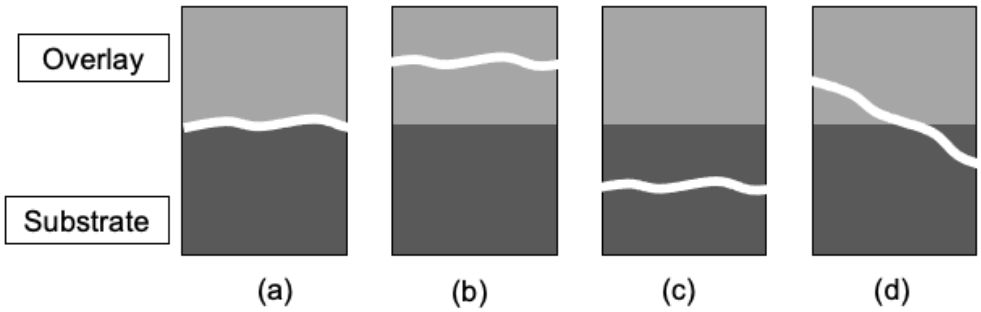

Figure 2.3 Concrete-to-concrete bond test specimen failure modes: (a) adhesive failure; (b) cohesive failure in overlay; (c) cohesive failure in substrate; (d) mixed failure.

2.2.2 Durability of interface bond

Shotcrete-concrete interface bond is similar to a concrete-to-concrete bond which has been well studied and thus is also included in the literature review to help understand the bond characteristics between shotcrete and concrete substrate. Concrete repair is used to extend the service life of a structure. Hence, the concrete-to-concrete interface bond should withstand external loads, temperature, moisture, and environmental exposure changes for an extended period. Concrete constructions are susceptible to cyclic freezing and thawing weather conditions in cold climates, accelerating material deterioration. Freeze-thaw-related cracking occurs due to the expansion of saturated water inside the concrete (Hanjari et al., 2011). Such cracks eventually reduce the mechanical properties and adversely affect the durability of a structure (Marzouk & Jiang, 1995). In other words, the fracture behavior of concrete is influenced by crack development, which depends partially on the freeze-thaw resistance (Ma et al., 2017) and pores.

Since there is already a mechanical property mismatch at the interface bond, it is critical to evaluate the effect of freezing and thawing in bi-layer composites. Such durability concerns have been investigated under the freeze-thaw accelerated conditioning

cycles (Jacobsen et al., 1996; Powers, 1945, 1955), and this method is well-documented (ASTM International, 2008). In a combined study of micromechanical and microstructural properties of concrete-to-concrete interface bonds, Zuo et al. (2020) showed that the coupled heat-cool and dry-wet cycles result in more severe deterioration than the heat-cool or dry-wet cycles individually. While the bond deterioration that results from heat-cool cycles was found mainly due to the reduction in interlocking areas at the bond interface, deterioration in coupled cycles (heat-cool and dry-wet) has been affected additionally by a decrease in adhesive bonds at the interface. Benzarti et al. (2011) investigated the accelerated aging behavior of the interface bond between concrete-to-carbon fiber-reinforced polymer (CFRP). While the humid aging significantly decreased the pull-off interface bond strength of non-carbonated concrete strengthened with CFRP, it had an insignificant influence on the bond of carbonated concrete-to-CFRP. This outcome has been attributed to the moisture diffusion from the non-carbonated concrete to the adhesive bonded interface. The bond failure of the non-carbonated concrete-to-CFRP interfaces has evolved from substrate failure to interface and mixed failure modes with humid aging. When comparing with polymer-modified concrete (PMC) overlays, styrene-butadiene rubber (SBR)-based PMC overlays have shown better interface bond durability with concrete substrates than acrylic-based PMC (Sadrmomtazi & Khoshkbijari, 2017).

Permeability is another durability issue related to the ability of concrete to resist the ingress of fluids into its pores. It is crucial to control permeability due to the potential harmful impacts it can cause, such as rebar corrosion, irrespective of whether the structure is monolithic or composite. Ding et al. (2019) used strain-hardening cementitious composites and roughened surfaces to reduce the permeability at the bond interface. Tayeh

et al. (2012) investigated the permeability of the normal concrete-UHPFC (ultra-high performance fiber concrete) based on rapid chloride permeability, gas, and water permeability tests. Results indicate that UHPFC is a suitable overlay material to improve resistance against chloride, gas, and water penetration. Qian and Xu (2018) successfully used a non-destructive ultrasonic pulse and rapid electrical test to evaluate the permeability of layered concrete composites with layers cast at different times.

2.2.3 Interface bond tests

Various tests are available to evaluate cementitious bi-material interfaces and choosing an appropriate characterization test requires knowledge of these test methods. Therefore, this section includes a comprehensive review of the different types of popular tests that could be used in this shotcrete-concrete interface study.

Figure 2.4 presents a compilation of the different types of interface bond strength tests for cementitious bi-material systems, based on previous studies (Kim & Bordelon, 2016; López-Carreño et al., 2017; Saucier et al., 1991). These tests are divided into tension, shear, combined shear-compression, and flexure tests. Figure 2.4(a) and (b) are both direct tension tests, where the pull-off test is the most popular *in situ* test method. Despite the differences in specimen shape, Figure 2.4(c) and (d) are splitting tensile tests classified as indirect tension tests. Figure 2.4(e)-(m) show pure shear testing, while Figure 2.4(n)-2.4(r) illustrate combined shear-compression tests. Flexure tests, also categorized under indirect tension testing, are shown in Figure 2.4(s)-(w). In the following, the most popular test methods in the literature are evaluated, and the results are compared and discussed.

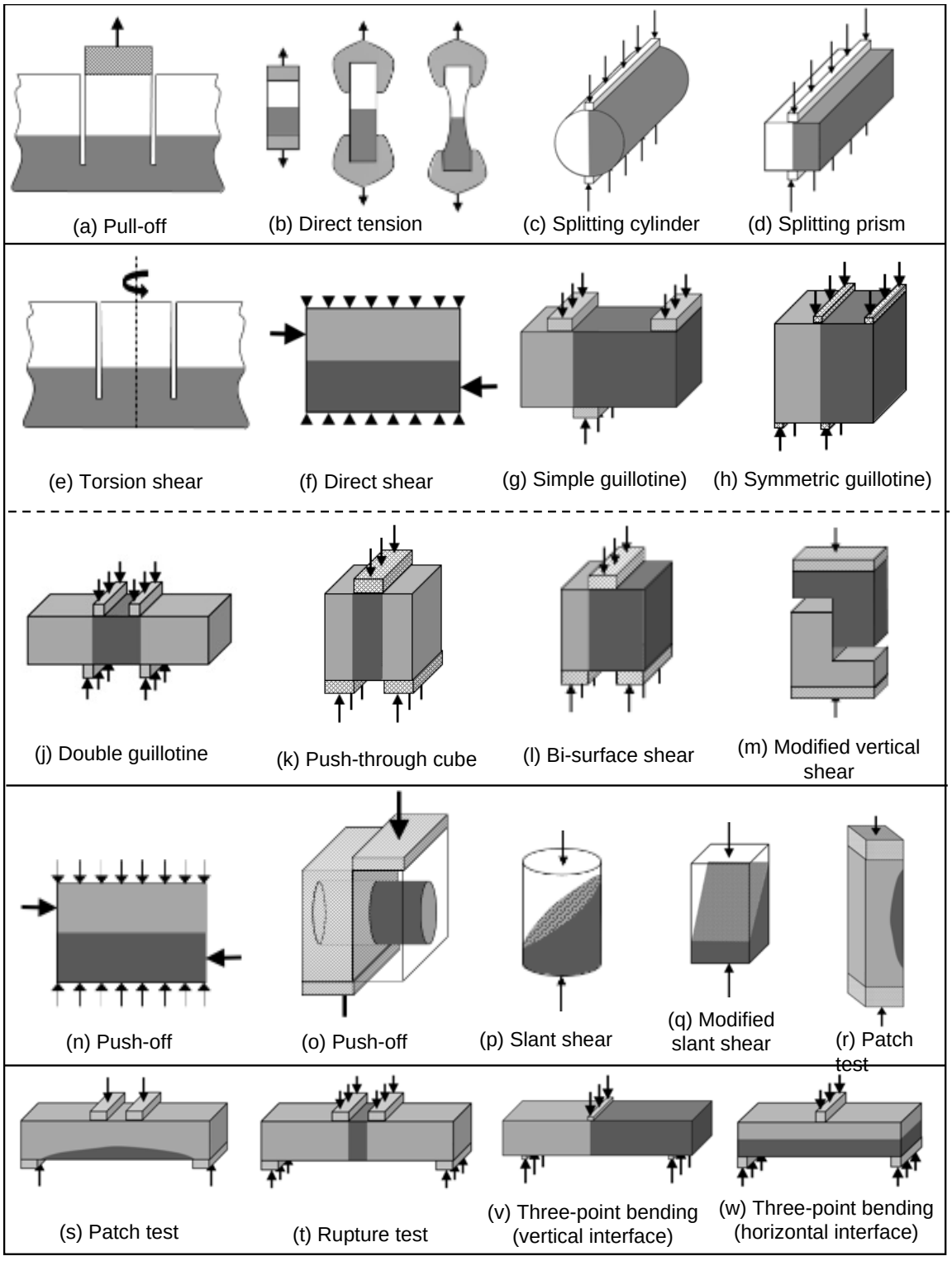

Figure 2.4 Strength tests for assessing concrete-to-concrete bond strength

2.2.3.1 Tension tests

The pull-out test (Figure 2.4(a)) has evolved into a standard test procedure (ASTM International, 2013b; British Standards Institution, 1999), and is the most popular *in situ* method for determining new-to-old concrete tensile bond strength in concrete repair (Bonaldo et al., 2005; Long & Murray, 1984). The test entails drilling a shallow core into a test slab, attaching a steel disk using epoxy to the top surface of the core, and then pulling out the still intact cylindrical specimen using a jack until it separates from the slab. Due to the uniform nature of the cylindrical core, the most prevalent problem with the pull-off test is that stress concentrations do not occur at a specific place. As a result, failure could occur in three areas: the substrate, overlay, or interface bond. Therefore, premature substrate failure, a type of cohesive failure, is frequently observed with the pull-off test, resulting in a low bond tensile strength (Zanotti & Randl, 2019), especially when the substrate and overlay materials have considerable variations in strength and stiffness. To ensure adhesive (interface) failure, Valipour and Khayat (2020) used a modified pull-off test specimen with a reduced bond area to induce stress concentrations at the bond interface. Despite the simplicity of the pull-off test, coring can cause microcracking in the substrate, weakening it and causing premature substrate cohesive failure. Another challenge is that the pull-off tests seem to report highly variable results with significantly high coefficients of variation (COV), such as 39% (Bonaldo et al., 2005), 40% (Ramos et al., 2012; Robins & Austin, 1995), and 67% (Valipour & Khayat, 2020), indicating the location dependency of the pull-off test. These differences could have resulted from location-specific material variations, such as the size and strength of aggregates at the testing location.

Additionally, coring induces torque at the interface bond, damaging and interfering with various specimen interface adhesive qualities, contributing to strength variations.

Despite these drawbacks, the pull-off test is efficient and straightforward. Thus, it is frequently employed in the industry and academia to characterize the concrete-to-concrete interface bonds (Rith et al., 2016).

On the other hand, direct tension tests in Figure 2.4(b) are performed in the laboratory to obtain tensile failure (Knab & Spring, 1989). However, to avoid large scatter in the test results, the specimen must be aligned with the load axis (Li, 1997), which is challenging in practice. Even with universal joints, there could be non-negligible bending moments due to misalignments. In most test setups, the tensile load is transmitted to the specimen through either glued metalheads or grips. Small compact specimens are often accompanied by glued metalheads, which is time-consuming because glue hardening and cleaning take time. Furthermore, slender specimens are used with tension grips that allow rapid testing. However, such specimens are long and space-consuming and cannot be extracted from repaired concrete structures.

The splitting tensile test method (Arioglu et al., 2006; Espeche & León, 2011; Ramey et al., 1984), which evaluates the tensile bond strength of concrete repair materials, is the most extensively used indirect tension test (Figure 2.4(c) and (d)). The specimen geometry could be a prism (Geissert et al., 1999) or a cylinder the (ASTM International, 2011). In addition to the shape, the size of the splitting tensile test specimen also influences the interface bond strength (Li et al., 1999). The test involves applying a compression load along the length of the specimen at the bond plane. Although high compressive stresses are generated near the load application areas, the tensile stresses are generated at the bond plane due to Poisson's effect, which leads the specimen to split. This test is popular because

it is easy to perform, uses the same testing machine as a standard compression test, and has a higher bond area-to-volume ratio than other flexure tests.

Given the practical constraints of direct tension testing, tension is measured indirectly more accurately and conveniently in flexure tests. Figure 2.4(s)-(w) show some popular flexure tests that fall into this category, which require bending a narrow specimen to obtain maximal flexure strength. Nevertheless, in flexure testing, the bonding plane is subjected to a gradient of stresses, with just a small region experiencing the maximum stress. As a result, the main drawbacks of flexure tests are: (i) poor efficiency due to the low bond area to volume ratio and (ii) a minimal bond area that undergoes maximum stress. Abu-Tair et al. (1996) used a modified modulus of rupture test to analyze the interface bond in tension, as shown in Figure 2.4(t). In their study, a concrete beam was sliced in half along its length and sandwiched with a repair material in the middle to create the composite test specimen that undergoes four-point bending. Results indicate that this test is more sensitive to a change in repair material than to the substrate surface preparation technique. Austin and Robins (1993) investigated a new patch test that allows the specimen to be tested under compression or flexure, as indicated in Figure 2.4(r) and (s). The main advantage of the patch test method is its ability to transfer loads indirectly to the bond interface while maintaining a larger bond area to volume ratio than other flexure specimens (e.g., Figure 2.4(v)). These real-world load scenarios also subject the concrete-to-concrete interface bonds to indirect loading conditions more often than direct loads. The proposed patch test could detect debonding and is sensitive to repair material, surface roughness, bond quality, and surface moisture when subjected to compression (Austin & Robins, 1993). Nevertheless, in contrast to the pull-off and slant shear tests, the patch test has shown

sensitivity to the stiffness of the repair material. The flexure configuration of the patch test has shown to be more sensitive to the specimen geometry when ensuring adhesive (interface) failure.

2.2.3.2 Shear tests

Shear stresses are produced at the interface bond mainly due to shear forces, differential shrinkage, or a combination of the two. Therefore, sufficient shear strength at the interface bond is critical to avoid debonding. Pure shear is induced on the concrete-to-concrete interface bonds using either torsion or direct shear tests to determine the shear bond strength (Figure 2.4(e)-(m)). Nevertheless, pure shear is challenging to attain in practice due to the presence of bending moments in test procedures (Espeche & León, 2011).

Silfwerband (2003) first investigated torsion tests (Figure 2.4(e)) to evaluate the *in situ* pure shear strength of bonded concrete overlays. The method uses the same specimen as the pull-off test but applies a torsional load instead of a tensile load. Torsional shear tests avoid the bending moment that would occur in an ordinary shear test due to the application of parallel loads and has *in situ* capabilities, making them more convenient than shear tests. The jacking test is another type of *in situ* direct shear test where a hydraulic jack secured to the substrate is used to apply a shear force at the interface of a saw-cut overlay block of a field sample (Rosen, 2016). A steel plate is placed between the ram and the block to ensure uniform stress distribution and applying the shearing force as close as possible to the substrate surface reduces the overturning moment.

Conventional shear tests involve applying two parallel and opposite loads on both sides of the specimen interface bond (Figure 2.4(f)). However, the main drawback of such tests is that they lead to a bending moment in addition to the shear force; hence, they do

not truly emulate pure shear. To overcome this complication, the investigators used three-part push-through tests (Figure 2.4(k)) (Bahraq et al., 2021; Sadrmomtazi & Khoshkbijari, 2019). However, the specimen used in this test has two interfaces, which is rare in a practical scenario. Also due to the existence of two interfaces, this test is challenging to perform.

The most common direct shear test configuration (e.g. AAHSTO T323) works similarly to a guillotine, where steelheads apply shear loads at the bonding line (Shahrooz et al., 2000) (Figure 2.4(g)-2.4(j)). In such tests, greater stress concentrations occur along the edges of the specimen that come into contact with the steelhead. The specimen fails when the stresses at these small concrete regions exceed the shear strength, yielding a more local bond strength value than a global average value. The scatter in test test results is directly proportional to the magnitude of the stress concentrations (Li, 1997). Momayez et al. (2004) investigated a new bi-surface shear test (Figure 2.4(l)) in which a three-point bending load was applied to 150 mm cubes. The test method is sensitive to specimen size, overlay repair material, and surface roughness.

The L-shaped shear test (Figure 2.4(m)) or the Strategic Highway Research Program (SHRP) interfacial bond test is another direct shear test method used to evaluate concrete-to-concrete interface bonds (Shahrooz et al., 2000). Using L-shaped and Z-shaped shear test specimens, Zhang et al. (2020) discovered that the interface bond strength is sensitive to substrate carbonation when testing self-compacting concrete overlays. The bond interface orientation of the Z-shaped test influenced the bond strength and the failure mode Zhang et al., 2020). Climaco and Regan (2001) successfully used L-shaped tests to

evaluate the effectiveness of different bond coats. However, these tests have a low bond area to volume ratio reducing their efficiency.

Ray et al. (2005) and Roy et al. (2014) used a direct shear specimen for bi-layer concrete, following the guidelines given for the block shear tool used with composite wood specimens (ASTM International, 2013a). The authors have modified the specimen geometry to a butterfly double-wedge type symmetrical specimen to provide effective lateral confinement in tension while applying shear loads.

2.2.3.3 Combined shear and compression tests

Combined shear and compression tests use a compressive force perpendicular to the bonding plane, reducing the effect of local stress concentrations found in guillotine tests and resulting in a more representative value of average bond strength. Mechanical tightening commonly applies compression forces, preventing test specimens from moving laterally. However, this variable compressive load increases with the shear force, resulting in an unknown compressive load at failure and, thus, lacks comparability to other tests.

Slant shear test is the most popular combined shear-compression test that involves the compression testing of a composite cylinder. The standard cylindrical specimen is made such that the bonding plane is inclined 60 degrees to the horizontal. If a modified test is conducted, it should be noted that the slant shear strength is sensitive to this bond angle (Austin et al., 1999). Zanotti et al. (2014) investigated the bond behavior of fiber-reinforced cementitious repair materials using a slant shear test with varying slant angles. It was identified that the shear bond strength is a function of the slant angle to the vertical but not a material property—the lower the slant angle, the lower the shear bond stress. Due to the inclination in the bond plane, the applied compression force transforms into a compressive force and a shear force which are normal and parallel to the bond surface, respectively.

Due to normal shear, the friction forces are more prominent in these tests leading to larger measured shear forces at the interface bond. Modified slant shear tests use a prism instead of a cylinder (Saldanha et al., 2013; Wall & Shrive, 1988), and the specimen shape and size influence the slant shear bond strength (Diab et al., 2017). The slant shear test is the most common and standard method to test the bond strength involving the resin-based/polymer-based composite materials (ASTM International, 2005; BSI British Standards, 1984), and it is widely used to evaluate other types of concrete-to-concrete interfaces (Abu-Tair et al., 1996; Saucier et al., 1991). Although the nature of the test setup imposes stresses on the entire bond interface, it is impossible to extract the specimens from a field overlay.

Furthermore, depending on the compressive strength of the substrate and overlay, this test results in either adhesive interface debonding or cohesive crushing of the weaker concrete layer (substrate or overlay), with the latter leading to a lower bound strength (Saldanha et al., 2013). Saucier et al. (1991) investigated a new shear-compression test device using a compact bi-layer composite specimen, which subjects a cubic specimen to fail under shear. This test procedure has allowed a compromise between the testing time, accuracy, and space. Mohamad et al., (2015) has successfully linked friction and cohesion coefficients to roughness parameters in concrete-to-concrete bonds using the push-off test in Figure 2.4(n). Qian et al. (2014) investigated a new frustum specimen, which exerts the combined shear and tensile forces along with the bond interface of cement-based repair materials when subjected to compression.

2.2.3.4 Fracture tests

Despite the quality, concrete structures carry inherent flaws, such as micro-cracks, air voids, and pores, even before applying any external loads. More defects, such as

microcracks, can form during repair procedures, especially when preparing the substrate surface. During construction stages and service loads, potential cracks along the interface of shotcrete overlay and substrate concrete may form, impairing integrity and shortening the service life of shotcrete structures. Cracks can further develop, leading to premature failure of the shotcrete-concrete interface. Bond fracture properties of shotcrete-concrete bi-layer composites are essential to predict potential crack initiation and propagation and evaluate the bond quality of shotcrete overlaying substrate concrete. As the load increases, isolated and randomly distributed internal microcracks propagate stably, while new ones are formed, eventually localizing into major cracks (Shah et al., 1995). The substrate-to-overlay composite system fails by cracking along the interface or kinking out, depending on whether the interface is weaker than the neighboring material layers. The failure will occur along the path of least resistance, and is governed by the fracture toughness rather than the compressive or tensile strengths (Li et al., 1995). Therefore, it is essential to utilize fracture mechanics-based tests in evaluating the bond performance of concrete bi-material interfaces. Figure 2.5 shows a few fracture test configurations for evaluating the fracture toughness or critical fracture energy of interface bonds in concrete repairs.

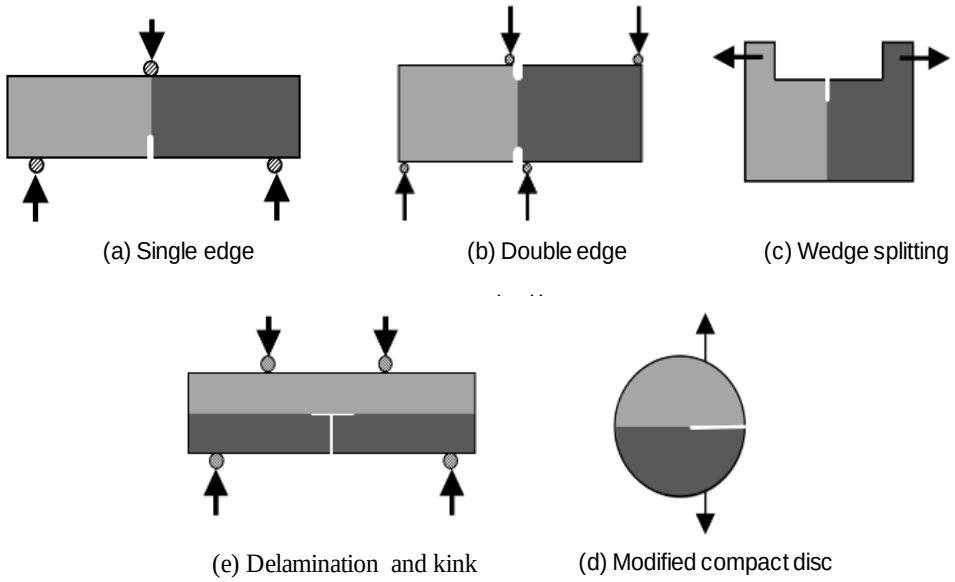

Figure 2.5 Fracture test methods to evaluate concrete-to-concrete interface bond

The most popular fracture mechanics-based test methods are three-point and four-point bending tests with different specimen geometries (Chbani et al., 2019). The geometries and configurations include single-edge notched beams (Lim et al., 2001; Shah & Kishen, 2011), double-edge notched (Bažant & Pfeiffer, 1986), delamination and kink test (ChiaHwan & Wei, 2014; Kamada & Li, 2000), and Chevron notched (Miarka et al., 2019). Wedge splitting tests are performed using a wedge to apply a compressive load, which translates to tensile loads as indicated in Figure 2.5(c), ultimately opening the crack. The shape of the test specimen could be derived from a cube (Tschegg et al., 1995; Tschegg et al., 2000; Kanellopoulos et al., 2009), cylinder with horizontal length axis (Hanjari et al., 2011), or cylinder with vertical length axis (Tschegg & Stanzl, 1991). Most of these tests are used to evaluate the Mode-I fracture behavior of concrete, while the double edge notched test (Figure 2.5(b)) subjects the specimen to a combined Mode-I (tensile) and Mode-II (in-plane shear) fracture loads. However, concrete is a very brittle material in

tension; thus, beam samples do not give good results for fracture behavior. Compact tension specimens (Farahani et al., 2017; Cifuentes et al., 2017; Dzugan et al., 2018) are used to determine the Mode-I fracture of brittle material more efficiently than bending tests. Other advantages of compact specimens are that they occupy lesser space and materials and, therefore, could be modified to fit inside a confined space in a testing or a curing machine. Single cantilever beam specimens with tapered cross-sections have been used to determine the Mode-I fracture properties of the concrete-fiber reinforced polymer (FRP) interfaces (Davalos et al., 2006). Single edge notch beam in anti-symmetric, four-point bending load has been used to determine the Mode-II fracture parameters of concrete (Swartz et al., 1988). The Iosipescu test evaluates the Mode-II in-plane shear of concrete (Iosipescu & Negoita, 1969).

2.2.3.5 Comparison of test methods

The substrate-to-overlay bond strength in concrete repair depends on the test method used. Specifically, the specimen size, geometry, and the type of stresses acting on the bond interface affect the force at failure. Therefore, it is necessary to understand how bond strength values are comparable across the literature. To this end, Momayez et al. (2005) investigated the relationship between the test results from slant shear, pull-off, splitting tensile, and new bi-surface shear tests. The results indicate that the bi-surface shear, slant shear, and splitting tensile strength values are 7.3, 1.8, and 1.1 times higher than the pull-off tensile strength. It is evident that the pull-off and splitting prism tests, which are both the tensions tests (direct and indirect), yield comparable values.

In contrast, bi-surface shear strength was closer to twice the direct tensile strength values. The highest bond strength value of the slant shear test is attributed to the existing

compressive stresses that increase interlock and friction forces. In contrast, the low bond strength of the pull-off test is attributed to the lack of frictional forces.

In an investigation of the bond strength of latex-modified concrete overlays, Yun et al. (2004) found that the overlay thickness influences the stress distribution at the interface. Sabah et al. investigated the bond strength of fiber-reinforced concrete as a concrete repair material, using slant shear, splitting tensile, and pull-off tests (Sabah et al., 2019). Similar to previous studies, the slant shear test has shown the highest average bond strength, which increased with the age of the composite system.

In comparing two methods used to test the bond between concrete and repair materials, Abu-Tair et al. (1996) found that the slant shear test is more sensitive to surface preparation, while the modified modulus of rupture test is more sensitive to the repair material. Delatte et al. (2000) found that the shear bond strength of properly cured concrete-to-high early strength concrete bond is approximate twice the tensile bond strength at a given maturity.

Appendix 1 indicates the bond strengths from different bond tests in the literature, while Table 2.2 shows the corresponding bond strength ratios. The bond strength ratio is the ratio of particular bond strength to the corresponding pull-off tensile strength. Pull-off tensile strength has been used as the denominator for the bond strength ratio because it seems to have the most conservative bond strength values across multiple investigations. Therefore, depending only on the pull-off tensile strength data can potentially underestimate the actual bond strength in applications susceptible to shear stresses. Additionally, it is vital to remember that the substrate-to-overlay bond strength in concrete repair depends on numerous factors, including the composition of overlay and substrate,

quality control conditions, and surface preparation techniques. Hence, cross-literature comparisons should be made with caution. Using a bond strength ratio has normalized these disparities to some extent.

Table 2.2 Minimum and maximum interface bond strength ratios to tensile pull-off strength (refer to Appendix 1)

Reference	Notes	Splitting Prism	Splitting Cylinder	Guillotine Shear	Jacking Shear	Bi-surface shear	Slant Shear	Torsion Test
Momayez et al. (2005)	Min	1.01				1.42	1.66	
	Max	1.16				8.26	7.53	
Rosen (2016)	Min			1.27	0.34		7.55	
	Max			2.16	1.60		10.19	
Pultorak (2016)	Min			2.07	1.04		24.47	
	Max			4.10	3.31		120.72	
Sabah et al. (2019)	Grooved		2.87				10.35	
	Sandblasted		3.26				13.70	
Silfwerband (2003)	Sandblasted							2.27

Figure 2.6 indicates the maximum and minimum bond strength ratios for each test considered in Appendix 1 and Table 2.2. The slant shear ratio varied within a broader range than the other test methods, ranging from 1.66 to 120 in this set, and recorded the highest bond strength ratio. The rest of the tests have shown comparable results with the pull-off tensile strength. Nevertheless, more thorough investigations are needed to compare bond strengths across various bond test data. The ACI 546.3R Guide to Material Selection for Concrete Repair provides acceptable bond strength values for different test types and materials (American Concrete Institute, 2014).

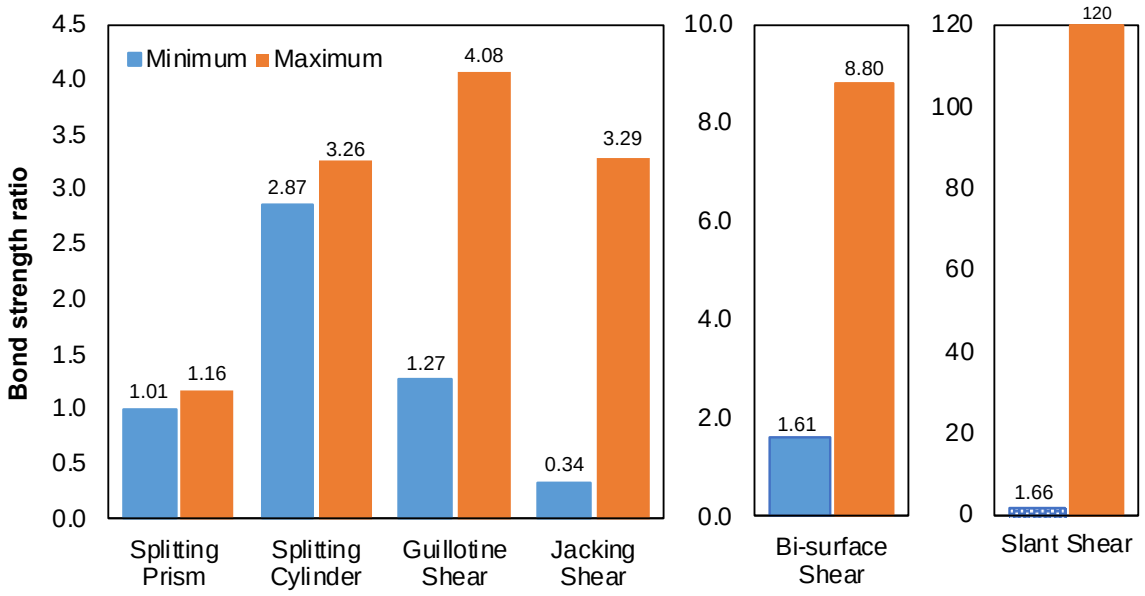

Figure 2.6 Range of bond strength ratios compared to pull-off tensile strength.

2.2.3.6 Factors affecting bond performance

Bond strength of concrete repairs depends on numerous factors, including aggregate interlock, interface adhesion, and friction; hence, preparation of the substrate surface is vital to ensure a monolithic bond. While the soundness, cleanliness, moisture condition, bonding agent, and roughness of substrate influence the bond adhesion, the porosity, meso-structure and micro-structures of the overlay transition zone (OTZ) affect the bond cohesion (Espeche & León, 2011). Aggregate shape, size, and surface preparation affect the friction and interlock (Momayez et al., 2005). Generally, the bond adhesive mechanism is governed by the mechanical anchorage between the old-new concrete layers that are influenced by the chemical adhesive forces at the micro-scale (Espeche & León, 2011; Rashid et al., 2020). Investigations have indicated that the OTZ is the weakest zone in the vicinity of the substrate-to-overlay interface bond (Rashid et al., 2020).

The factors affecting the composite action of concrete repairs are broadly categorized into the substrate characteristics, overlay characteristics and application

techniques, and environmental conditions, as indicated in Figure 2.7, primarily based on Silferbrand (1990) and Courard et al. (2014).

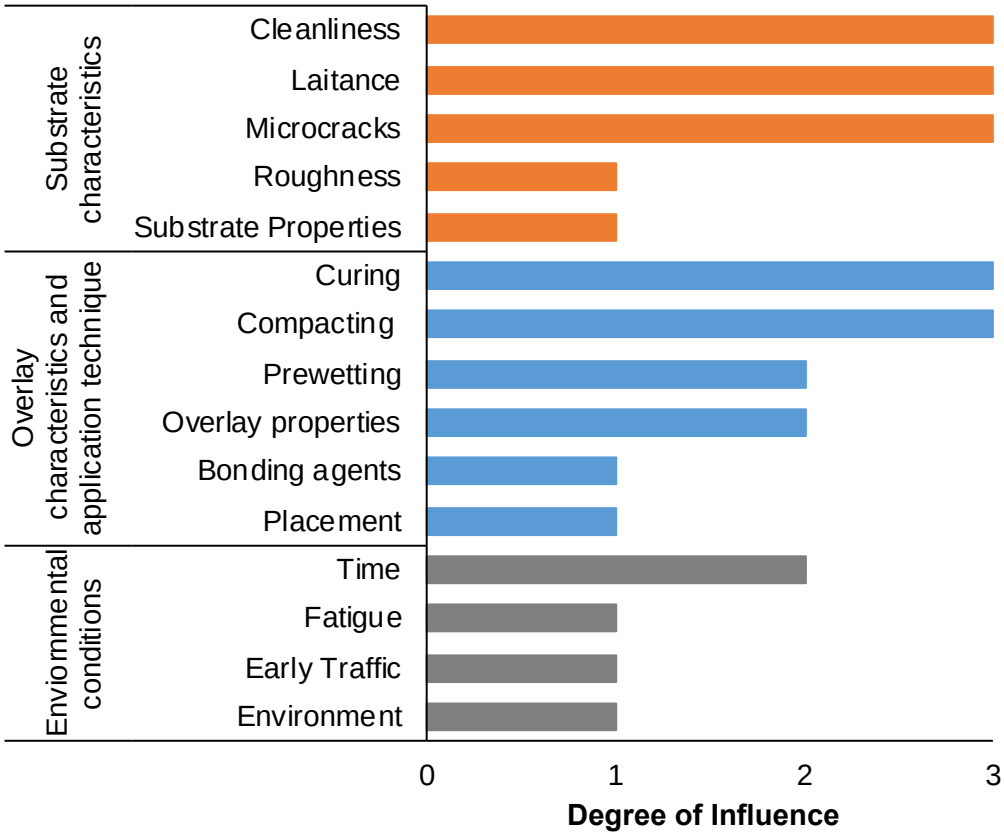

Figure 2.7 Factors influencing concrete-to-concrete bond strength: 1-minor influence, 2-medium importance, and 3-major influence (Silfwerbrand, 1990)

Substrate characteristics that influence an excellent bond include the absence of microcracking, non-formation of a laitance layer, appropriate surface roughness, surface cleanliness, and substrate layer properties. Prewetting, proper curing, adequate compaction, proper placement, and bonding agents are the application techniques that increase bond strength. Other factors influencing the interface bond strength include time and temperature differences in the two layers, fatigue, overlay properties, and other environmental conditions. An unclean substrate surface with contaminants (e.g., dust, grease, or oil) reduces friction. The contaminants create a preventive layer, thus hindering

proper interlock between the substrate and the shotcrete overlay. In a concrete-to-concrete repair, the water in the overlay will not only aid the cement hydration of the fresh overlay material, but a certain amount of water will also migrate into the capillaries of the substrate concrete due to the imbalance in moisture conditions. The rate of water migration from the overlay to the substrate depends on the moisture content of the substrate concrete layer. Although all these factors influence the old-to-new concrete bond, Silfwerband (1990) emphasized the most prominent as substrate cleanliness, microcracking, laitance, curing, and compaction.

Momayes et al. (2004) investigated the effect of specimen size, maximum aggregate size, type of repair material, interface roughness, and age on the shear and tensile strength of the interface bond. The results indicate that the bond strength increased with an increase in surface roughness, use of silica fume, and age at testing, while it decreased with the size of the specimens. The curing temperature and mix proportioning influence the tensile and shear bond strength (Delatte et al., 2000). Curing can minimize early-age shrinkage, reducing the overlay cracking (Silfwerbrand & Beushausen, 2005). The interface can have a weaker bond if temperature differentials occur while the overlay has not hardened (Dhir, 1984).

Sealers cover cracks and voids on the concrete substrate hinder the movement of unwarranted materials, such as water and chlorides. They also aid in reducing or preventing rebar corrosion, freeze-thaw, carbonation, and sulfate damage. Some popular sealers are high molecular weight methacrylic sealing compounds, epoxy-based sealing compounds, silane, and siloxane sealing compounds. However, applying sealers on the substrate concrete before the overlay placement reduces the interface bond strength (Shahrooz et al.,

2000). Nevertheless, a mild surface preparation technique, such as sandblasting after the sealer, restores partial bond strength. Primers can also be used on the substrate surface to improve the bond quality (Xiong et al., 2002).

Climaco and Regan (2001) used slant shear tests to identify the substrate conditions for a sound concrete-to-repair material interface bond. Their results indicated that a repair concrete overlay can bond well to substrate concrete even without bonding aids, provided that the substrate surface is dry and roughened to expose the aggregates with no damage in the concrete adjacent to the interface.

Several researchers have reported the importance of substrate moisture conditions in achieving a good bond (Emmons, 1994; Erhard & Chorinsky, 1986; Farzad et al., 2019; Zhang et al., 2020). While dry substrates may absorb too much moisture, which reduces the amount of water available for hydration, the excessively wet substrate surfaces may hinder the absorption of repair materials and increase the water/cement (w/c) ratio of concrete at the interface, thus reducing the bond strength (Bissonnette et al., 2012). Therefore, saturated surface dry (SSD) condition is considered the best state. However, Beushausen et al. (2017) discovered that prewetting the substrate surface before placing an overlay had no added benefits and might sometimes negatively impact the shear bond strength at the interface, regardless of the substrate compressive strength. Absorption of overlay/bonding agent material into the substrate concrete is vital for the quality of the bond, which is hindered by the clogged pores in a wet substrate that reduces the bond strength (Beushausen, 2010). Júlio et al. (2004) also concluded that the influence of substrate prewetting is insignificant to the pull-off bond strength and slant shear bond strength of the concrete repair. Geissert et al. (1999) used the splitting prism test method

to indicate that the dry or damp substrate surfaces have better bond strength than saturated wet conditions in concrete-to-concrete repairs. On the other hand, the bi-surface shear test has shown sensitivity to the substrate moisture condition in concrete repair work (Santos et al., 2012).

Bentz et al. (2018) compared the microstructural development at the substrate-overlay bond interface at different moisture contents using X-ray and neutron images after subjecting concrete-cementitious grout bonds to slant shear and pull-off tests. The dry roughened substrate has demonstrated a greater slant shear strength, likely due to the densification of the repair material layer next to the dry substrate. On the other hand, SSD substrates have indicated a higher pull-off tensile bond strength, likely due to better consolidation of the overlay material and improved hydration in the interface region brought on by water. In other words, the slant shear test favors dry roughened substrates, whereas pull-off tests favor substrates in SSD conditions. These findings suggest that different substrate qualities affect the bond strength differently when evaluated using various testing techniques.

Overall, no conclsuive findings on the effects of moisture condition on bond strength were achieved.

2.2.3.7 Surface preparation techniques

Bond development between the substrate and the overlay is influenced by the degree of substrate surface preparation. Some factors are the moisture and cleanliness of the substrate surface, depth and texture of the roughened surface, substrate surface's moisture and cleanliness, the roughened surface's depth and texture, substrate surface preparation technique, and the extent of aggregate exposure on the substrate surface (Whitney et al., 1992). Figure 2.8 shows the substrate surface after subjecting to some

popular surface preparation techniques, including as-cast, wire-brushed, and shot-blasted, which have very different surface textures. Courard et al. (2014) highlighted the significance of surface roughness in forming the substrate-to-overlay bond and claimed that the substrate compressive strength is less critical to bond development if a proper surface treatment regime is followed. Nevertheless, the aggressive surface treatments, such as jackhammering and hydro-demolition, cause more substrate near-surface microcracking than the dry sandblasting and polishing (Courard et al., 2014). Júlio et al. (2004) ranked surface preparation techniques as sandblasting, wire-brushing, and partially chipped, from most effective to the least. Santos et al. (2007) correlated roughness parameters, such as maximum peak-to-valley height, total roughness height, and maximum valley depth, to the corresponding bond strengths.

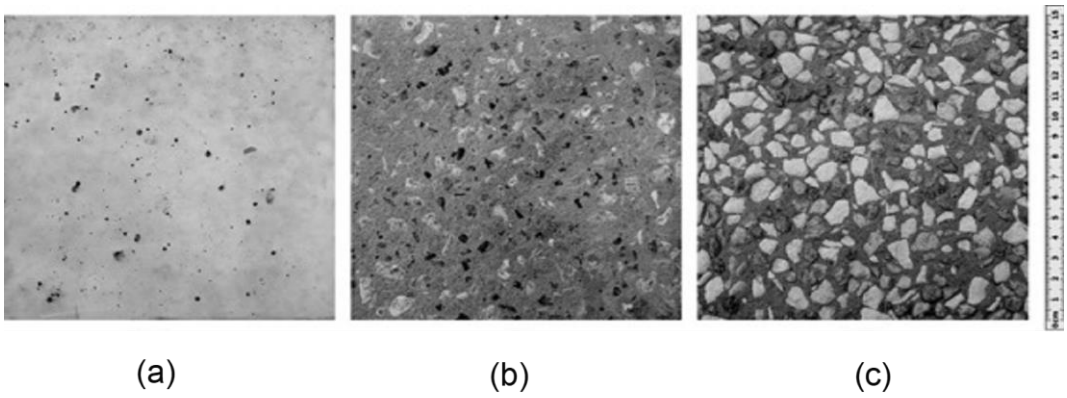

Figure 2.8 Substrate surface preparation: (a) as-cast; (b) wire-brushed; and (c) shot-blasted (Santos et al., 2007)

The surface preparation method directly influences the roughness and soundness of the substrate surface in the concrete repair (Austin et al., 1995), and several surface preparation techniques are available, as stated hereafter. Although vigorous surface preparation techniques lead to rough substrate surfaces, they may also induce microcracks that make the interface weaker (Silfwerbrand, 1990; Talbot et al., 1994). The existence of

surface defects such as microcracks leads to an effective reduction in contact area at the bond interface, making the bond more vulnerable to tensile loads (Austin et al., 1995). Furthermore, microcracks tend to grow with crack tip stress concentrations, which further reduces the tensile bond strength of the interface. The surface roughness of the substrate concrete affects the bond strength of cementitious overlay material more than polymer-modified repair materials (Momayez et al., 2005). In comparing the slant shear bond strength due to different substrate surface preparation techniques, the surfaces with 6 mm deep grooves have shown the most superior bond compared to the hand-brushed and mechanical wire-brushed surfaces (Diab et al., 2017).

Tayeh et al. (2013) compared the influence of surface preparation technique on the bond between substrate concrete and ultra-high performance fiber concrete repair. The authors characterized and compared the substrate-to-overlay interface bond for different substrate preparation techniques, namely, as-cast, sandblasted, wire-brushed, drilled holes, and grooved, using the splitting tensile and slant shear tests. Under the given surface preparation techniques, the sandblasted substrate surface provided the best mechanical bond. Sabah et al. (2019) also found sandblasting to be more effective than grooving when preparing a concrete substrate surface. Sandblasting has been more effective than the wire-brushed or as-cast substrate surface preparation techniques when the bond strength was measured using the slant shear and splitting tensile strength tests (Tayeh et al., 2013). Youm et al. (2021) investigated the bond behavior of normal-strength concrete to UHPC interfaces using slant shear tests for different inclination angles and substrate roughness. Smooth surfaces have predominantly led to sliding interface failure. In contrast, the failure

of sandblasted roughened surfaces transitioned from concrete crushing failure to near-interface concrete cracking as the inclination angle increased.

Abu-Tair et al. (1996) compared the influence of different substrate surface preparation techniques on the slant shear and tensile bond strength between concrete substrate and repair materials. Out of smooth as-sawn, wire-brushed, needle-gunned, and hand-chiseled substrate surface preparation techniques, the needle-gunned method indicated a cohesive failure in the substrate 90% of the time. In contrast, the hand-chiseled method showed the highest interface bond strength in the slant shear.

While shotblasting and sandblasting sound similar, they are entirely different processes. Shotblasting involves using centrifugal force to shoot abrasive media onto a receiving surface while sandblasting uses compressive air to propel the material. In a study evaluating the single-lap shear bond behavior of concrete-to-CFRP layers, Soares et al. (2019) identified that sandblasting is more effective than grinding. All specimens have been subjected to cohesive failure of the concrete substrate instead of the adhesive failure at the epoxy layer, regardless of the substrate surface preparation technique. Júlio et al. (2005) reported that applying bonding agents, such as epoxy resin, does not affect the bond strength of a properly surface-prepped concrete substrate, and sandblasting is more cost-effective than using a bonding agent. Scarifying machines use a rotating cutting tool to scar the hardened concrete surface. Due to the cutting process, scarifying mechanisms generate microcracks at the substrate surface (Haber et al., 2018). Haber et al. (2018) found that the hydro demolition creates fewer microcracks than scarifying and still manages to give a greater degree of roughness, as indicated in Figure 2.9.

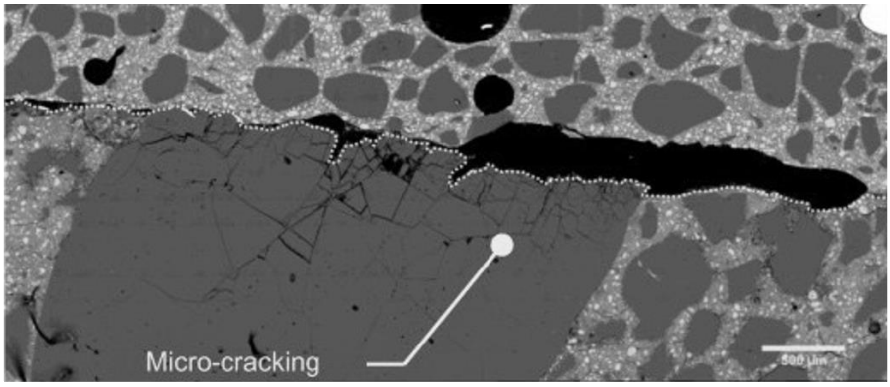

(a) Scarification - distressed aggregate in laboratory concrete sample

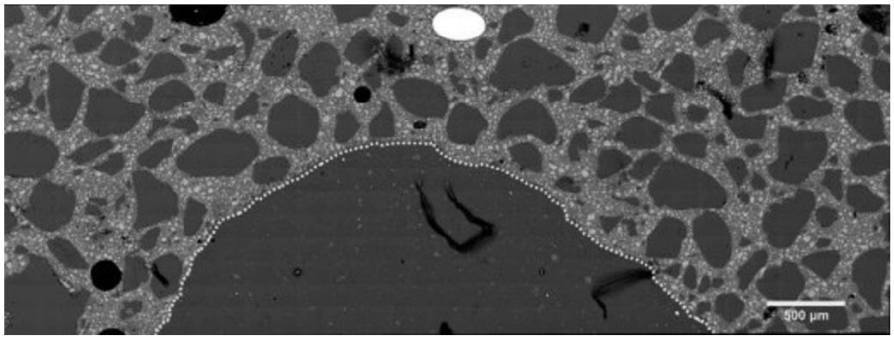

(b) Hydro demolition - Intact aggregate in laboratory concrete sample

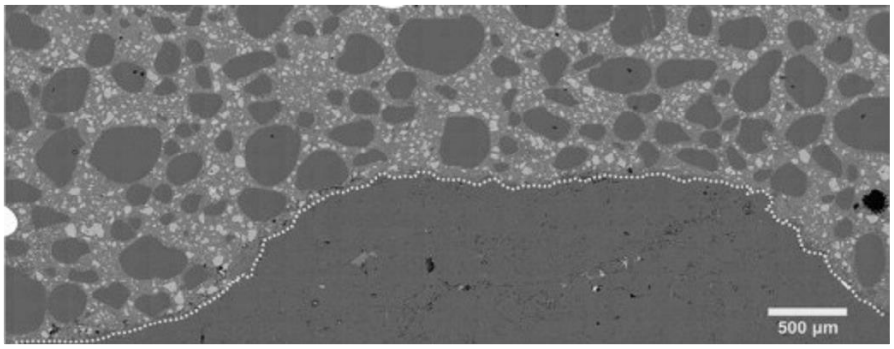

(c) Diamond grinding - Intact aggregate in field concrete sample

Figure 2.9 Microstructural damage on the substrate surface due to different surface preparation techniques (Haber et al., 2018)

Despite the high surface roughness, the grooved substrates reported the lowest tensile bond strengths because overlay materials do not fill out the grooves, thus resulting in a low contact area (Harris et al. 2011). Table 2.3 summarizes a few test results that

indicate the interface bond strength from several studies. In general, it can be seen that sandblasting gives reasonable bond strength values in both tension and shear tests. It has reached a shear bond strength value as high as 10.9 times the as-cast specimen. Sandblasting seems to be a popular surface preparation technique comparing the table values and other literature cited above. All the surface preparation techniques considered in Table 2.3 have recorded superior bond strengths compared to the as-cast specimens.

Table 2.3 Interface bond strengths for different surface preparation techniques

Reference	Test	As-cast	Wire-brushed	Chipped	Sandblasted	Shotblasted	Waterjet	Hand-scrubbing	Drilled holes	Grooved
Silfwerbrand (1990)	Pull-off			160	345		286			
Julio et al. (2004)	Slant shear	189	1548	905	2049					
Santos and Julio (2011)	Slant shear	1769	2038		2426	2814		3060		
	Splitting prism	268	274		307	334		451		
Santos et al. (2012)	Bi-surface shear	200	280			532				
Tayeh et al. (2012)	Slant shear	1259	1849		2583				1780	2019

A combination of individual material properties, construction techniques, and quality control procedures influences the bond between substrate concrete and overlay repair materials. For example, the factors affecting individual concrete layer strength, such as curing, concrete mix composition, concrete age, and degree of consolidation, affect the strength of the composite bi-layer material. Proper curing will reduce moisture loss at the interface, leading to appropriate hydration. Adequate vibration of the overlay concrete ensures proper consolidation, minimizing the amount of entrapped air near the bond

interface, hence minimizing voids. Due to the localized reduction in the contact area between the substrate and the overlay, the presence of voids may lead to inconsistent and inaccurate bond strength values.

2.3 Industry survey results

To better understand shotcrete industry practices and identify problem areas, WSU conducted an online survey in collaboration with the WSDOT. The survey was distributed to industry professionals, shotcrete researchers, and state DOTs. The following section provides a summary of the survey findings based on over 30 responses and previous studies.

2.3.1 Test methods to evaluate shotcrete performance

The survey participants reported that the two most common failure modes concerning shotcrete are compressive strength failure and debonding from the substrate. The said failure modes are assessed using the compression testing of core samples and pull-off direct tensile test of test panels, respectively. However, the pull-off direct tensile test has the in-situ capability out of these two. This test is performed simply by attaching a disk to the surface of the shotcrete, drilling around it, and pulling the whole setup out. It is essential to carefully align the specimen along the loading axis to avoid any larger scatters in the results, which is difficult to control in a practical scenario. Most practitioners prefer using disks with a diameter of 2" (50 mm) for the pull-off direct tensile tests per ASTM C1583/C1583M requirement. Nevertheless, this is the minimum diameter required, and thus, some practitioners prefer larger diameters such as 3" (75 mm) or 4" (100 mm). Nonetheless, this test frequently detects premature substrate failure rather than interface bond failure, as indicated in Figure 2.10, resulting in a lower bound tensile bond strength.

Despite the in-situ capabilities of the pull-off test, it is evident that some practitioners do not test the bond strength or still prefer testing the compressive strength of cored samples and visual inspections. Plastic shrinkage cracking and adhesion loss are two other failure modes concerning shotcrete.

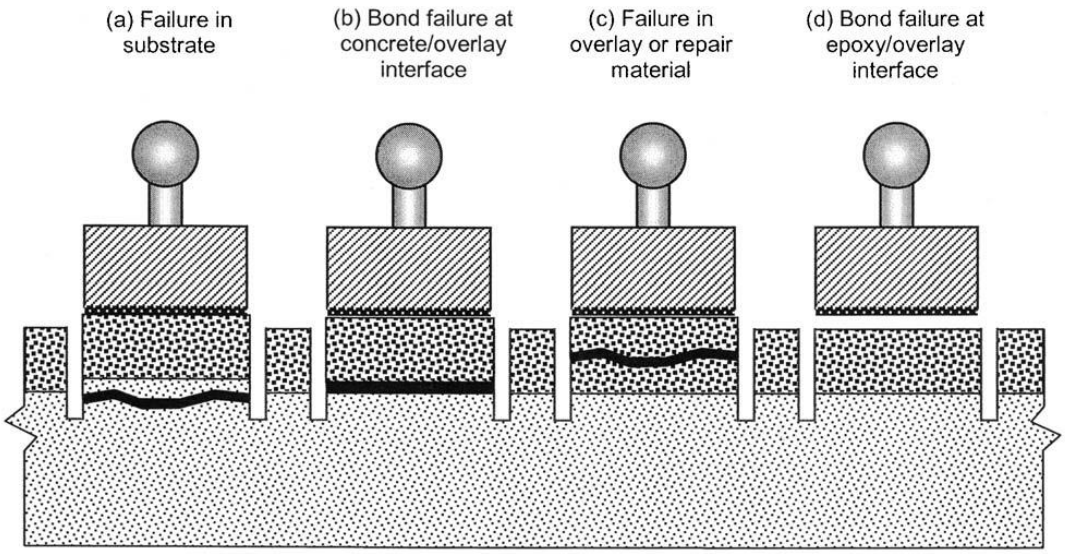

Figure 2.10 Pull-off test failure modes (ASTM C1583)

Figure 2.11 indicates that the preferred non-destructive test method in the industry is the hammer test. This test is favored as a preliminary test to identify problem areas, followed by other tests if an anomaly is detected. Due to reliability issues, many practitioners do not use non-destructive tests at all. Ultrasonic pulse velocity is also considered a suitable technique. However, the concerns over the quality of results in a densely reinforced area remain. These issues suggest the necessity for an improved, cost-effective testing method. The most preferred in-service test method is to evaluate the compressive strength of cored samples. In such tests, contractors core the specimens from areas with little or no rebars by locating them before the tests with GPR, profometers, and other rebar locating methods.

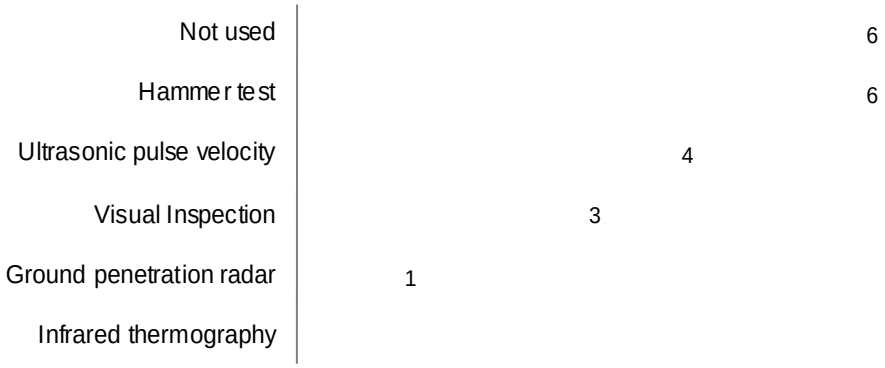

Figure 2.11 Non-destructive test methods used for quality inspection of shotcrete overlays

2.3.2 General practices

As discussed in the previous sections, the integrity of shotcrete applications relies heavily on the ability of the overlay to effectively bond to the substrate concrete, especially in repairs. To this end, properly preparing the receiving surface is vital to ensure an adequate bond between the substrate and the overlay to ensure cleanliness, remove laitance, and improve roughness. Hence, the survey asked the preferred surface preparation techniques used in the industry, which are indicated in Figure 2.12. According to the survey responses sandblasting is the most popular method, followed by chipping and hydro-demolition.

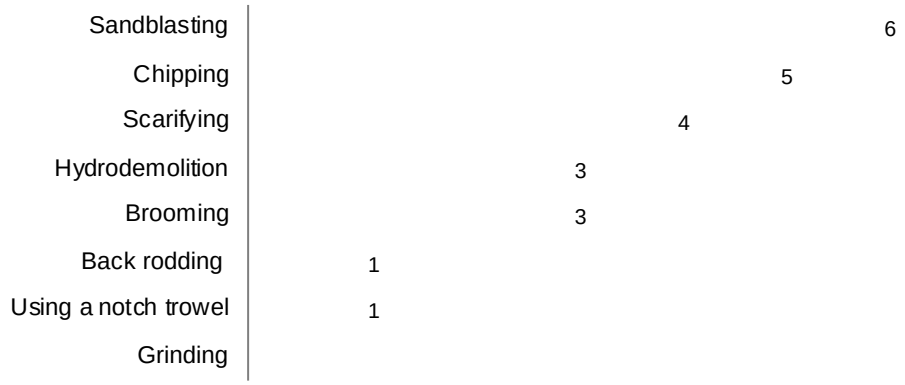

Figure 2.12 The popularity of substrate surface preparation techniques (the numbers are responses received)

Shotcrete generally is characterized by a lower water cement ratio (w/c) and small nominal maximum aggregate size, suggesting a higher paste content, which leads to shrinkage-related issues. Therefore, another critical factor in ensuring a proper bond, according to Silfwerbrand (1990), is curing, which could also influence shotcrete's drying shrinkage cracking behavior. Adequate curing will reduce moisture loss at the interface, leading to proper hydration. Curing can minimize early-age shrinkage, reducing the overlay cracking (Silfwerbrand & Beushausen, 2005). Therefore, the shotcrete survey investigated the common methods of curing used in shotcrete construction. Figure 2.13 indicates that the most common curing method for vertical shotcrete walls is use of a curing compound.

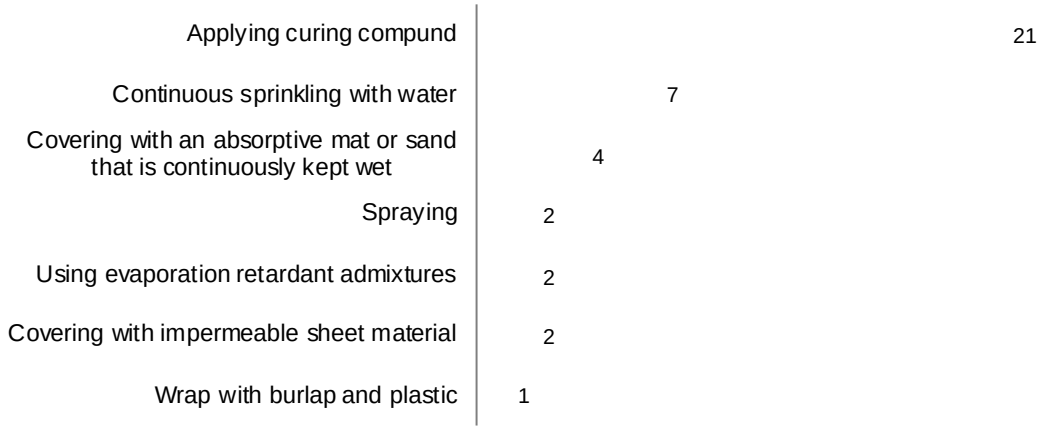

Figure 2.13 Common curing methods for vertical shotcrete walls

However, practitioners have also mentioned that the curing method depends on many factors, including weather conditions and the location the shotcrete layer (i.e., internal or surface). The literature suggests that curing compounds reduce the interface bond strength between the concrete substrate and shotcrete. Therefore, the survey asked the methods to ensure adequate shotcrete-shotcrete or concrete-shotcrete bond strength when using curing compounds. In summary, most practitioners preferred curing compounds for the final flash coat. It is typically removed by hydro or sandblasting before shooting the next layer if curing compounds are used in an internal layer. Some practitioners use mechanical connections between layers for better bond strength and thus don not remove the curing compounds before shooting the next layer. Mechanical connections include dowels to provide an additional bond and load transfer to the structure with shear and lateral resistance. Dowels also add rigidity to the reinforcing steel, secure its placement during vibrations, and reduce the risk of future spalling. Other practitioners mentioned that they do not take additional precautionary measures to ensure adequate bond strength even after curing compounds. When curing compounds may not be the most economical solution, early drying shrinkage cracking can be postponed with prolonged

moisture curing. Therefore, this survey also investigated the typical duration of prolonged moisture curing, and the results are shown in Figure 2.14. The most common curing period is seven days.

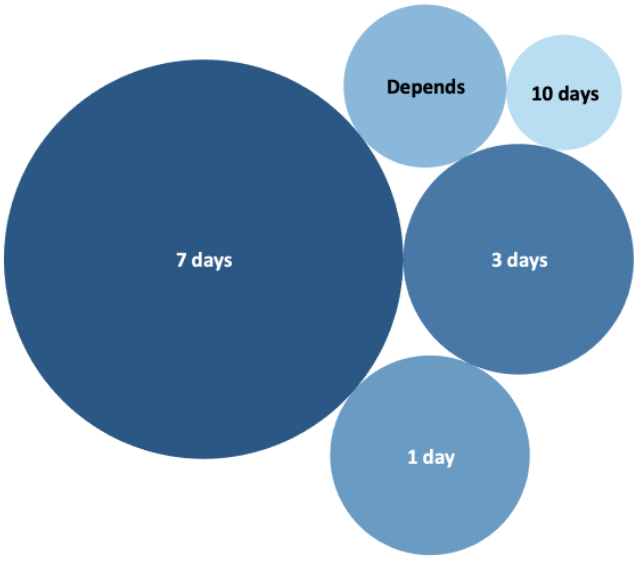

Figure 2.14 Common durations of prolonged moisture curing regimes

2.3.3 Multi-layer shotcreting

The survey further investigated the use of multiple shotcrete layers in construction. It is evident from the answers that most practitioners favored single layer shotcreting over multilayer shotcrete constructions to ensure monolithic behavior. They preferred shooting the structural shotcrete layer at once and finishing with the top-down final coat. Therefore, the most common number of layers in multilayer shotcreting was two. However, some practitioners have mentioned using multilayer shotcreting in thick walls with congested reinforcement. There were different answers as to the maximum thickness of a wall that could be shot at a single layer. Some practitioners have mentioned 18" (450 mm) thick walls, whereas some have limited it to 4" (100 mm) thick walls, suggesting that multilayer shotcreting is an area that must be addressed through specifications. It is also apparent from

the responses that cast-in-place concrete is more economical than shotcrete beyond a particular thickness. According to the responses, the substrate or the final flash-coat is more likely to fail than the internal shotcrete layers.

Figure 2.15 shows the time after which the successive layer is placed in shotcrete multilayer construction. Some practitioners believe that if the receiving surface is adequately prepared, the delay does not matter. The survey also reresponses indicated that it depends on the site conditions and the application which has a range of 1” - 24" (25mm - 600 mm) for the initial shotcrete layers and 1” - 2" (25 mm - 50 mm) for the final flash coat. It was also evident that the most common failure mode in multilayer shotcrete construction is subsequent layers debonding from the adjoining layers. However, the practitioners strongly believe that debonding could be avoided through proper surface preparation of the receiving surface.

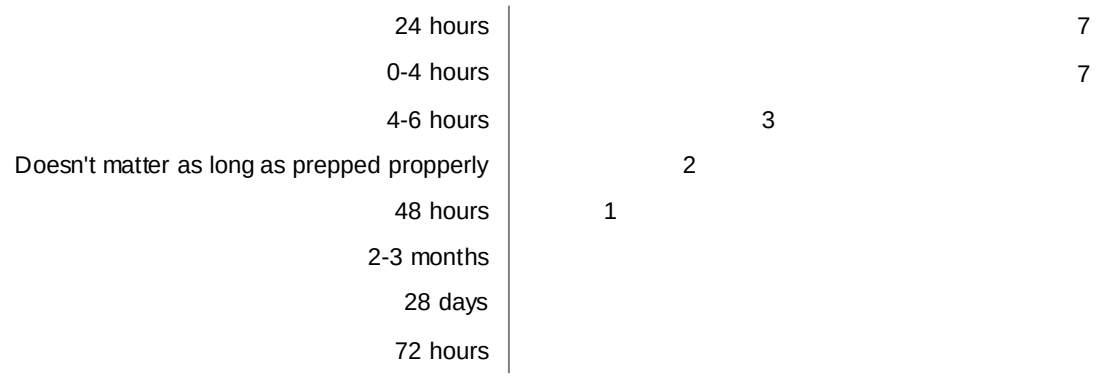

Figure 2.15 Common delay between shotcrete layers in multilayer shotcreting

If it is found that the bond strength is below a particular value, then the preferred corrective action seems to be to remove and replace the shotcrete in the areas in question. However, when such corrective steps are taken, practitioners ensure that the receiving surface is prepared correctly and in the SSD state. Nevertheless, the literature indicates contradicting results on the substrate moisture condition. However, several authors have

reported the importance of substrate moisture conditions in achieving a good bond (Emmons, 1994; Erhard & Chorinsky, 1986; Farzad et al., 2019; Zhang et al., 2020).

2.3.4 Long-term durability of shotcrete

Figure 2.16 indicates the factors affecting the long-term durability and deterioration of shotcrete. According to most practitioners, freezing and thawing cycles lead to material deterioration of concrete more frequently than the other factors mentioned. The freeze-thaw durability of shotcrete could be improved with a well-distributed internal air void system (air content and spacing factor) of the hardened concrete. Literature indicates that shotcrete loses 6-10% air during placement (Choi et al., 2016), suggesting the importance of adding air-entraining admixtures to improve the freeze-thaw resistance.

Figure 2.16 Long-term durability issues of shotcrete

2.3.5 Quality assurance of shotcrete

Practitioners adhere to the methods listed in ACI 506.4R to guarantee the quality of shotcrete during the construction phase (ACI Committee 506, 2019). These methods include having third-party experts perform visual inspections, using only ACI-certified nozzlemen who have experience with similar projects, using mock-up panels to qualify nozzlemen, and laboratory testing of core samples. Furthermore, the mix designs are reviewed to ensure the correct mix, while materials and equipment are checked to ensure

they are up to the standards required. These tests include periodic testing of compressive strength, workability, air content, temperature, and grading. Round determinate panel tests (RDP) are performed when toughness is a concern, especially in fiber-reinforced shotcrete. Practitioners perform random wall core tests to ensure that shadowing is not present in densely reinforced shotcrete sections. Hammer sounding is done in some cases no earlier than 28 days after the shotcrete is placed to detect delamination.

Further, quality inspections ensure that the requisite mesh tightness, proper surface preparation with a clean but rough receiving surface, and adequate surface prewetting are achieved to ensure SSD conditions. After preparation of the substrate, inspections begin to ensure that shotcrete is placed at the correct angle and distance, followed by proper curing. Continuous monitoring ensures even placement of shotcrete and quality of construction. In summary, all aspects of shotcrete placement, including design, materials, equipment, and craftsmanship, are monitored to guarantee shotcrete quality in the construction stage. According to the survey results, practitioners mostly use visual inspections to ensure shotcrete quality during the in-service phase. Other methods include hammer sounding, pull-off tests, and core sample testing. These inspections typically occur on an annual or biennial basis.

2.3.6 Summary of the industry survey

The online survey results are summarized below to understand shotcrete industry practices and identify problem areas.

- Debonding and compressive strength failure are the two most common failure modes concerning shotcrete structures.

- Although the pull-off direct tensile test has *in situ* capability, practitioners still prefer laboratory compressive testing of core samples taken from mock-up test panels.
- Hammer sounding is the most common form of non-destructive testing method used by shotcrete practitioners. Nevertheless, this method is mainly used as a preliminary assessment technique to identify problem areas for further testing. However, an equal portion of practitioners does not use any non-destructive tests.
- Proper substrate surface preparation is necessary to ensure monolithic behavior in shotcrete construction, and sandblasting is the most common preparation process. Before shooting, bringing the receiving surface to the SSD state is vital.
- Industry practitioners prefer shooting a single structural layer of shotcrete over multilayer shotcrete constructions, followed by a final coat. However, in situations where multiplayer construction cannot be avoided, there is no consistent responses with regard to the maximum layer thickness that can be applied at once. The substrate or final flash coat is more likely to fail than the internal layers of shotcrete. It is also apparent that the successive layer is placed within four hours or one day after shooting the preceding shotcrete layer in general practice.
- Curing is vital for maintaining shotcrete quality, and the use of curing compounds seem to be the most popular with vertical shotcrete walls. However, the curing compound needs to be removed unless it is used on the final flash coat, and the surface needs to be adequately prepared before a successive shotcrete layer is placed. Otherwise, instead of curing compound, prolonged moisture curing can be utilized. The most common moisture curing duration for shotcrete is seven days.

- According to the survey participants, freezing and thawing is the most detrimental factor affecting long-term durability of interface bond between shotcrete and substrate.
- Several Quality Assurance (QA) and Quality Control (QC) procedures are available to ensure shotcrete quality in the construction phase. Industry professionals, however, often rely on visual inspections to ensure shotcrete quality in the in-service phase.
- When the shotcrete does not meet the appropriate requirements, the common practice is to remove the shotcrete layer in the area in question and adequately prepare the receiving surface to ensure sufficient roughness and SSD condition before placing a new shotcrete layer.

2.4 Chapter summary

Based on the extensive literature review and the industry survey results, this report will address the following.

- The effect of the substrate surface preparation technique on the interface bond between the shotcrete overlay and the concrete substrate.
- The effect of the test method in determining the performance of shotcrete-to concrete interface bonds.
- The effect of freezing and thawing on the durability of the shotcrete-concrete interface bonds.
- The influence of surface texture on the quality of shotcrete-concrete interface bonds.

Chapter 3. MATERIALS AND EXPERIMENTAL PROGRAM

The goals of this Phase III study are to mainly investigate the influence of surface preparation on the short-term and long-term bond characteristics of the shotcrete-concrete interface bonds. The following section summarizes the materials and the experimental program for both short- and long-term freeze-thaw durability characteristics of the interface bond.

3.1 Raw materials and mix design

The experimental investigation utilized Type I-II Portland cement ASTM C150 and coarse aggregates with a nominal maximum size of 3/8" (9.5 mm) for the concrete layer. A local ready-mix concrete company, Premix-Inc, Pullman, WA, provided the coarse aggregates and sand, and the grain size distributions of those materials from sieve analysis meet the requirements of AASHTO #8 and WSDOT Class 2 sand, respectively. The corresponding specific gravity based on ASTM C127 (and water absorption based on ASTM C128) of the coarse aggregates and sand in concrete are 2.69 (1.21%) and 2.64 (1.89%), respectively. The grain size distributions of coarse aggregate and fine sand from sieve analysis in accordance with ASTM C136 are presented in Table 3.1. The water-cement ratio (w/c) of the concrete mix is 0.48. The shotcrete overlays were cast by The Conco Construction Companies, Kent, WA. The specific gravity (and water absorption) of the coarse aggregates and sand in shotcrete are 2.68 (1.25%) and 2.65 (2.14%), respectively. The water-cementitious material ratio (w/cm) of the concrete mix is 0.39, with a density of 143.9 lb/ft^3. The shotcrete mix incorporates two types of cementitious materials, Type I-II Portland cement and Class F fly ash ASTM C618. Table 3.2 indicates

the details of the concrete (reference mix obtained from WSDOT) and shotcrete mix designs used in the experimental program.

Table 3.1 Grain size distribution of aggregates (cumulative % passing)

Sieves, mm (mesh)	Cast-In-Place (CIP) Concrete		Shotcrete	
	Coarse Aggregates	Fine Aggregates	Coarse Aggregates	Fine Aggregates
12.5 (1/2")	100	-	100	
9.53 (3/8")	91	100	94.8	100
4.75 (#4)	14	99	13.1	98
2.36 (#8)	0.2	84	0.3	84.2
1.18 (#16)	0.1	66	0.1	68
0.6 (#30)	-	44	0.1	47.5
0.3 (#50)	-	20	0.1	22.8
0.15 (#100)	-	4	0.1	5.1
0.075 (#200)	-	1.3	0.1	1.7
Specific Gravity (SSD)	2.68	2.65	2.67	2.65
Water Absorption, %	1.21	1.89	1.25	2.14

Table 3.2 Typical shotcrete and cast-in-place concrete mix proportions (per yd^3)

Mixture	Cement (lb)	Fly Ash (lb)	Coarse Aggregate (lb)	Sand (lb)	Water (lb)	AEA (oz)	WRA (oz)
CIP Concrete	564	-	1830	1270	272	-	-
Shotcrete	705	50	860	2000	292	1-20	13-70

3.2 Sample preparation

Since the study focused on the shotcrete-concrete interface bond, all the specimens consisted of two layers. The substrate concrete layer was prepared in the WSU laboratory. The concrete was mixed in a portable drum mixer with a volume of 26 gals (0.1 m^3). Two types of specimens were cast for the strength and fracture mechanics-based tests. The surface of the hardened concrete was prepared using three common methods before applying the shotcrete layer, namely chipping, pressure-washing, and sandblasting, by The Conco Construction Companies in Kent, WA. Based on the survey results, chipping and sandblasting are two of most commonly used surface preparation methods. Pressure-washing is another frequently used method and is also available for The Conco Company. Chipping was carried out using a chipping gun, a lightweight handheld concrete breaker. Sandblasting involved using compressive air to shoot abrasive media, specifically sand, onto a receiving. After chipping or sandblasting, the surfaces were air-blasted to remove dusts. Pressure washing used high pressured water to treat the receiving surface. Figure 3.1 shows the concrete panels for bond strength tests after surface preparations and Figure 3.2 shows the panels for double-wedge samples after surface preparations.

Since the goal of the study is to characterize the quality of the bond between the substrate and overlay, shotcreting was done as closely as possible to the field condition. A qualified nozzleman from the Conco Companies cast the shotcrete overlay at the Conco site in Kent, WA. The concrete substrate panels were placed vertically against a wall. Shotcrete was shot to the concrete substrates without pre-wetting.

Figure 3.1 Concrete panels for bond strength samples after surface preparations: (left) pressure-washed; (middle) chipped; and (right) sandblasted

Figure 3.2 Concrete panels for double-wedged samples after surface preparations: (left) sandblasted; (middle) pressure-washed; and (right) chipped

3.2.1 Cylindrical samples for bond strength tests

After mixing, fresh concrete was poured into 28" x 28" x 1.175" (610 mm x 610 mm x 30 mm) oiled wooden molds to cast concrete panels, as indicated in Figure 3.3. All the specimens were externally vibrated using a vibrating table. The panels were initially sprayed with water and covered with plastic sheets for 24 h, after which they were demolded. Next, the panels were continuously spray-cured for seven days and left covered with plastic for 28 days, during which they were watered occasionally. The panels were then air-cured until they were transported to the field.

After shotcreting, the panels were transported back to WSU laboratories, 4" (100 mm) diameter cylinders were cored from the panels using a water jet to prepare the cylindrical specimens for the shear and tensile strength tests. Figure 3.44 indicates the

preparation of the samples. One of the advantages of using a water jet is eliminating the possible damage to the interface bond by the torque-driven coring.

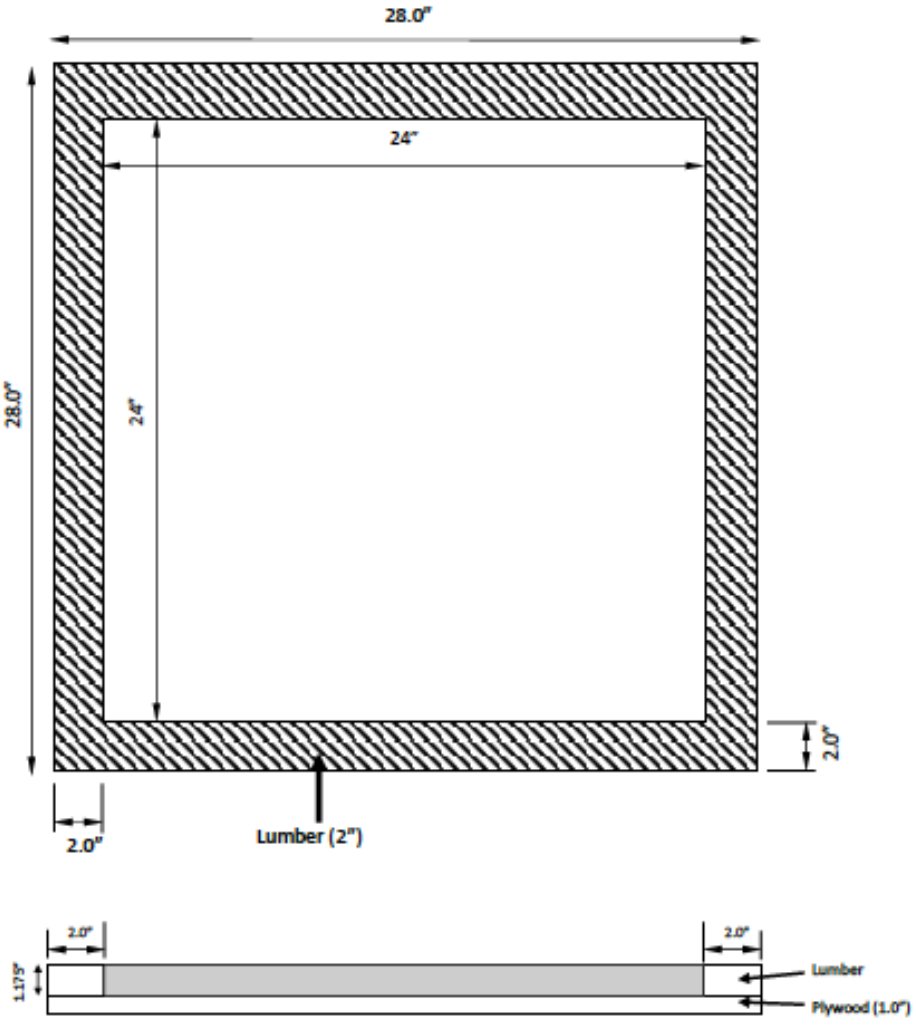

Figure 3.3 Plan view and elevation of the bond strength specimen mold

Figure 3.4 Cylindrical sample preparation for the shear and tensile bond strength tests

3.2.2 Double-wedged butterfly specimen

3.2.2.1 Specimen geometry and loading

As indicated in Figure 3.5, a double-wedged butterfly specimen was designed to test shotcrete-concrete interface bonds. An initial finite element analysis using the virtual crack closure technique (VCCT) based on linear elastic fracture mechanics was conducted using ABAQUS software to determine the geometry (wedge angle, θ) and the initial crack length ($a_0 = 0.9$") of the specimen. The crack length was created by placing a tape of 0.9" in width on the ends of substrate concrete before placing the shotcrete. The test fixture for the specimen was designed to impart both Mode-I (crack opening mode) and Mode-II (in-place shear) loads, as indicated in Figure 3.6(a) and (b), respectively.

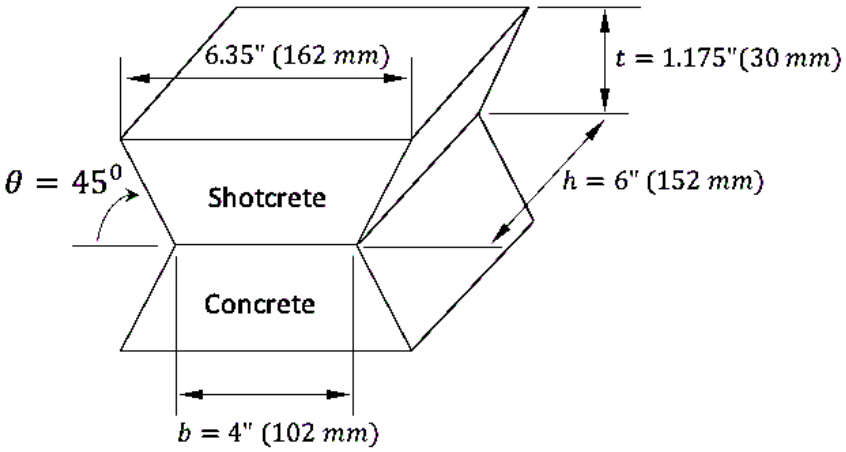

Figure 3.5 Double-wedged butterfly specimen geometry

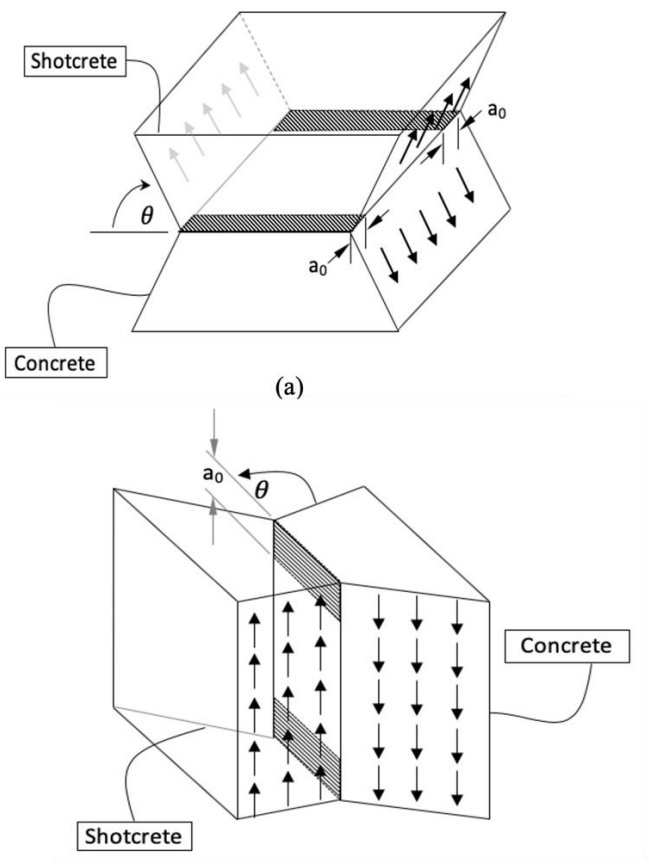

Figure 3.6 Different fracture modes on the double-wedged butterfly specimen; (a) Mode-I fracture loading, (b) Mode-II fracture loading

3.2.2.2 Specimen preparation

Figure 3.7 indicates the mold for the double-wedged butterfly specimens. One panel consists of 12 specimens. The samples were separated by steel bars in the longitudinal direction, while all the other parts of the mold were made of wood. In addition, there is a plywood board at the bottom of the mold to contain the concrete, as indicated in Figure 3.7.

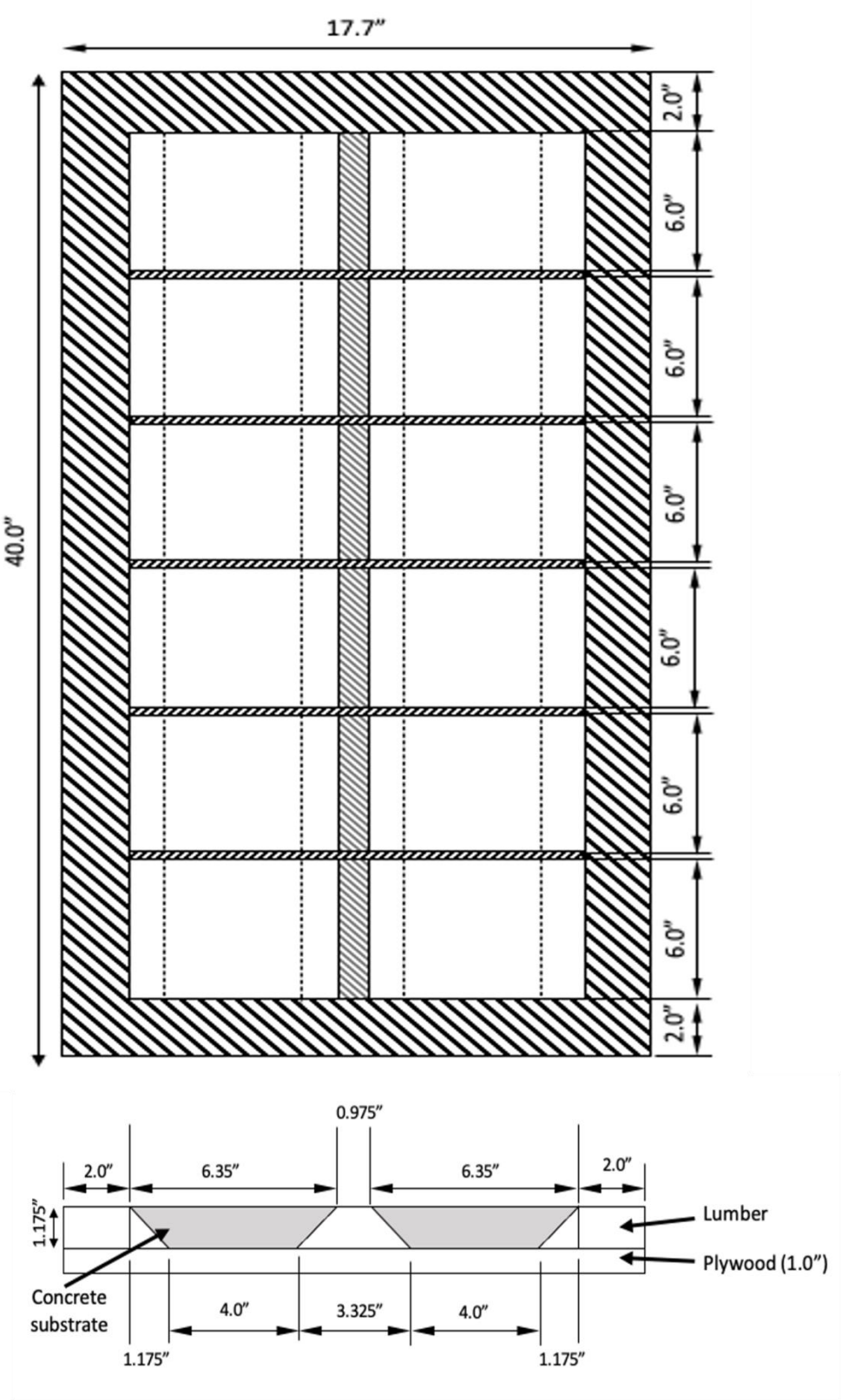

Figure 3.7 Plan view and elevation of the butterfly specimen mold

A schematic of the general procedure for preparing the butterfly specimens is indicated in Figure 3.8. The specimens are composed of two layers: the concrete substrate and the shotcrete overlay. The concrete substrate was-cast in the WSU concrete lab. After mixing, the fresh concrete was poured into oiled wooden molds to cast the concrete layer, as indicated in Figure 3.8(a). All the specimens were externally vibrated using a vibrating table. The panels were initially sprayed with water and covered with plastic sheets for 24 h, after which point they were demolded and kept in a lime bath until the time of transportation. The specimens were taken out of the lime bath, air-dried, and put back in molds.

The dried concrete specimens were put back in the initial mold as indicated in Figure 3.8(b). Then, the whole setup was turned upside down, as shown in Figure 3.8(c). After that, plywood layer-1 in Figure 3.8(c) was removed to prepare the molds and the concrete substrate for the shotcrete layer. To this end, three layers of 0.9” masking tape were used in the place of the cracks (two edges), to simulate an initial crack (see Figure 3.6). After that, the molds were lubricated before affixing the plywood (layer-1) over the top. The plywood layer-1 in Figure 3.8(c) could be substituted with bubble wraps for transportation purposes. Then, the specimen butterfly panels were transported to a site in Kent, WA to cast the shotcrete layer. Note that by casting the concrete layer of the butterfly specimen upside down (interface at the bottom, as Figure 3.8(a)), it is ensured that the interface layer is naturally smooth. This way, the effect of the substrate surface preparation technique can be truly evaluated.

Figure 3.8(d) indicates the completed double-wedged specimens, which were air cured until the time of transportation in the lumber molds. A second plywood layer was

fixed on top of the whole setup before transporting back to the WSU laboratories to protect the specimens, as indicated in Figure 3.8(d).

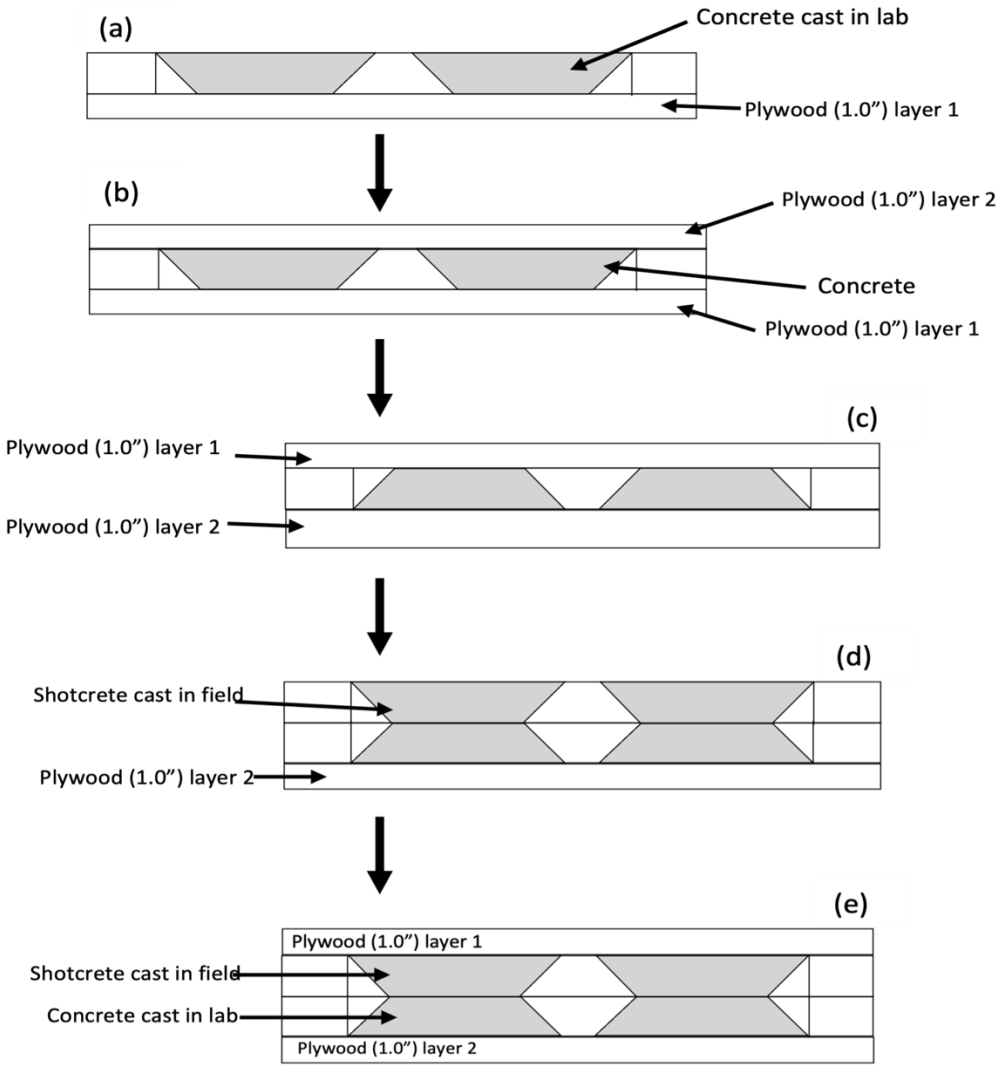

Figure 3.8 Preparation of double-wedged butterfly specimens

Before casting the overlay, the surface of the substrate concrete panel has been prepared using different techniques: sandblasting, pressure washing, and chipping. As a benchmark, a few of the substrate surfaces were left unprepared, or as-cast. After that, the shotcreting process was conducted by an ACI-certified nozzleman to cast the overlay. Note that, until the day of casting the shotcrete layer, the specimen panels were left exposed to

the air. It is also essential to make sure that the concrete layer is in the configuration in Figure 3.8(c) just prior to shooting the shotcrete layer.

Figure 3.9 shows the complete process from preparation of the mold to the final product of the double-wedged specimen.

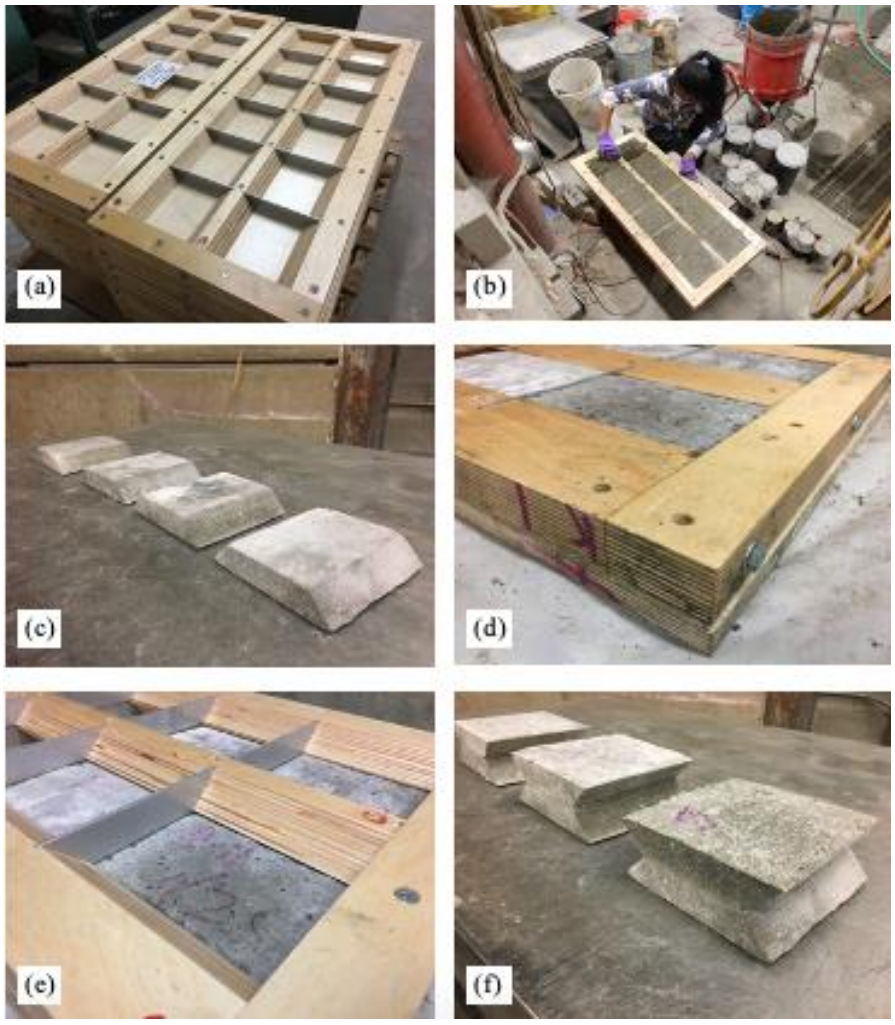

Figure 3.9 Double-wedged specimen preparation: (a) specimen mold, (b) substrate preparation, (c) demolded concrete substrate, (d) remolded concrete substrate, (e) molds turned over before spraying the shotcrete layer, and (f) final specimen.

3.3 Experimental testing plan

A series of tests were conducted to evaluate the hardened properties of the concrete and the strength and fracture mechanics characteristics of the shotcrete-concrete interface bonds. Shear, tensile, and fracture bond tests were performed over a 10-month period. The long-term durability evaluation of the shotcrete-concrete interface bond under rapid F-T conditions was performed after curing the specimens for 28 days. However, note that from the time after transporting the base concrete substrate to The Conco Company until the time of casting the top shotcrete overlay, the concrete specimens were exposed to the air to simulate realistic field condition of substrate concrete. The procedures of the above tests are briefly discussed in the following sections.

3.3.1 Tensile bond strength tests of interface bond

Figure 3.10 shows the tensile bond test setup for the shotcrete-concrete interface bond. The bi-layer cylindrical samples were attached to two steel discs at the top and bottom using epoxy. An MTS servo-hydraulic testing machine was used to test the specimens in a displacement-controlled mode with a 0.0254 inch/min (0.1 mm/min) loading rate. The displacement and peak tensile load upon failure of the interface bond were measured using a linear voltage differential transducer (LVDT) attached to the loading arm. At the unconditioned stage (no freezing or thawing), five specimens for each of the four different surface preparation techniques were tested for tension. The tensile bond strength was calculated as the peak tensile load per unit area of the interface. Figure 3.11 indicates a schematic of the loads applied to the cylindrical specimen.

Figure 3.10. Tensile strength test of shotcrete-concrete interface bond

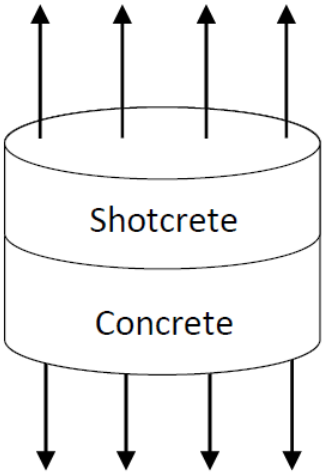

Figure 3.11 Schematic of tensile loading configuration on the cylindrical specimen

3.3.2 Shear bond strength tests of the interface

Figure 3.12 presents the shear bond test setup for the shotcrete-concrete interface bond. The cylindrical specimen was inserted into the stationary part of the fixture, which firmly holds the specimen, while a shear-type guillotine load was applied to the bond interface. It is critical to align the loading plane with the interface bond to ensure bond failure. Although this test setup is similar to test method of Iowa 406-C, the guillotine was

loaded with a MTS servo-hydraulic testing machine with a displacement-controlled loading at a 0.0254 inch/min (0.1 mm/min) loading rate. The loading part of the fixture, which rests entirely on the shotcrete overlay of the specimen, weighs 11 lbs (5 kg). The displacement and peak shear load upon failure of the interface bond were measured using an LVDT attached to the loading arm. Four specimens for each of the four different surface preparation techniques were tested for shear at the unconditioned stage. The shear bond strength was calculated as the peak shear load per unit area of the interface. Figure 3.13 indicates a schematic of the loads applied to the cylindrical specimen.

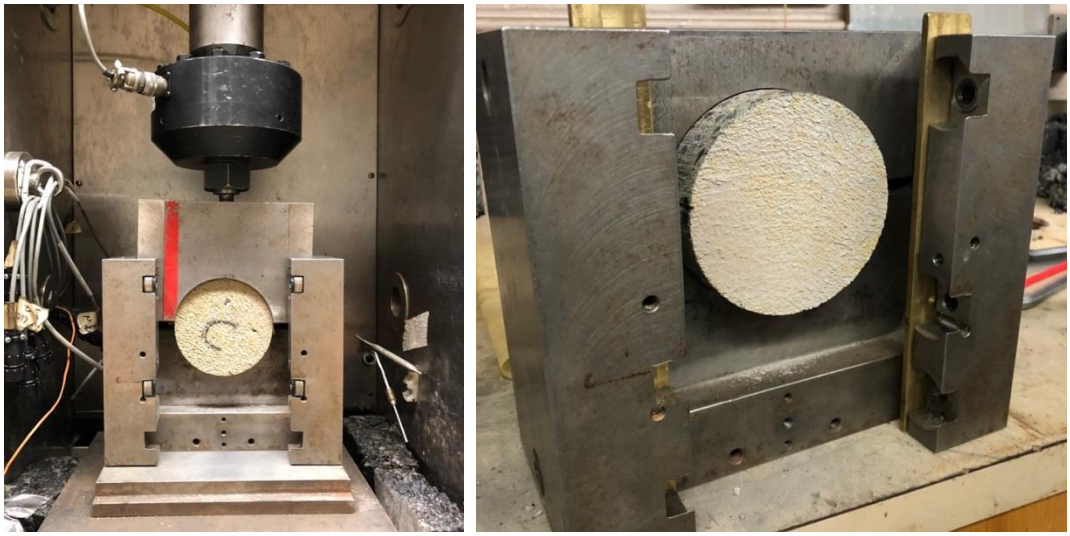

Figure 3.12 Shear strength test of shotcrete-concrete interface bond

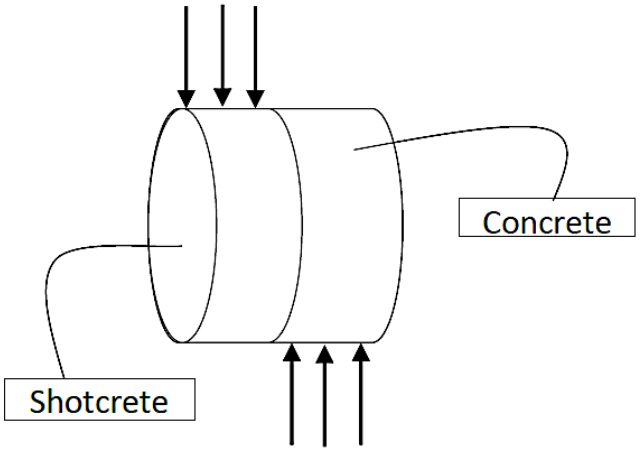

Figure 3.13 Schematic of the shear loading configuration on the cylindrical specimen

3.3.3 Fracture-based tests

Fracture-based tests were conducted based on a specially designed fracture-based test fixture for the compact butterfly double-wedged specimens. A schematic of the fixture is indicated in Figure 3.14. The specimens were held in position by four angle wedges which can be used to test specimens with various widths. Note that the fixture has been designed to optimize material usage and reduce weight. The fixture is made of a combination of steel and aluminum parts.

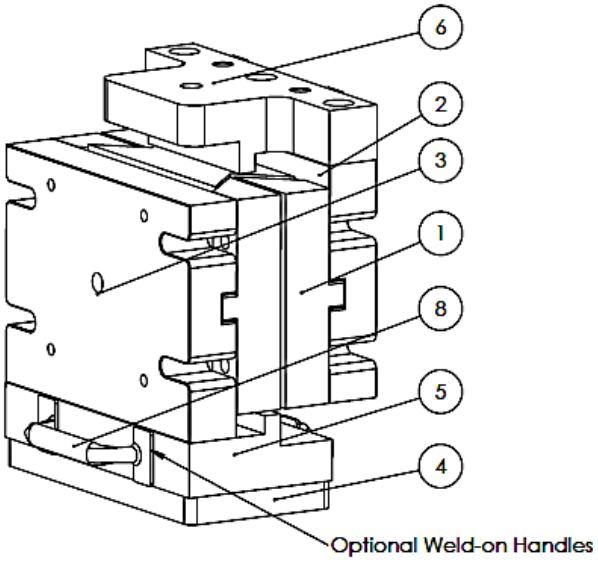

ITEM NO.	PART NUMBER	QTY.
1	Angle Wedge 3	4
2	Back Tapped	1
3	Back Counterbored	1
4	Base	1
5	Lower Shear	1
6	Upper Shear	1
7	Sample	1
8	1650A1	3

Figure 3.14 Schematic of fixture design for fracture-based tests

3.3.3.1 Mode-I fracture tests

Mode-I fracture is the crack opening of the specimens, in which the specimen is subjected to a tensile load as given in Figure 3.15 (loading direction indicated with red arrows) which is achieved by turning the test fixture by 90° and removing the top and bottom parts. Hence the apparatus weighs less in this instance. In this configuration, the load was applied to the specimen at the angle wedges, in contrast to the shear configuration. The specimens were loaded at a constant rate of 0.0254 inch/min (0.1 mm/min) using the loading arm. The displacement and the applied load were measured using an LVDT attached to the loading arm. The load vs. displacement curve was constructed using the data, and the fracture energy was computed as the area under the curve per unit area of the fractured surface.

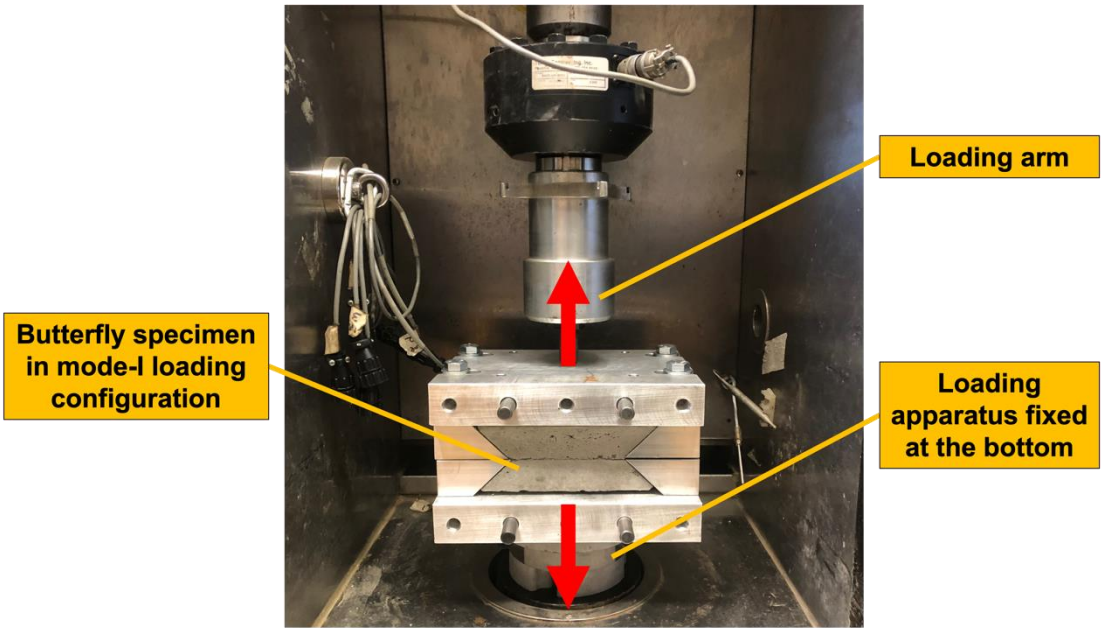

Figure 3.15 Mode-I fracture test configuration of butterfly double-wedged specimen

3.3.3.2 Mode-II fracture tests

Mode-II fracture is the in-plane shear configuration of fracture loads, in which component number 6 (upper shear) in the Figure 3.14 is used to load the specimen. It imparts a shear force closer to the bond plane using a strip of 0.5 inches (12.7 mm). The specimens were loaded at a constant rate of 0.0254 inch/min (0.1 mm/min). The displacement and the applied load were measured using an LVDT attached to the loading arm. The load vs. displacement curve was constructed using the data, and the fracture energy was computed as the area under the curve per unit area of the fractured surface. In this case, it is the area of the intact bond interface before fracture. The fracture test fixture with a specimen in shear configuration (leading to Mode-II fracture) is indicated in Figure 3.16. The four black nylon screws on either side of the vertical surfaces of the fixture were used to align the specimen bond plane with the loading part. Six specimens for each

substrate surface preparation technique were tested for unconditioned and conditioned samples at 300 F/T cycles.

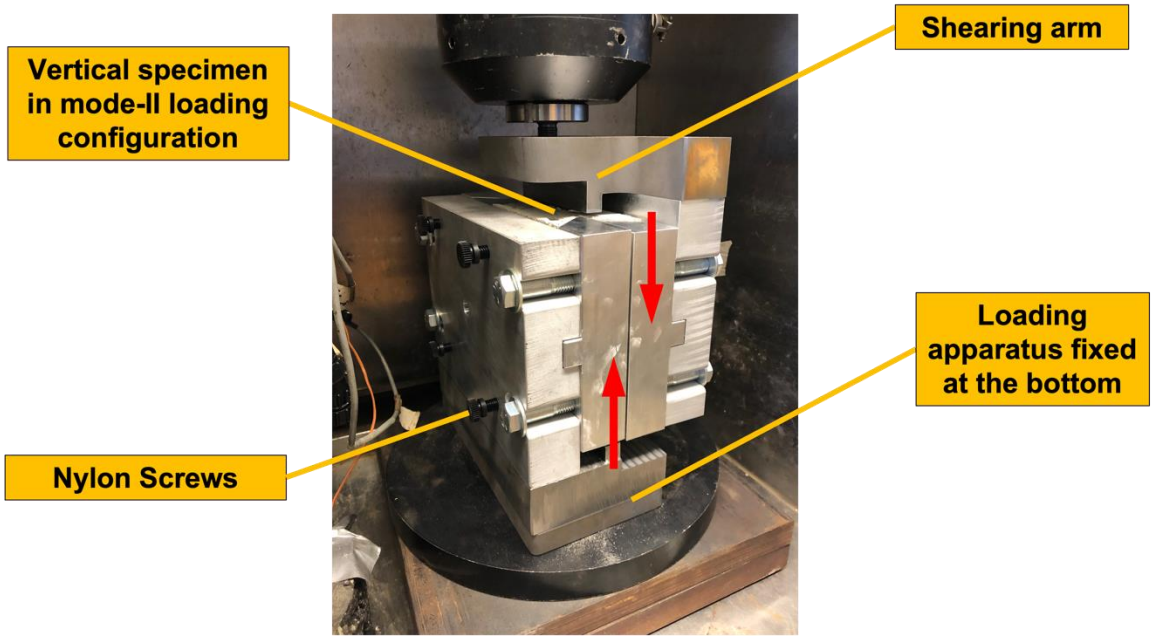

Figure 3.16 Mode-II fracture test configuration of the butterfly double-wedged specimen

3.3.4 Rapid freeze and thaw test

The durability study focused on evaluating the frost resistance of the shotcrete-concrete interface bond. More than 60 cylindrical specimens with 4 inches (100 mm) diameter and 30 mm thickness were subjected to rapid freezing and thawing, per ASTM C666 Procedure A. The temperature was varied between -0.4 °F (-18 °C) and 39.2 °F (4 °C) at a frequency of about eight cycles per day. Tensile bond tests were performed on fifteen samples for each of the four surface preparation techniques at 100, 200, and 300 F/T cycles. The specimens were not entirely submerged in water, and the water level was maintained about 0.4 inches (10 mm) above the shotcrete-concrete interface bond because the focus is on the durability of the bond interface rather than on individual material layers.

3.3.5 Laser texture scans of the substrate surface

A laser scanner was used to better analyze the effect of the substrate surface preparation technique on the quality of the shotcrete-concrete substrate bonds. Three-dimensional 3D graphs of the substrate concrete surface after the bond failure for strength and fracture test specimens were captured. The key measurement parameters were the mean profile depth (MPD) and the estimated texture depth (ETD). The mean profile depth was computed in accordance with ASTM E2157 (ASTM International, 2015). The profile is segmented into 100 mm baselines, and each baseline is divided into two halves. Figure 3.17 illustrates the calculation of the mean segment depth, which is calculated as the difference between the average of the two peaks of each segment and the profile average. Once the test is repeated for different segments, the average of all is expressed as the MPD (Gendy & Shalaby, 2007). In contrast, the ETD is calculated as a function of MPD, according to the ASTM E2157. Please note that the texture scans were obtained in mm.

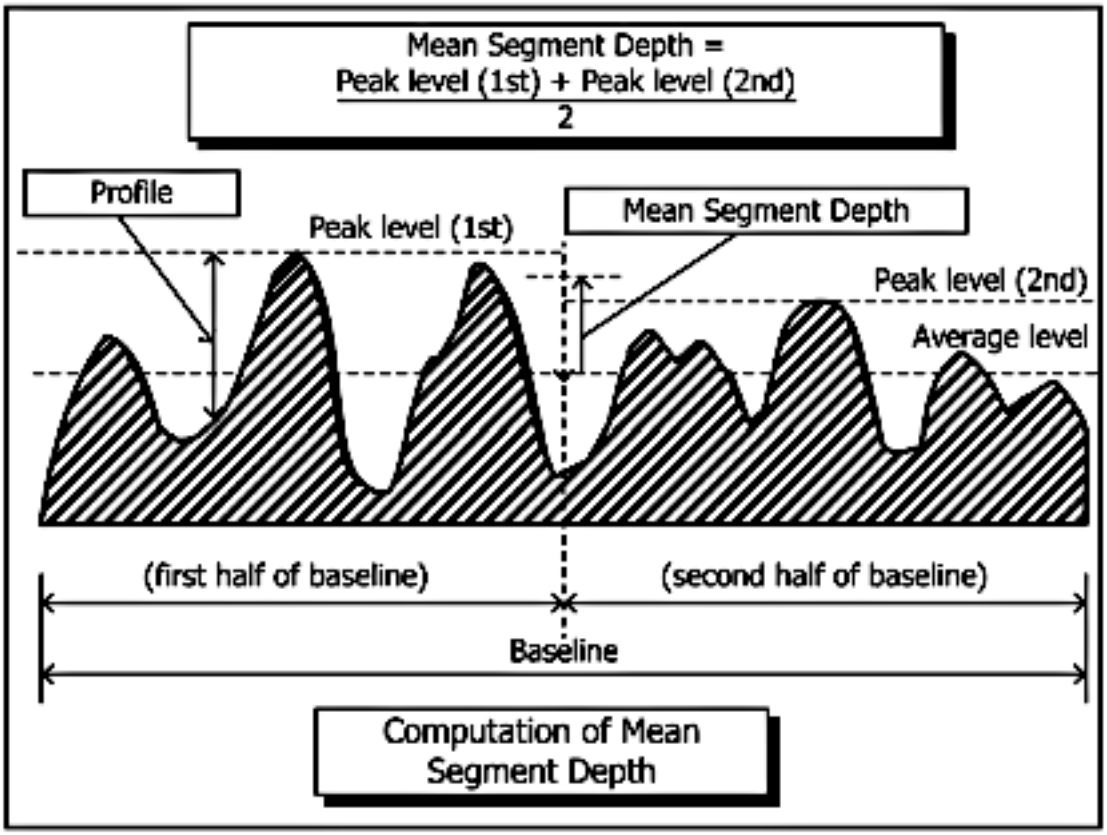

Figure 3.17 Procedure for computing the mean segment depth (ASTM International, 2015)

ASTM E2157 lists two equations for metric and imperial units as follows. The texture scanner directly showed the MPD and ETD values, along with the 3D texture plots.

$$ETD\ in\ mm = 0.2 + (0.8 \times MPD) \quad (1)$$

$$ETD\ in\ inches = 0.008 + (0.8 \times MPD) \quad (2)$$

Chapter 4. TEST RESULTS AND ANALYSIS

In this chapter, the results of the experiments introduced in Chapter 3 were presented, and an analysis was performed to interpret the data better. The 28-day compressive strength of the concrete is 4,410 psi (30 MPa), while the shotcrete is 6,990 psi (48 MPa).

4.1 Short-term bond behavior

The short-term (without freeze-thaw cycles) bond strength of the shotcrete-concrete interface was computed in terms of shear and tensile strengths. The tensile and shear strength tests used five and four specimens for each surface, respectively. The specimens were tested afer three months from the time of casting the shotcrete layer.

4.1.1 Short-term (no F/T cycle) tensile bond strengths of unconditioned samples

Figure 4.1 indicates the peak tensile strengths of the shotcrete-concrete bi-layer composite specimens. The peak tensile strengths have varied in ascending order as as-cast (AC), sandblasted (SB), pressure-washed (PW), and chipped (C) samples. The peak tensile strengths of the chipped samples are more dispersed, compared to the as-cast specimens, denoted by a relatively shorter box plot. The chipped, pressure-washed, sandblasted, and as-cast specimens have mean tensile bond strengths of 284 psi (1.96 MPa), 225 psi (1.55 MPa), 120 psi (0.83 MPa), and 45 psi (0.31 MPa), respectively, as indicated in Figure 4.1. The respective bond tensile strengths of each specimen are indicated in Table 4.1.

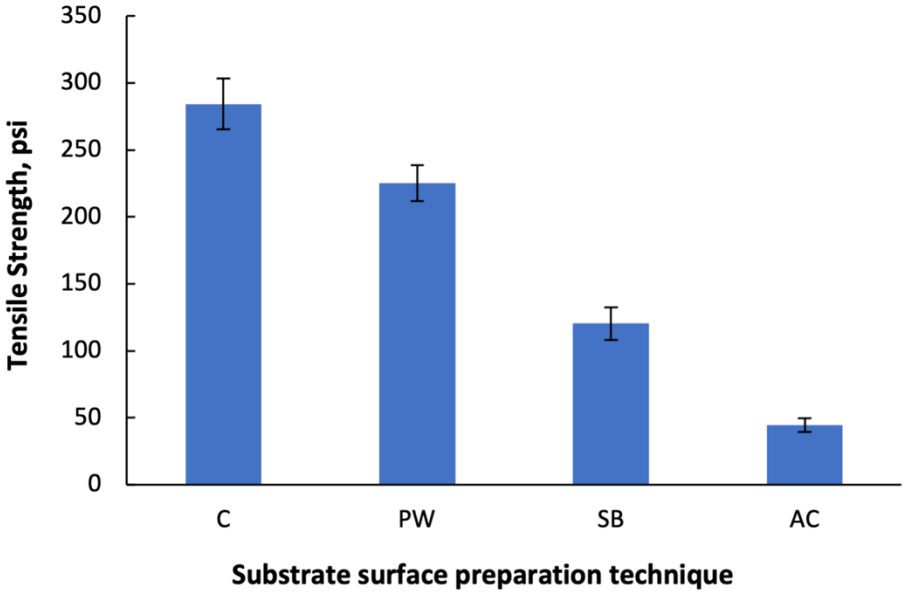

Figure 4.1 Tensile bond strength with substrate surface preparation technique

Table 4.1 Tensile bond strengths of unconditioned samples (psi)

Specimen No.	C	PW	SB	AC
1	313	182	134	36
2	248	230	144	60
3	282	208	130	51
4	339	256	120	31
5	240	250	74	45
Mean	284	225	120	45

The specimens with chipped substrate surfaces exhibit the highest tensile strength, indicating that they are the most tension resistant. This could be due to the better interlocking that is governed by the better roughness due to the chipped substrate surface. The tensile bond strength of pressure-washed samples appears to have an advantage over

sandblasted samples. As expected, the as-cast (unprepared) surface was the least resistant to tensile loads, emphasizing the need for substrate surface preparation in shotcrete repairs. The specimens with chipped, pressure-washed, and sandblasted substrate surfaces were 6.3, 5, and 2.7 times more resistant to tensile loads than unprepared substrate specimens, respectively. The specimen sets described above had a coefficient of variation (COV) of 14.86%, 13.51%, 22.7%, and 25.7%, respectively.

ACI 506.R-16 states that an adequately applied shotcrete with sufficient consolidation on a properly prepared substrate surface usually develops a bond strength greater than 145 psi (1 MPa) (ACI Committee 506-R, 2016, p. 506). It also states that the bond strength could be measured by direct tension or shear tests and that the usual method is to use the pull-off tension test, as described in ASTM C1583 (ASTM International, 2013b). In that sense, all the chipped and pressure-washed samples are well above the limit, while sandblasted and as-cast specimens did not surpass the considerable limit of bond strength. However, note that the direct tension pull-off tests differ from the laboratory tensile test setups. For instance, the pull-off test is intended to use a tensile force to pull and separate the still intact specimens from a substrate surface, which introduces additional stiffness to the specimen. In contrast, the laboratory tensile test specimens are fully cored and separated from the rest of the substrate using a water jet. Moreover, the water jet to separate the samples from the original panel may have a different influence on the substrate to overlay interface bond than using a core bit, which is the conventional method used in pull-off tests. Coring induces microcracking at the shotcrete-concrete interface bonds, reducing the bond strength. Furthermore, there could be some bending caused by the laboratory testing setup due to the eccentricity of load application. All the above reasons

might raise the question of whether the laboratory tensile strength and pull-off tension tests are directly comparable. Nevertheless, assuming they are, in a conservative sense, the results in Table 4.1 could be compared with the pull-off tensile strength tests from other studies.

Figure 4.2 shows the interfaces of the failed samples in tension. Note that the specimen section attached to the steel disk is the concrete substrate, while the other part is the shotcrete overlay in Figure 4.2. The number of aggregates exposed on the substrate surface due to surface preparation decreases from chipped to pressure-washed to sandblasted to cast specimens. A closer inspection revealed that the aggregates of the substrate concrete layer were more exposed in the chipped samples indicating a rugged surface, followed by pressure-washed samples. Hence, chipped samples indicated a more cohesive failure in the substrate concrete paste, followed by pressure-washed samples. In contrast, the sandblasted samples showed more adhesive failure, while the as-cast specimens failed completely by adhesive failure. There are no aggregates visible on the smooth as-cast (unprepared) surface of the substrate, as indicated in Figure 4.2(d).

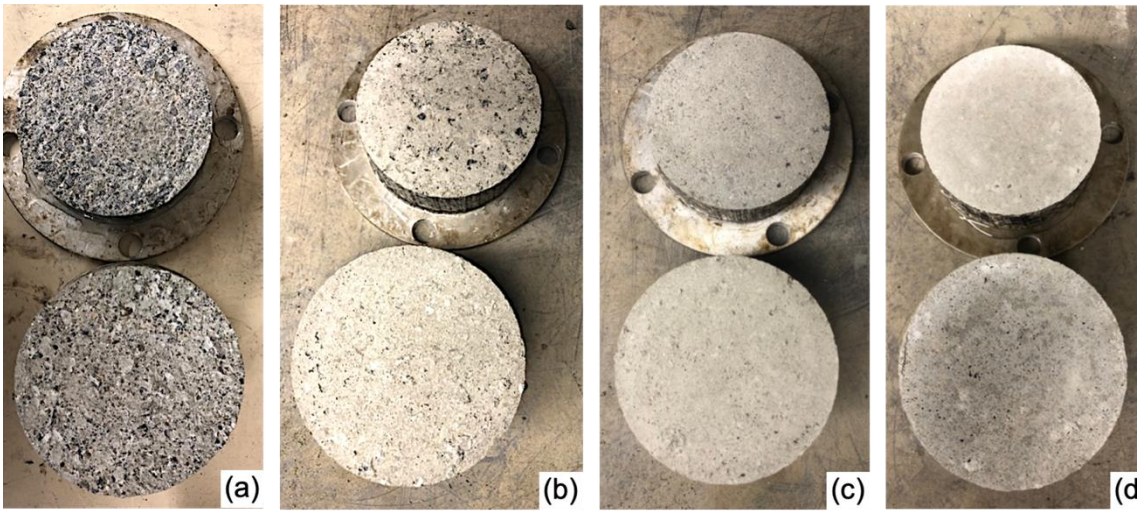

Figure 4.2 Interface bond failure of the shotcrete-concrete specimens under tensile load; (a) chipped, (b) pressure-washed, (c) sandblasted, (d) as-cast (unprepared)

Figure 4.3 presents a simple image analysis conducted for the four types of substrate surfaces using Python for the four types of substrate surfaces. A mask is created using a specified RGBs (red, green, and blue) range to cover the non-aggregate regions based on color. RGB model uses red, green, and blue colors in combination to produce a wide range of other colors. The region of interest is indicated with dark blue pixels, while the mask is shown in yellow. The ratio of dark blue pixels on the circular part of the image is then expressed as a ratio of the total pixels of the circular area of the image. This analysis helps identify the aggregate exposure as a percentage of the total area of the substrate surface. The exposure of aggregates for chipped, pressure-washed, sandblasted, and as-cast specimens were 30.07%, 9.19%, 3.76%, and 0.08%, respectively. This was in line with the visual indications of more cohesive type failure on chipped samples, as opposed to the as-cast samples. However, this analysis would be inaccurate if there were many visible pores on the substrate surfaces, as the image analysis may consider those regions as aggregates. The aggregate exposure correlates with the tensile strength variation of the specimens.

Based on this image analysis, it was decided to investigate the substrate surface texture further using a laser scanner, which is discussed separately.

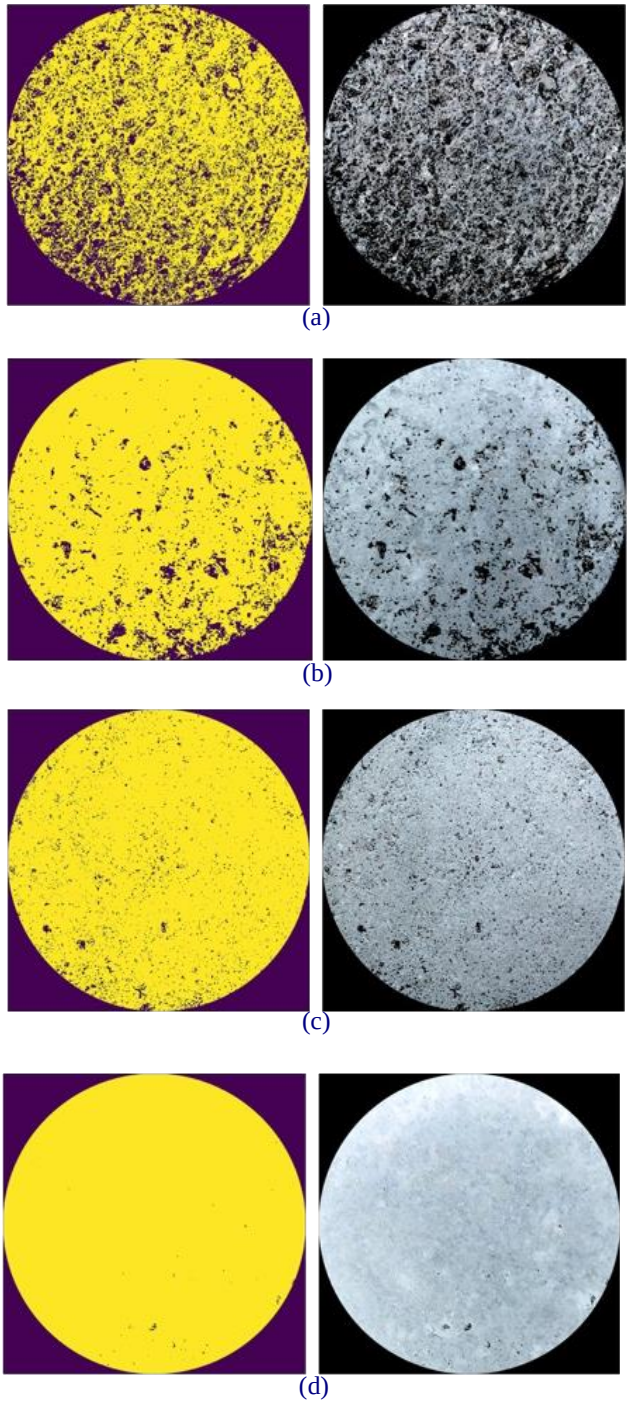

Figure 4.3 Image analysis for the substrate's texture (a) chipped, (b) pressure-

washed, (c) sandblasted, (d) as-cast (unprepared)

4.1.2 Short-term shear bond strengths of unconditioned samples

Figure 4.4 indicates the shear bond strengths of the shotcrete-concrete bi-layer composite specimens, in an ascending order as AC, PW, SB, and C samples. The chipped samples' peak shear force is more dispersed than the cast and pressure-washed specimens. The maximum shear strengths are shown in Table 4.2. Note that the pressure-washed and sandblasted specimens have only four specimens each due to a few discrepancies in the specimen diameter that occurred when extracting specimens using the waterjet.

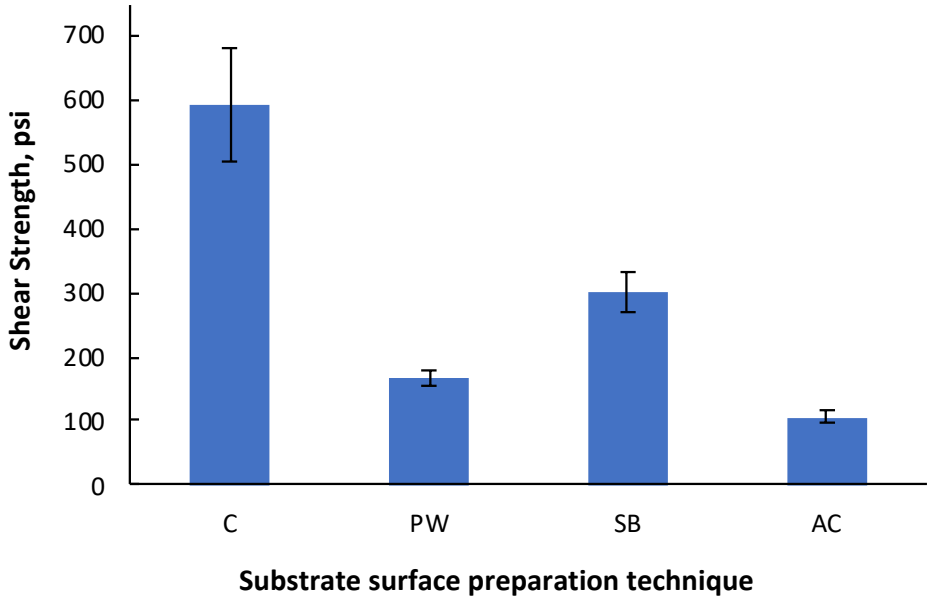

Figure 4.4 Shear bond strength variation with substrate surface preparation technique

Table 4.2 Shear bond strengths of unconditioned samples (psi)

Specimen	C	PW	SB	AC
1	426	196	387	133
2	496	160	236	93
3	779	164	288	90
4	748	140	287	100
5	520	-	-	109
Mean	594	165	299	105

The chipped, pressure-washed, sandblasted, and as-cast specimens have mean shear bond strengths of 594 psi (4.09 MPa), 165 psi (1.14 MPa), 299 psi (2.06 MPa), and 105 psi (0.72 MPa), respectively. The specimens with chipped substrate surfaces exhibit the highest mean shear force and, thus, the maximum shear strength, suggesting that they are the most shear resistant. This could be due to, again, the better interlocking governed by, the better roughness of the chipped substrate surface and the higher exposed aggregates. The shear bond strength of sandblasted samples is greater than the pressure-washed samples. As expected, the as-cast (unprepared) surface was the least resistant to shear loads, emphasizing the need for substrate surface preparation in shotcrete repairs. The specimens with chipped, pressure-washed, and sandblasted substrate surfaces were 5.65, 1.57, and 2.85 times respectively, more resistant to shear loads than unprepared substrate specimens. ACI 546.3R-14 specified that the shear bond strength should be 300 psi or higher for a good bond performance. Only samples with chipped and sandblasting surface preparations can meet this requirement.

The specimen sets had high coefficients of variation (COV), with 29.86%, 14.23%, 21.20%, and 18.64%, respectively. In general, the COVs of shear tests were higher than those of the tensile tests, indicating that the shear behavior of the shotcrete-concrete interface bond is more sensitive to local variations in substrate surface texture than tensile behavior. In addition, the direct shear test imparts stress concentrations in some areas of the specimen. Differences in local stress concentrations from specimen to specimen may have also contributed to the higher variations in measured values.

Figure 4.5 shows the interface of the failed samples in shear. As opposed to the substrate texture of the tensile bond failure, the sandblasted specimen substrates in shear showed more exposed substrate aggregates when compared with the pressure-washed counterparts. The chipped surface had more exposed cohesive regions, followed by sandblasted and pressure-washed specimens. As before, as-cast specimens indicated a complete adhesive failure resulting in a smooth substrate surface after failure, as indicated in Figure 4.5(d). Chipped samples showed more cohesive failure in the substrate concrete, followed by sandblasted samples. In contrast, the pressure-washed samples indicated more adhesive failure, with little to no cohesive failure. Note that in Figure 4.5, only the concrete substrate surfaces are shown.

Figure 4.5 Interface bond failure of the shotcrete-concrete specimens under shear load; (a) chipped, (b) pressure-washed, (c) sandblasted, (d) as-cast (unprepared)

One of the common difficulties with the direct shear setup is that the loading plane must completely align with the bond plane (interface). However, this was particularly difficult because the waterjet cores were not perfectly smooth on the circumferential surfaces. Therefore, the bond would sometimes be loaded slightly to the sides of the shotcrete or the concrete. Moreover, when the loading plate interface is located in shotcrete, local cohesive failure in shotcrete occurred, as indicated in Figure 4.6. This is another reason for the larger dispersions in shear bond test results when compared to the tensile bond strength results. The compressive strength of the shotcrete is often higher than bond strength; hence, shotcrete cohesive failure leads to a greater shear bond strength value.

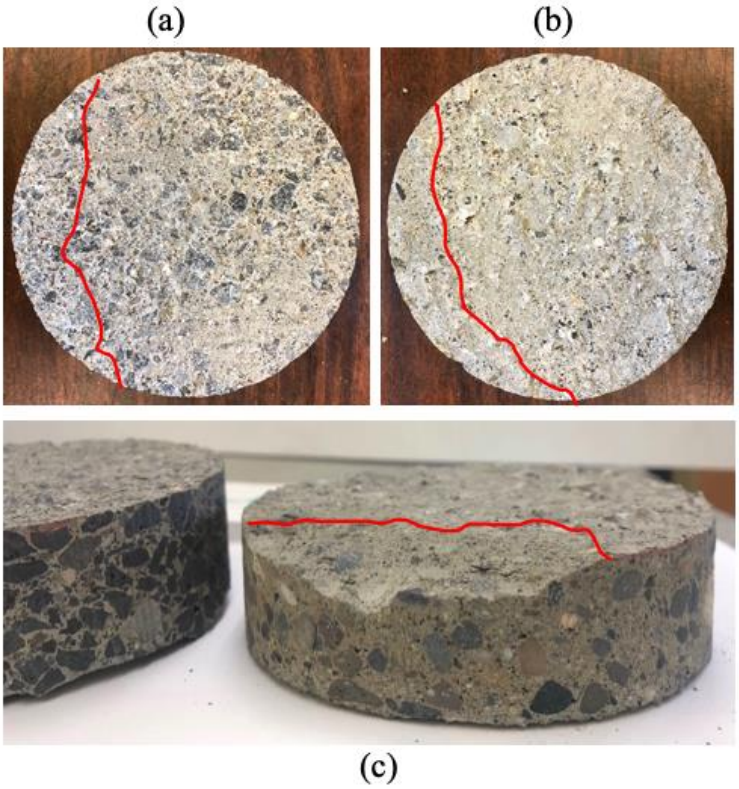

Figure 4.6 Localized failure due to localized stress concentrations on shear specimens: (a) concrete substrate, (b) shotcrete overlay, and (c) elevation of the shotcrete overlay.

4.1.3 Short-term Mode-II fracture behavior of unconditioned butterfly samples

The butterfly double-wedged fracture test specimen was initially designed for the Mode-II in-plane shear fracture. Therefore, this section explains the behavior of the proposed specimen in mode-II first, and then discusses the mode-I tests in the next section. The Mode-II fracture tests were performed on six specimens of each substrate surface preparation technique. Once the load-displacement curve was obtained from the MTS machine, the data was analyzed using Python since the data files were relatively large. The area under the load-displacement curve and the individual plots were obtained using python. In general, a few different load-displacement curves were observed, and two of them (brittle failure and ductile failure) are indicated in Figure 4.7, not pertaining to a

particular substrate surface preparation technique. The most common failure mode for shotcrete-concrete interface bonds is represented in Figure 4.7(a). Although small, there is some softening after the peak load in Figure 4.7(a).

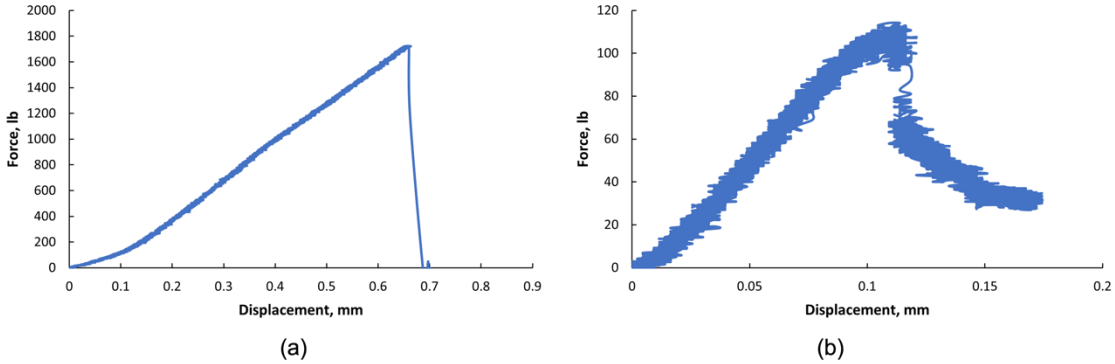

Figure 4.7 Different types of load-displacement curves for Mode-II fracture tests of the shotcrete-concrete interface bond: (a) brittle failure; (b) ductile failure

Figure 4.8 indicates the variation of fracture energy with substrate surface preparation techniques. Fracture energy is computed as the area under the load-displacement curve per unit area of the cracked surface (initially intact area). The fracture energy has varied in ascending order as as-cast, pressure-washed, sandblasted, and chipped samples, similar to the variation reported in the shear strength test. Note that the specimens are loaded in shear in both shear strength and Mode-II fracture energy tests. However, unlike the strength tests, adhesive failure was more prominent in the Mode-II fracture tests. Nevertheless, the chipped samples may have exhibited a slightly mixed-mode failure with more apparent adhesive failure. Regardless, a microstructural characterization is necessary to analyze the near failure interface region definitively. The fracture energies for the respective surface preparation technique are shown in Table 4.3, and note that six specimens were tested for each surface preparation technique.

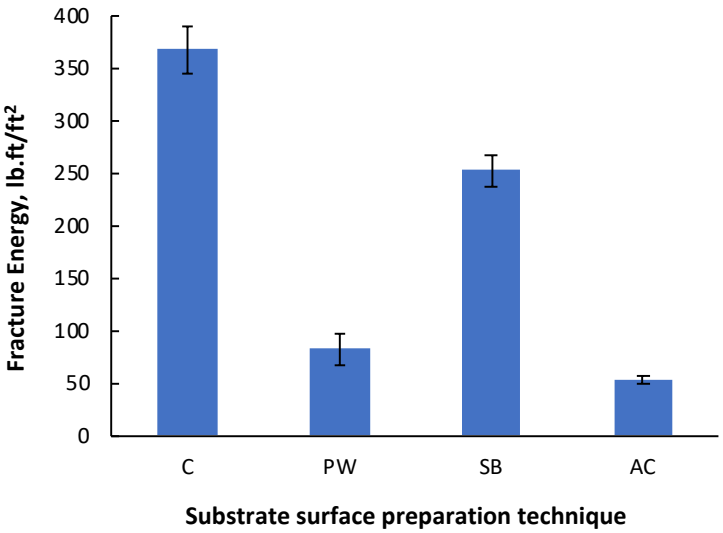

Figure 4.8 Mode-II fracture energy variation with the substrate surface preparation techniques

Table 4.3 Mode-II fracture energies of unconditioned samples (lb.ft/ft^2)

Specimen	C	PW	SB	AC
1	350	87	244	52
2	404	94	212	64
3	354	37	316	66
4	410	39	233	53
5	269	117	271	45
6	420	121	240	44
Mean	368	82	253	54

The chipped, pressure-washed, sandblasted, and as-cast specimens have mean fracture energies of 368 lb.ft/ft^2 (498 J/m^2), 82 lb.ft/ft^2 (112 J/m^2), and 253 lb.ft/ft^2 (343 J/m^2), and 54 lb.ft/ft^2 (40 J/m^2), respectively. The specimens with chipped substrate surfaces exhibited the highest mean fracture energy, suggesting that they are the most

resistant to in-plane shear-type (sliding) fracture. This could be due to the better interlocking governed by the superior surface texture, as indicated in Figure 4.9(a). The sandblasted specimens reported the second-highest fracture energies, which are in line with the rougher surface texture shown in Figure 4.9(c). As expected, the as-cast specimens indicated the least resistance to in-plane shear fracture, further emphasizing the need for substrate surface preparation in shotcreting work.

The specimens with chipped, pressure-washed, and sandblasted substrate surfaces were 6.81, 1.53, and 4.68 times, respectively, more resistant to in-plane shear fracture than unprepared substrate specimens. The COV of the specimens above is 15.45%, 44.6%, 14.36%, and 17.18%, respectively. The specimens were prepared in individual molds on larger panels. The small confined regions might have affected uniform surface preparation and shotcreting, influencing the dispersion of the data. These local variations in the substrate surface may have influenced the differences in the fracture behavior of individual specimens.

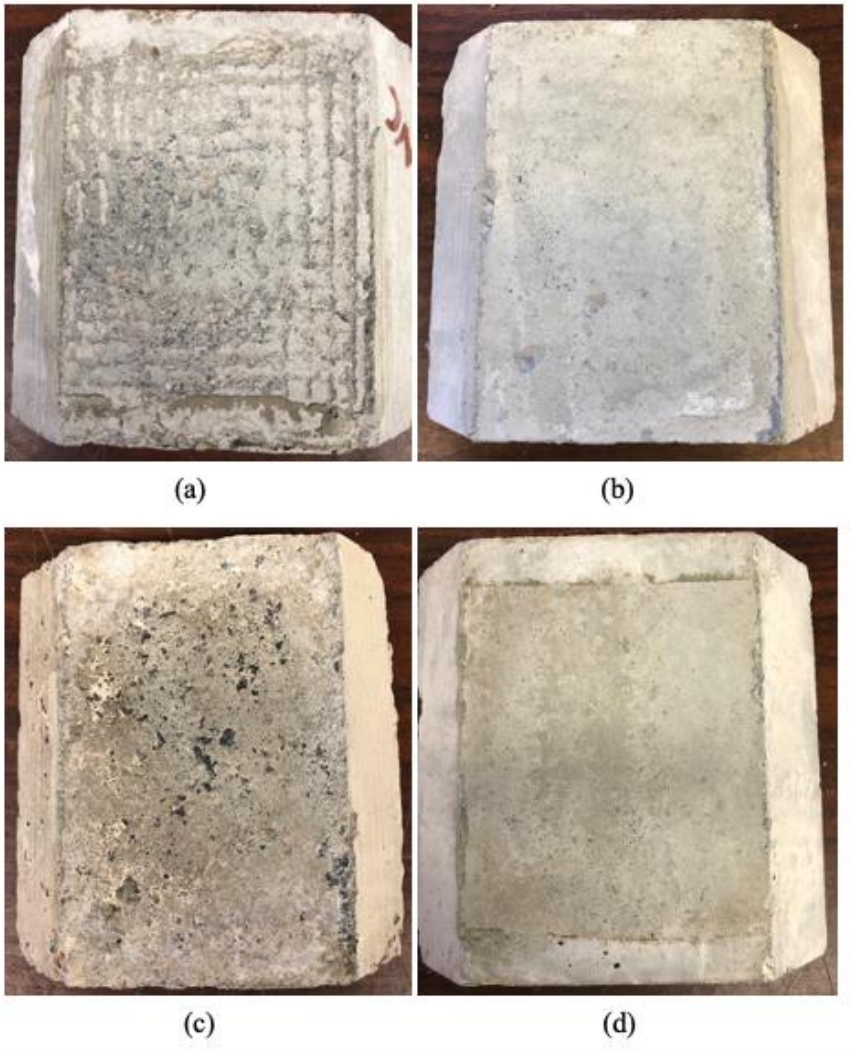

Figure 4.9 Concrete substrate of the Mode-II fracture test failure plane of (a) chipped, (b) pressure-washed, (c) sandblasted, and (d) as-cast specimens

4.1.4 Short-term Mode-I fracture behavior of unconditioned samples

The primary purpose of the butterfly test method is to evaluate the Mode-II fracture behavior of cementitious bi-layer composites. The mode-I fracture test was only performed on the as-cast specimens to compare the results with the Mode-II fracture behavior. Figure 4.10 indicates the Mode-I fracture test distribution for the as-cast specimens, with a mean value of 29.75 lb.ft/ft^2 (40.33 J/m^2). The individual specimen readings are indicated in

Table 4.4. The COV of the results is 84%, with a six-specimen average, indicating the need to investigate further the ability of the proposed test method to evaluate the mode-I fracture energy through a larger population size.

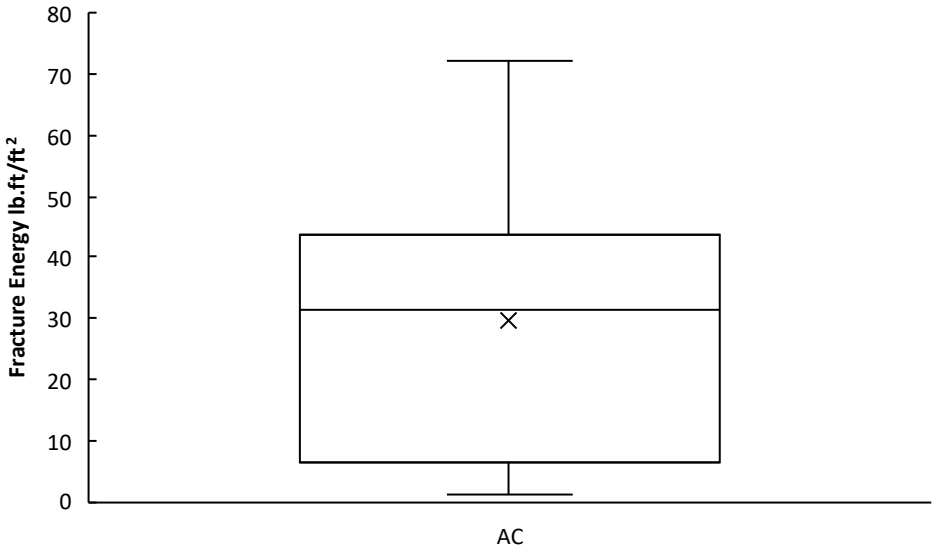

Figure 4.10 Distribution of the Mode-I fracture test for as-cast specimens

Table 4.4 Mode-I fracture energies of unconditioned samples (lb.ft/ft^2)

Specimen	**Mode-I (AC)**
1	1
2	8
3	72
4	33
5	34
6	30
Mean	30

4.1.5 Variations in surface texture with substrate surface preparation technique

Figure 4.11 toFigure 4.13 indicate the 3D plots of the substrate surface texture of the failure plane for tension, shear, and fracture test specimens. The failure surface of each test showed different surface textures and hence were discussed separately in this section. Figure 4.11 indicates the failure surface scans of the tensile bond tests. In Figure 4.11(a), the chipped surfaces have the roughest surface, followed by the pressure-washed and sandblasted samples. Table 4.5 (in English unit) andTable 4.6 (in Metric unit) show that the chipped, pressure-washed, sandblasted, and as-cast specimens reported estimated texture depths (ETD) of 0.0225 inches (0.568 mm), 0.0123 inches (0.309 mm), 0.0101 inches (0.253 mm), and 0.0086 inches (0.216 mm), respectively. ETDs of the chipped, pressure-washed, and sandblasted specimens were 2.63, 1.43, and 1.17 times the ETD of the as-cast specimens. These variations align with the tensile bond strength ratios (6.3, 5, and 2.7), discussed in Section 4.1.1.

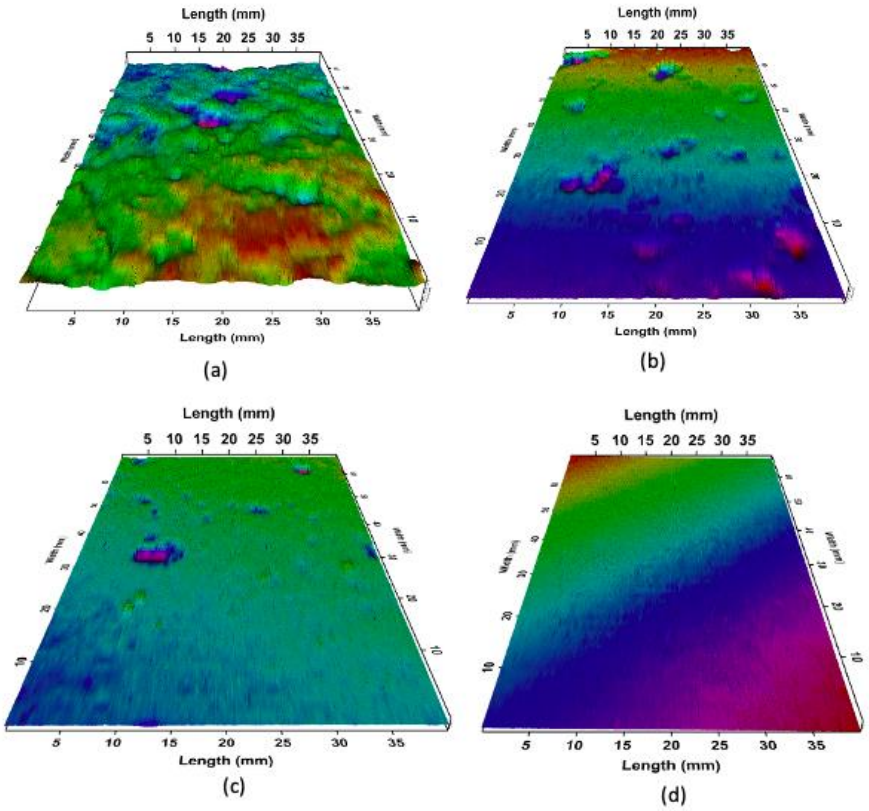

Figure 4.11 3D surface texture maps of substrate failure surface after tensile strength tests for (a) chipped, (b) pressure-washed, (c) sandblasted, and (d) as-cast specimens

Table 4.5 Mean profile depth (MPD) and the estimated texture depth (ETD) of the tension, shear, and Mode-II fracture test specimens (inches)

Surface Preparation	MPD-Tension	ETD-Tension	MPD-Shear	ETD-Shear	MPD-Mode II	ETD-Mode II
Chipped	0.0181	0.0225	0.0127	0.0181	0.0087	0.0150
Pressure-washed	0.0054	0.0123	0.0015	0.0092	0.0027	0.0102
Sandblasted	0.0026	0.0101	0.0022	0.0098	0.0045	0.0116
As-cast	0.0008	0.0086	0.0007	0.0085	0.0026	0.0101

Table 4.6 Mean profile depth (MPD) and estimated texture depth (ETD) of the tension (-T), shear (-S), and Mode-II fracture (-F) test specimens (mm)

Surface Preparation	MPD-Tension	ETD-Tension	MPD-Shear	ETD-Shear	MPD-Mode II	ETD-Mode II
Chipped	0.4600	0.5680	0.3220	0.4570	0.2220	0.3780
Pressure-washed	0.1370	0.3090	0.0390	0.2310	0.0690	0.2550
Sandblasted	0.0660	0.2530	0.0570	0.2450	0.1150	0.2920
As-cast	0.0200	0.2160	0.0170	0.2140	0.0660	0.2530

Figure 4.12 shows the scanned surface texture of the shear test specimens. Here, the chipped surfaces have the highest roughness, just as before, but followed by sandblasted, pressure-washed, and as-cast specimens. Note that, this behavior is contradicting with the tensile bond test failure surface textures, in which the pressure-washed sample had a greater ETD than the sandblasted specimen failure surface. However, the chipped, pressure-washed, sandblasted, and as-cast shear strength specimens reported ETDs of 0.0181 inches (0.457 mm), 0.0092 inches (0.231 mm), 0.0098 inches (0.245 mm), and 0.0085 inches (0.214 mm), respectively. In other words, the ETDs of the chipped, pressure-washed, and sandblasted specimens were 2.14, 1.08, and 1.14 times the ETD of the as-cast specimens. These variations align with the shear bond strength ratios (5.7, 1.6, and 2.9), discussed in section 4.1.2.

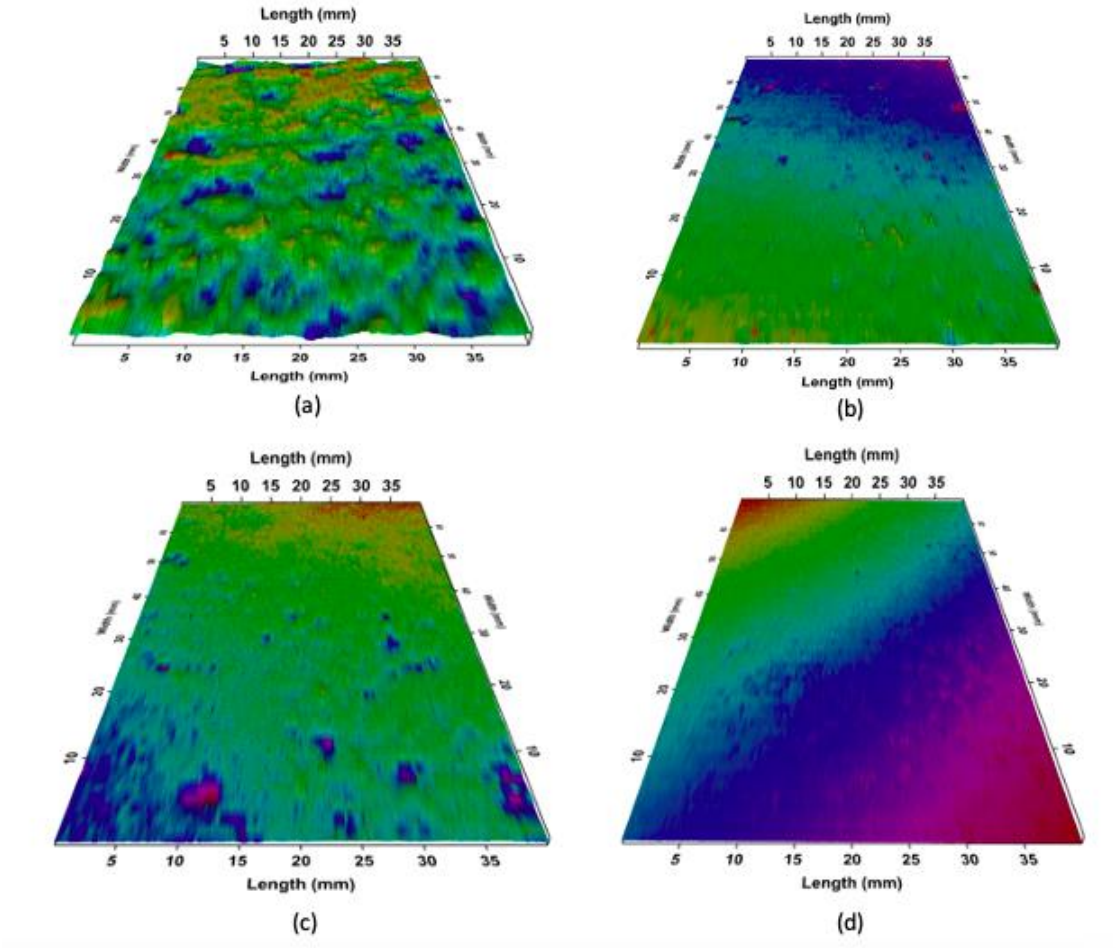

Figure 4.12 3D surface texture maps of the substrate failure surface after shear strength tests for (a) chipped, (b) pressure-washed, (c) sandblasted, and (d) as-cast specimens

The failure surfaces from the proposed Mode-II fractures tests are shown as 3D surface scans in Figure 4.15. The chipped surfaces exhibited the highest roughness, while the as-cast surfaces indicated the lowest ETDs, which is in line with both shear and tensile failure surfaces. However, sandblasted Mode-II fracture surfaces exhibited a higher ETD than pressure-washed surfaces. This texture behavior was consistent with shear failure but contradicted with the tensile failure surfaces. The reported ETDs for chipped, pressure-washed, sandblasted, and as-cast specimens' ETDs as 0.0150 inches (0.378 mm), 0.0102

inches (0.255 mm), 0.0116 inches (0.292 mm), and 0.0101 inches (0.253 mm). ETDs of the chipped, pressure-washed, and sandblasted specimens were 1.49, 1.01, and 1.15 times the ETD of the as-cast specimens. These variations were in line with the Mode-II fracture energy ratios (6.8, 1.5, and 4.7), discussed in Section 4.1.3.

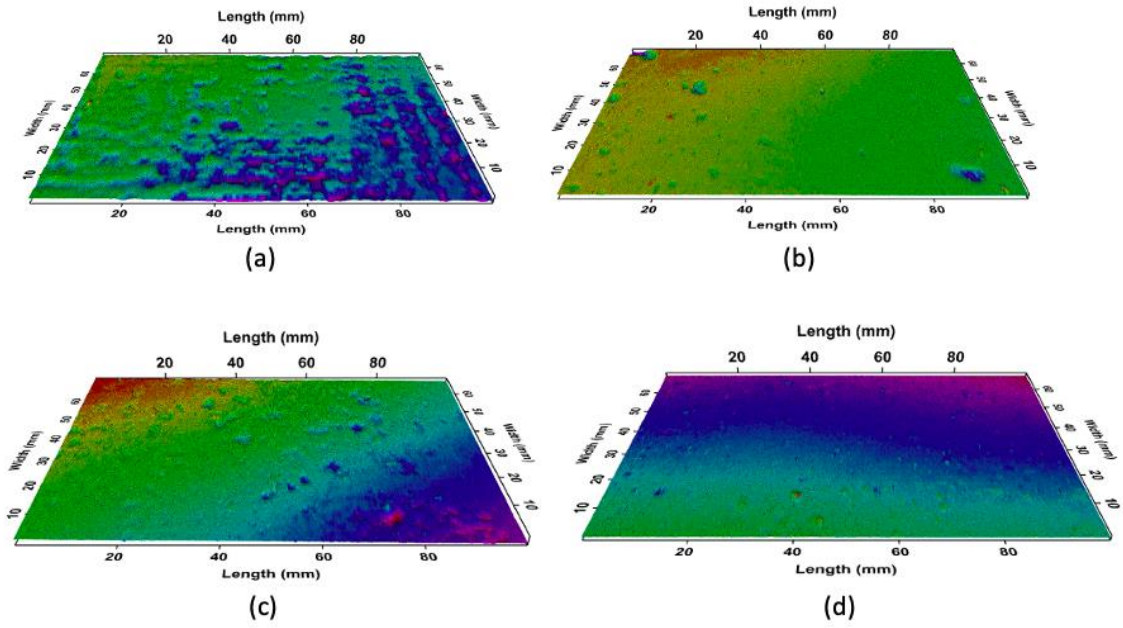

Figure 4.13 3D surface texture maps of substrate failure surface in Mode-II fracture tests for (a) chipped, (b) pressure-washed, (c) sandblasted, and (d) as-cast specimens

Note that the surface texture scans of cylindrical specimens were confined to a region of 40 mm x 70 mm, and for the double-wedged specimens it was a 70 mm x 100 mm. Figure 4.14 shows the variation in texture depth for each surface type. In terms of chipped surface preparation, tensile specimens have shown the highest texture depth after tests, followed by shear and Mode-II fracture specimens; although the tensile strengths are smaller than the shear strengths. In contrast, pressure-washed samples clearly show a higher ETD value for the tensile test samples than the shear test samples. In general, Mode-II fracture surfaces of pressure-washed, sandblasted, and as-cast specimens have shown a

higher ETD than shear or tensile test specimens in each category. However, sandblasted and as-cast specimens show comparable ETDs for shear and tension tests indicating uniformity in surface preparation across these panels. Note that the surface texture scans were obtained after the failure of the composite specimens and hence, may not reflect the actual texture depth before casting the shotcrete layer. Nevertheless, the shear and tension strength tests reported cohesive-dominated mixed-mode failure, while adhesive failure dominated Mode-II fracture tests. Hence, the actual surface texture could be more closely related to the Mode-II fracture surfaces than the bond strength test surfaces indicated here.

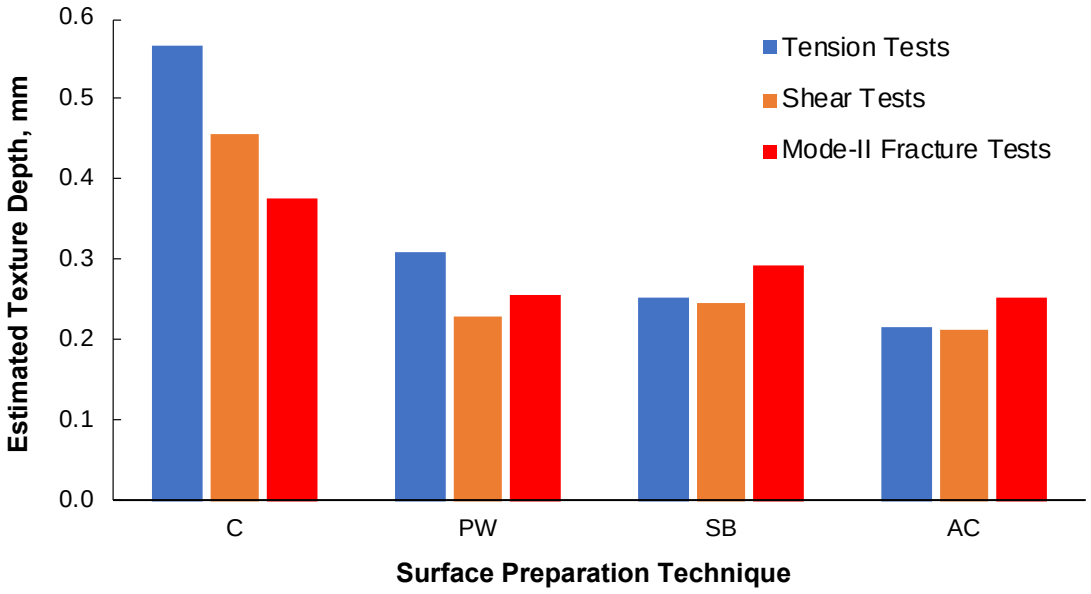

Figure 4.14 Variation in the estimated texture depth (ETD) for three tests versus four surface preparation techniques

4.1.6 Comparison of shear and tensile strength tests

Figure 4.15 indicates the shear and tensile bond behavior of different specimens with different surface preparation techniques. In general, chipped, sandblasted, and as-cast specimens showed shear bond strengths of more than two times the tensile bond strength values. In contrast, pressure-washed samples were tensile-dominated, with a tensile bond

strength of 1.37 times the shear bond strength, as indicated in Table 4.7. The mean shear strength to tensile strength ratio of the chipped, pressure-washed, sandblasted, and as-cast specimen interface bonds are 2.09, 0.73, 2.49, and 2.35, respectively. Also, note that the shear bond strength results are more scattered than tensile bond strength values in chipped and sandblasted specimens, as represented by the standard error bars. It could be due to the local variations of cored specimen surfaces, misalignment of the bond plane with the loading plane, and localized stress concentrations at the bond interface due to the loading mechanisms of the shear test. More microstructural characterizations are needed to understand the mechanisms of failure at each interface due to shear and tensile test loads.

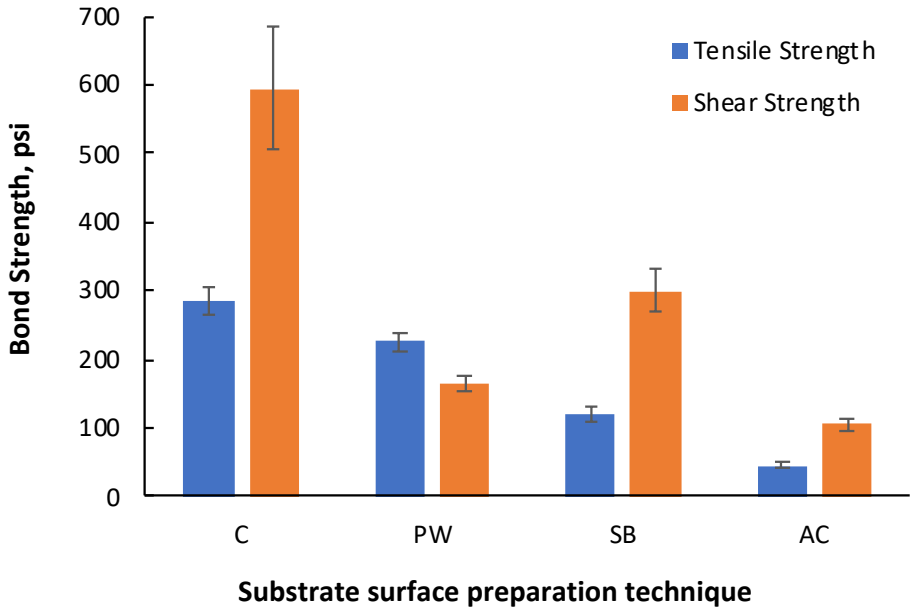

Figure 4.15 Variation of shear and tensile bond strengths of unconditioned cylindrical samples

Table 4.7 Comparison of shear and tensile bond strengths

	C	PW	SB	AC
Tensile Strength (psi)	284	225	120	45
Shear Strength (psi)	594	165	299	105
Shear Strength/Tensile Strength Ratio	2.09	0.73	2.49	2.35

4.1.7 Comparison of the Mode-I and Mode-II fracture tests

Figure 4.16 indicate the behavior of Mode-I and Mode-II fracture tests of unconditioned, as-cast, butterfly double-wedged specimens. Note that the variation of individual results of the Mode-I test is significantly higher for the given sample size (six samples each) than for the Mode-II test, as indicated from the error bars (±10.24 lb.ft/ft^2 for Mode-I and ±3.78 lb.ft/ft^2 for Mode-II fracture). The test reported Mode-I and Mode-II fracture energies of 30 lb.ft/ft^2 (40.33 N/m^2) and 54 lb.ft/ft^2 (73.16 N/m^2). In other words, the Mode-II fracture energy is 1.81 times greater than the mode-I fracture energy of as-cast samples. Note that the as-cast sample surfaces are smooth and reported overall lowest Mode-II fracture energies out of all substrate surface preparation techniques.

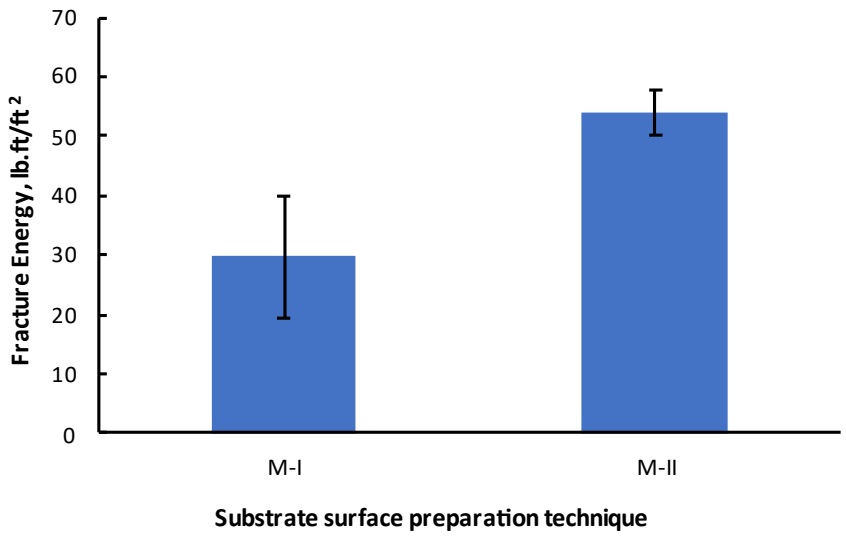

Figure 4.16 Comparison of Mode-I and Mode-II fracture energy of as-cast specimens

4.1.8 Comparison of surface preparation techniques and overall short-term bond quality

Figure 4.17 presents the unitless normalized bond parameters for different surface preparation techniques at an unconditioned state. The unitless bond parameters are obtained by dividing by each test's respective as-cast specimen readings; hence, the values for the as-cast specimens for all test types are 1.00. In general, the chipped and sandblasted samples are Mode-II fracture dominated with normalized bond parameters of 6.8 and 4.7, respectively. In contrast, the pressure-washed samples are tension dominated with a bond parameter of 5.0 for the normalized tensile strength. Among all the substrate surface preparation techniques, chipped surfaces indicated the highest bond strengths and Mode-II fracture energy values, indicating superior bond quality. Hence, it is safe to assume that chipping is the best technique considered in this study. On the other hand, the as-cast

samples showed the lowest bond strengths and mode-II fracture energies, indicating poor bond quality and the importance of substrate surface preparation in shotcreting work.

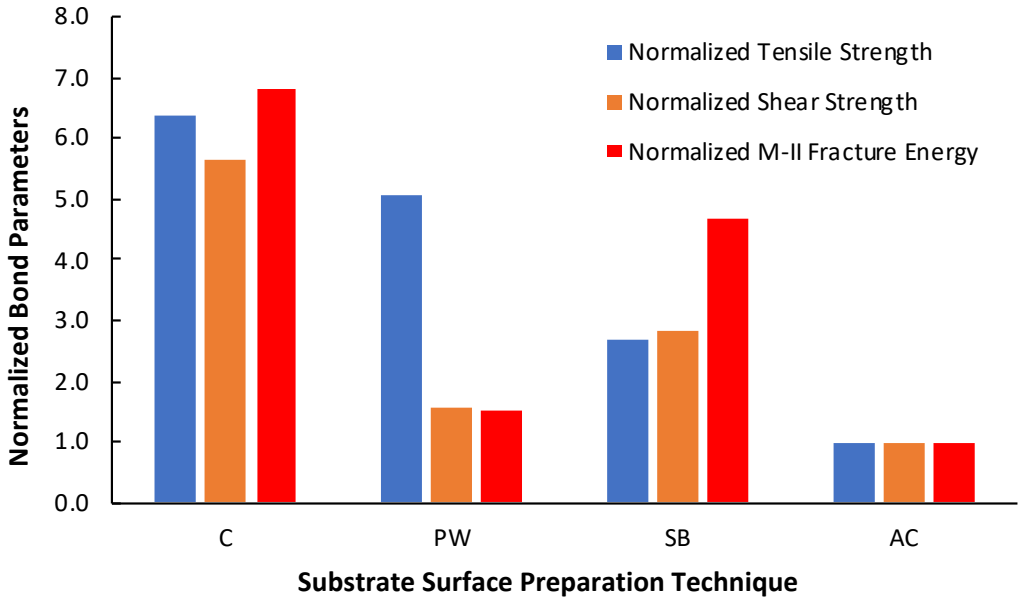

Figure 4.17 Variation of bond parameters with substrate surface preparation technique

In contrast, the differentiation between the pressure-washed and sandblasted specimens is more complicated. The pressure-washed specimens reported mean tensile strength, shear strength, and fracture energy of the bond as 225 psi (1.55 MPa), 165 psi (1.14 MPa), and 82 lb.ft/ft^2 (112 J/m^2). On the other hand, the sandblasted specimens reported mean tensile strength, shear strength, and fracture energy of the bond as 120 psi (0.83 MPa), 299 psi (2.06 MPa), and 253 lb.ft/ft^2 (343 J/m^2). If the usual benchmark of 145 psi (1 MPa) is considered in direct tension tests (ex: pull-off test), this batch of sandblasted specimens would be deemed unsatisfactory with a tensile bond strength of only 120 psi; hence, better bond quality is achieved by the pressure-washed substrate. The reason for the bond quality variations could be due to the process of surface preparation. Sandblasting involves using sand (an abrasive material) projected at a higher velocity to the receiving

surface. Due to the impact force, sandblasting leads to a much rougher surface through abrasion than pressure washing, but may leave residues of sand and dust, even the surface after sandblasting has been air-blasted. Therefore, it is recommended to wash the substrate surface after sandblasting. The tensile bond strength could be sensitive to these residues (dust and sand) left from sandblasting, hence giving a lower tensile bond strength. In contrast, pressure-washing involves using a forceful stream of water to remove dust and dirt from the surface giving a much cleaner surface. It could be the reason for a higher tensile bond strength. Due to the high-pressure water, this may remove a few aggregates from the surface contributing to the surface texture variations.

However, the sandblasted specimens exhihitedsuperior resistance to shear loads and mode-II fractures with 1.81 and 3.08 times the respective pressure-washed sample values. The additional friction induced by the rougher surface, the shear bond strength, and Mode-II fracture energy (shear-type loading) of sandblasted specimens may have recorded a higher bond strength/fracture energy value than the pressure-washed specimens. In an instance where tensile loads are prominent, pressure washing could be a better solution (ex: overhead structures). On the other hand, in shear-dominated loading applications (ex: slope stabilization), the sandblasted specimens seem to perform better. Either way, when there are existing cracks in the system (debris or foreign objects on substrate concrete), the sandblasting specimens seem to have more resistance to crack propagation than the pressure-washed specimens.

Figure 4.18 indicates the correlation between estimated texture depth (in mm) and the normalized bond parameter. Note that the metric units are used here instead of the imperial units due to the scale of the ETD which includes values less than a millimeter. It

is apparent that all the test results could be represented relatively accurately with linear curves. For each test, higher the mean profile depth (hence the estimated texture depth), higher the normalized bond parameter. The solid red line indicated the 145-psi limit mentioned in the ACI-506-R as a ratio of the as-cast specimen tensile bond strength ratio. In general, it seems any ETD larger than 0.294 mm (or a mean profile depth of 0.0875 mm) would give reasonable bond strengths. Surface roughness can be measured in accordance with ASTM E2157, "Standard Test Method for Measuring Pavement Macrotexture Properties Using the Circular Track Meter," or ASTM D8271, "Standard Test Method for the Direct Measurement of Surface Profile of Prepared Concrete." A roughness of 0.294 mm is equal to 11.6 mils. As a result, alternatively, the ICRI's CSP No. 4 (or higher) which corresponds to a surface roughness of 15±2 mils can be specified.

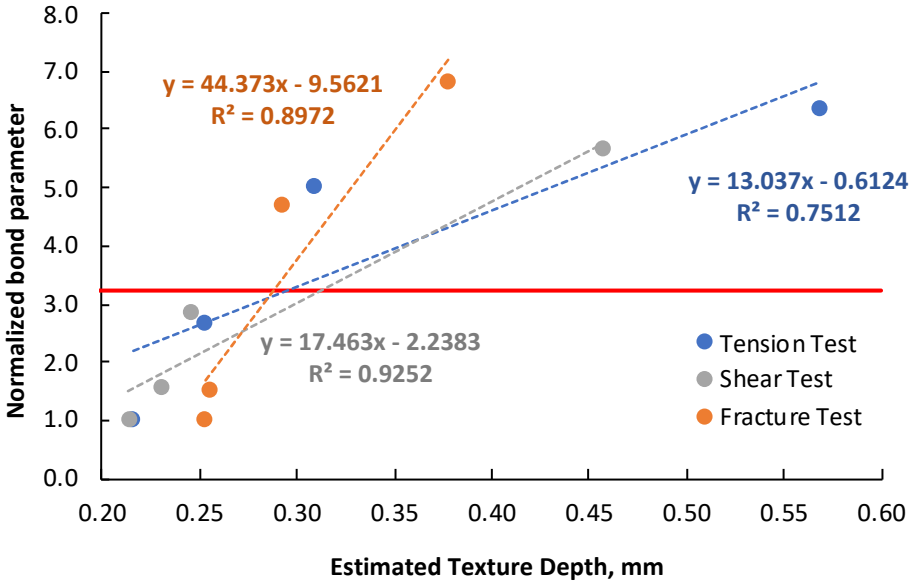

Figure 4.18 Variation of normalized bond parameter with the estimated texture

depth

4.2 Long-term behavior

The durability of the shotcrete-concrete interface bonds was analyzed to determine the effectiveness of using different surface preparation techniques in freeze-thaw cyclic weather. The results are presented below with respect to mass loss and the change in tensile bond strength.

4.2.1 Material deterioration and mass loss

The visual changes in the bond interface due to freeze-thaw action are exhibited in Figure 4.19 to Figure 4.22, for cycles 0, 100, 200, and 300. The exposed aggregates on the concrete substrate were reduced with the increasing number of F/T cycles. Close inspection indicates that the concrete cohesive failure is more prominent at low cycles, whereas adhesive bond failure is more common in high cycles. Almost all the chipped, pressure-washed, and sandblasted specimens indicated mix-mode failure with varying concrete cohesive and bond adhesive failures. Nevertheless, cohesive shotcrete failure was minimum in the tension bond tensile tests. In addition, more pores are observed on the surface of the concrete substrate at a higher number of conditioning cycles. The aggregate exposure of the concrete varied depending on the type of substrate surface preparation technique at each cycle.

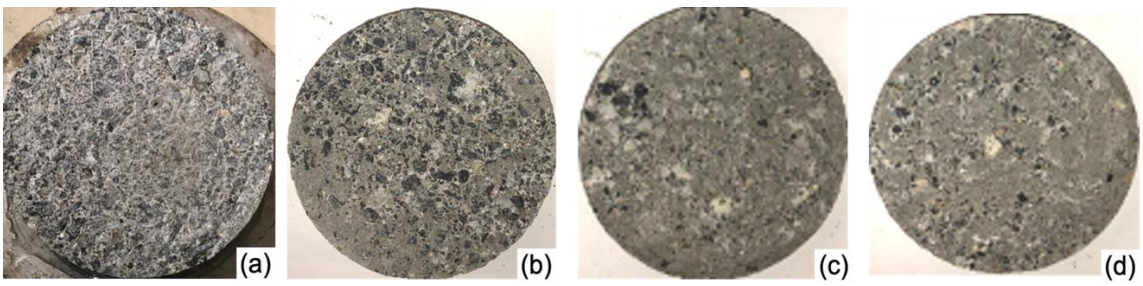

Figure 4.19 Appearance of chipped samples at different freeze-thaw cycles: (a) 0-

cycles, (b) 100-cycles, (c) 200-cycles, and (d) 300-cycles

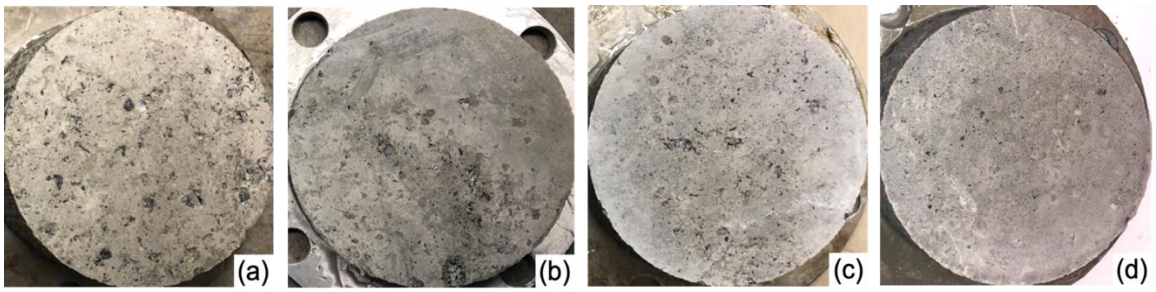

Figure 4.20 Appearance of pressure-washed samples at different freeze-thaw cycles: (a) 0-cycles, (b) 100-cycles, (c) 200-cycles, and (d) 300-cycles

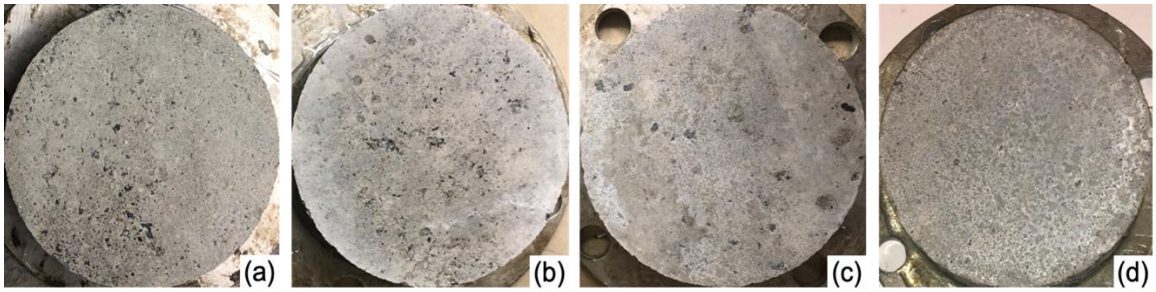

Figure 4.21 Appearance of sandblasted samples at different freeze-thaw cycles: (a) 0-cycles, (b) 100-cycles, (c) 200-cycles, and (d) 300-cycles

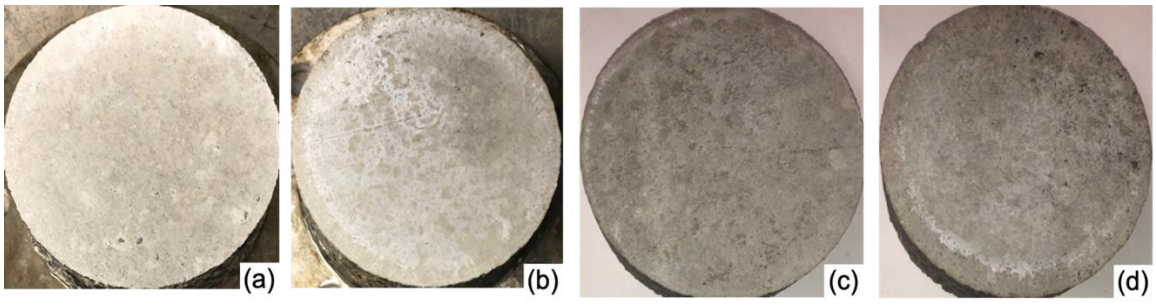

Figure 4.22 Appearance of as-cast samples at different freeze-thaw cycles: (a) 0-

cycles, (b) 100-cycles, (c) 200-cycles, and (d) 300-cycles

Furthermore, the appearance of pores increased with the number of cycles, indicating a reduced effective contact area at the bond interface. Note that this study did not quantitatively evaluate the percentage of adhesive or cohesive failure. Instead, this study aims to observe general trends of shotcrete-concrete substrates as the specimens are subjected to cyclic freezing and thawing conditions. The mass loss of the specimen is given in Figure 4.23, which indicates the deterioration of the two materials. Note that the mass loss of sandblasted sample at 100 F/T cycle appears to be an outlier due to sample variations. However, the mass loss due to only the bond deterioration cannot be separately measured. The mass loss percentages are 1.19%, 1.4%, 1.64%, and 1.92%, respectively, for the chipped, pressure-washed, sandblasted, and as-cast specimens. The microstructure behavior at the bond interface would be interesting to investigate to better understand the deterioration mechanisms in the bond region. Although no specific allowable mass loss limit is mentioned in standards, Kevern et al. (2010) has used an acceptable mass loss for pervious concrete as 15%.

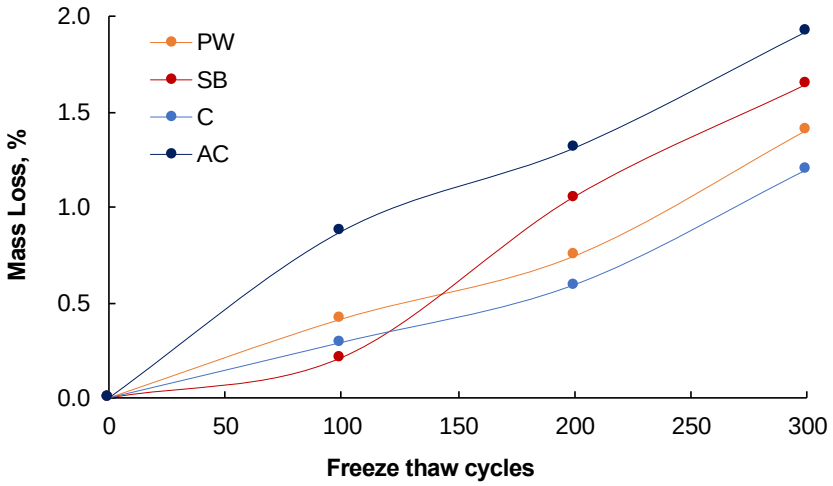

Figure 4.23 Mass loss of specimens due to freeze-thaw cycles

4.2.2 Tensile strengths of freeze-thaw conditioned samples

Table 4.8 to Table 4.11 show each specimen's maximum tensile bond stress at each freeze-thaw cycle. In Table 4.8 to Table 4.11, the fist number(s) before the letter in the column of "Specimen ID" is the number of F-T cycles. Adhesive failure indicates that the failure occurs at the interface only, whereas cohesive failure indicates the failure occurs inside shotcrete or concrete substrate. However, the cohesive failure location is often close to the interface. "Cohesive-C" indicates cohesive failure in concrete, and "Cohesive-S" indicates cohesive failure in shotcrete. Besides adhesive failure, in the presence of slight cohesive failure, it was denoted as "Mix." In more prominent cohesive failure cases, the failure mode was listed in brackets. For an example, if the bond interface had a mix failure mode and the more aggregates were exposed on the concrete substrate, it was deemed as "Mix (conc.)", to indicate that the cohesive failure in the concrete substrate was prominent. As the number of freeze-thaw cycles increases, there is a general transition from mixed failure modes (with the more cohesive concrete type of failure) to adhesive failure. As indicated in Table 4.11, some of the as-cast specimens at 200 and 300 freeze-thaw cycles

failed even before the tests were performed, emphasizing the importance of substrate surface preparation to increase durability in shotcrete applications. These specimens are denoted with “Adhesive-NA, " indicating that the failure occurred before testing.

Figure 4.24 graphically represents the influence of surface preparation on the freeze-thaw durability of shotcrete-concrete interface bonds. Figure 4.25 shows the variation of the tensile strength of each specimen category (i.e., chipped, pressure-washed, sandblasted, and as-cast) for varying freeze-thaw cycles. The error bars in the figures indicate the standard error computed as the standard deviation over the square root of the sample size. The tensile strength was computed as the average of five specimen readings for each category (a total of 80 specimens).

Table 4.8 Peak tensile force and peak tensile strengths of the individual chipped specimens.

Specimen ID	Max. Tensile Force (lb)	Type of failure	Max. Tensile Strength (psi)	Tensile Force (lb)	Tensile Strength (psi)
0TC1	3932	Cohesive-C	313	3573	285
0TC2	3116	Cohesive-C	248		
0TC3	3545	Cohesive-C	283		
0TC4	4260	Cohesive-C	339		
0TC5	3010	Cohesive-C	239		
100TC1	3471	Mix (Conc.)	276	3135	249
100TC2	3100	Mix (Conc.)	247		
100TC3	2518	Mix (Conc.)	200		
100TC4	3804	Mix (Conc.)	303		
100TC5	2781	Mix (Conc.)	222		
200TC1	2918	Mix (Conc.)	232	2763	220
200TC2	2932	Mix (Conc.)	234		
200TC3	3586	Mix (Conc.)	286		
200TC4	2352	Mix (Conc.)	187		
200TC5	2028	Mix (Conc.)	161		
300TC1	2653	Mix (Conc.)	212	2312	184
300TC2	3093	Mix (Conc.)	247		
300TC3	2174	Mix (Conc.)	173		
300TC4	1747	Mix (Conc.)	139		
300TC5	1893	Mix (Conc.)	151		

Table 4.9 Peak tensile force and peak tensile strengths of the individual pressure-washed specimens

Specimen	Max. Tensile Force (lb)	Type of failure	Max. Tensile Stress (psi)	Tensile Force (lb)	Tensile Strength (psi)
0TPW1	2291	Mix (Conc.)	183	2830	225
0TPW2	2891	Mix (Conc.)	231		
0TPW3	2615	Mix (Conc.)	207		
0TPW4	3217	Mix (Conc.)	255		
0TPW5	3136	Mix (Conc.)	249		
100TPW1	1841	Mix (Conc.)	146	2498	199
100TPW2	2929	Mix (Conc.)	234		
100TPW3	2385	Mix (Conc.)	190		
100TPW4	2754	Mix (Conc.)	219		
100TPW5	2581	Mix (Conc.)	206		
200TPW1	2201	Mix (Conc.)	175	2143	171
200TPW2	1592	Adhesive	126		
200TPW3	2435	Mix (Conc.)	194		
200TPW4	2668	Mix (Conc.)	212		
200TPW5	1821	Mix (Conc.)	145		
300TPW1	1814	Adhesive	145	1580	126
300TPW2	2075	Mix (Conc.)	165		
300TPW3	1120	Adhesive	88		
300TPW4	1704	Adhesive	136		
300TPW5	1185	Adhesive	94		

Table 4.10 Peak tensile force and peak tensile strengths of the individual sandblasted specimens.

Specimen	Max. Tensile Force (lb)	Type of failure	Max. Tensile Strength (psi)	Tensile Force (lb)	Tensile Strength (psi)
0TSB1	1686	Mix (Conc.)	135	1514	121
0TSB2	1814	Mix (Conc.)	144		
0TSB3	1632	Mix (Conc.)	131		
0TSB4	1506	Mix (Conc.)	120		
0TSB5	933	Mix (Conc.)	74		
100TSB1	899	Mix (Conc.)	71	1232	98
100TSB2	1443	Mix (Conc.)	115		
100TSB3	1664	Mix (Conc.)	132		
100TSB4	996	Mix (Conc.)	80		
100TSB5	1158	Mix (Conc.)	93		
200TSB1	1068	Mix (Conc.)	86	1024	82
200TSB2	1571	Mix (Conc.)	125		
200TSB3	661	Adhesive	52		
200TSB4	1144	Mix (Conc.)	91		
200TSB5	677	Adhesive	54		
300TSB1	445	Adhesive	36	813	65
300TSB2	452	Adhesive	36		
300TSB3	953	Adhesive	75		
300TSB4	1039	Adhesive	83		
300TSB5	1176	Adhesive	94		

Table 4.11 Peak tensile force and peak tensile strengths of the individual as-cast (unprepared) specimens

Specimen	Max. Tensile Force (lb)	Type of failure	Max. Tensile Strength (psi)	Tensile Force (lb)	Tensile Strength (psi)
0TAC1	459	Adhesive	36	562	44
0TAC2	755	Adhesive	59		
0TAC3	636	Adhesive	51		
0TAC4	389	Adhesive	30		
0TAC5	569	Adhesive	45		
100TAC1	459	Adhesive	36	433	34
100TAC2	573	Adhesive	45		
100TAC3	531	Adhesive	42		
100TAC4	259	Adhesive	20		
100TAC5	342	Adhesive	28		
200TAC1	0	Adhesive-NA	0	36	3
200TAC2	124	Adhesive	10		
200TAC3	0	Adhesive-NA	0		
200TAC4	0	Adhesive-NA	0		
200TAC5	56	Adhesive	4		
300TAC1	0	Adhesive-NA	0	22	2
300TAC2	0	Adhesive-NA	0		
300TAC3	79	Adhesive	6		
300TAC4	34	Adhesive	3		
300TAC5	0	Adhesive-NA	0		

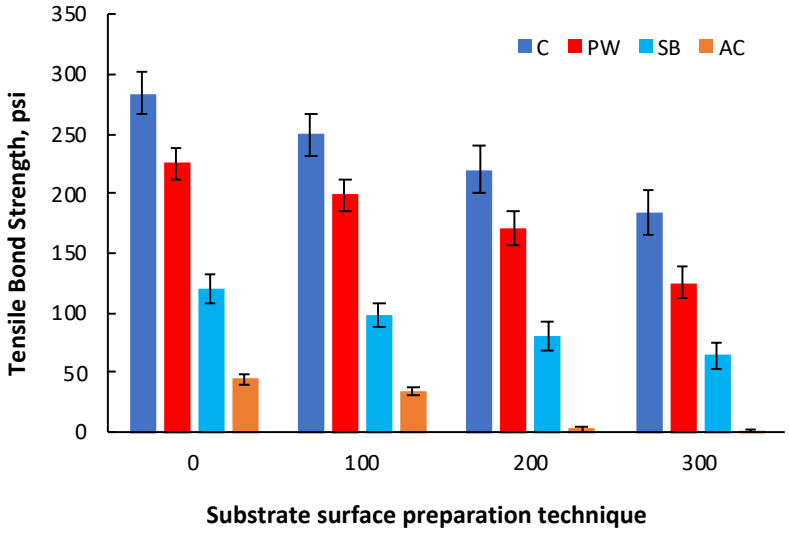

Figure 4.24 Variation of the tensile bond strength of specimens to freeze-thaw cycles

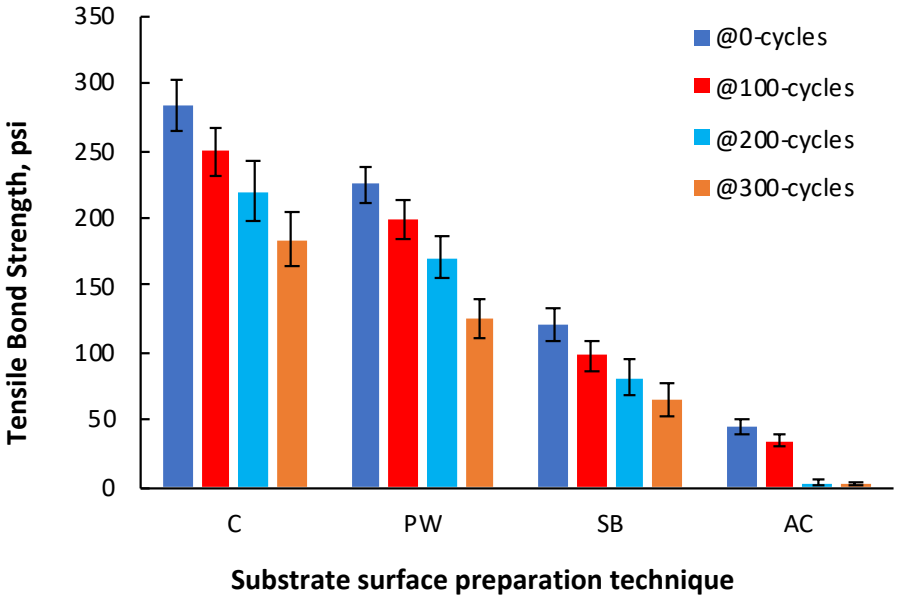

Figure 4.25 Tensile bond strength of freeze-thaw conditioned samples with different surface preparation techniques

According to Figure 4.24, the tensile bond strength reduces with the number of freeze-thaw cycles for each surface type. As shown in Figure 4.24, the chipped specimens reported the highest tensile bond strengths at each cycle, followed by the pressure-washed and sandblasted specimens. As expected, the unprepared surfaces (as-cast) are associated with the lowest bond strengths. Note that the as-cast specimens recorded significantly low tensile strengths at higher cycles, and some specimens failed even before testing, indicating the importance of surface preparation in cold regions. The tensile bond strength of unconditioned chipped, pressure-washed, and sandblasted samples was 6.4, 5.0, and 2.7 times larger than the as-cast specimen at 0-cycles. It has increased to 82.3, 56.2, and 28.9 times at 300-cycles indicating the rapid deterioration of the unprepared bond interfaces.

According to the results, the chipped surfaces are the most frost-resistant, while the as-cast samples are the least frost-resistant. As mentioned in Section 4.18, the tensile behavior of pressure-washed bond interfaces is better than the sandblasted bond interfaces. Therefore, note that these results are test-specific, and the ranking could switch between pressure-washed and sandblasted specimens in a different test method. However, confined to the testing parameters of the study, including the test method, the strength variation patterns of unconditioned samples have been carried forward to each freeze-thaw cycle, indicating that pressure washing performs better than sandblasting. Nevertheless, other tests are necessary to determine which surface preparation technique is more durable overall.

The type of failure indicates the visual representation of each sample after it failed. It could vary from adhesive failure to mixed failure modes, as discussed in the first part of this report. The mixed mode usually denotes the presence of both adhesive and cohesive

failure, either in the concrete or the shotcrete layer. A closer inspection of the failure surfaces revealed that cohesive failure in concrete was more common and prominent than the cohesive failure in shotcrete, especially at low F/T cycles. This was evident by the aggregate exposure in the concrete substrate and the apparent differences in the color of the concrete and shotcrete layers.

4.2.2.1 Relative Durability Factor (RDF)

The relative durability factor (RDF) factor of the test specimens is expressed as the ratio of tensile strength at a given freeze-thaw cycle concerning the tensile strength of a similar specimen at 0-cycles. Note that the tensile bond test is a destructive test and the test samples at each cycle differ. Nevertheless, the RDF helps to compare the tensile strength loss of each specimen category to determine the most durable surface preparation techniques. Table 4.12 indicates the RDF expressed as a percentage for each freeze-thaw cycle and Figure 4.26 indicates the RDF for each specimen category with freezing and thawing conditioning. Although there are some minor variations, in low cycles, the most durable bond interface is given in the chipped specimens with an RDF of 64.7% after 300 F/T cycles. In other words, the tensile bond strength of the chipped samples has reduced only by 35.3% due to frost action after 300 cycles. The pressure-washed and sandblasted specimens are close behind with an RDF of 56% and 54%, indicating that the tensile bond strengths of each category have reduced by 44% and 46%, respectively. Note that the durability factor of as-cast (unprepared) surfaces has reached 1% by the end of 300 F/T cycles, indicating that for the given samples, the tensile bonds strength of specimens with unprepared substrate surfaces has almost entirely failed under tensile loads 300 F/T cycles, further emphasizing the importance of substrate surface preparation in concrete repairs. ASTM C666 mentions a relative dynamic modulus limit of 60% at 300 freeze-thaw cycles.

Only chipped surface preparation can meet this criterion, though bond strength can differ from the dynamic modulus.

Table 4.12 Relative durability factors for different F/T cycles (expressed as a percentage)

F-T Cycles	C	PW	SB	AC
100-cycles	87.7	88.3	81.4	76.9
200-cycles	77.3	75.7	67.7	6.4
300-cycles	64.7	55.8	53.7	4.0

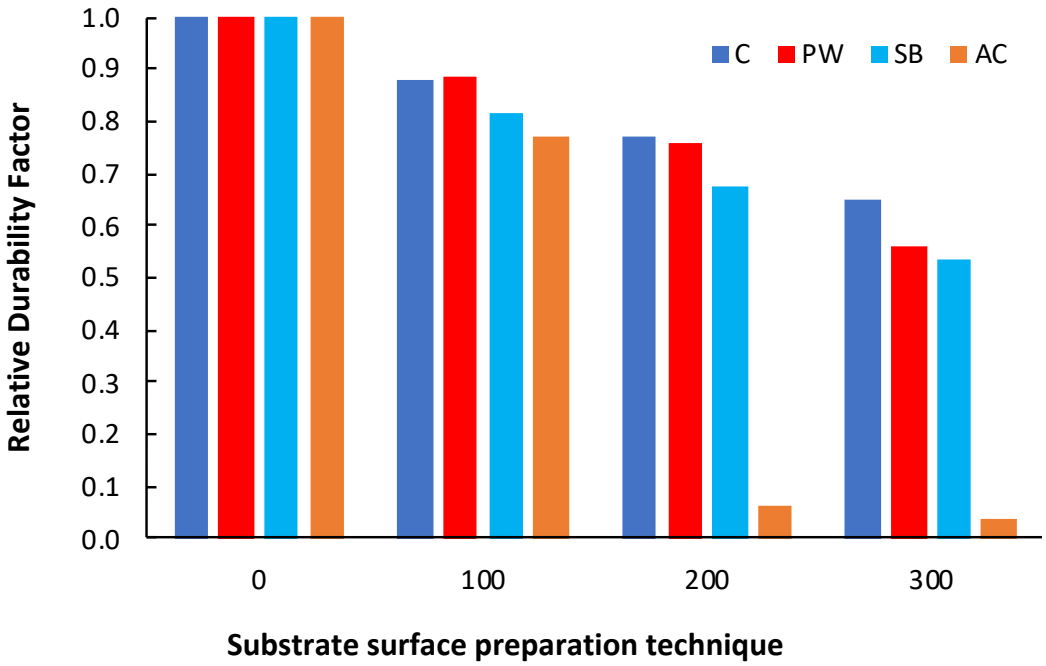

Figure 4.26 Variation of the relative durability factors with F/T cycles

4.2.2.2 Variation in the test data

Figure 4.27 to Figure 4.30 indicates a graphical representation of the variation of test data with respect to the standard deviation. It is evident that the tensile bond strength tests result in highly scattered data and that the variation increases with the number of

cycles for the specimens with prepared substrate surfaces. The COV of the chipped, pressure-washed, and sandblasted specimen samples varies between 14.9-24.1%, 13.5-16.2%, and 22.7-42.1%, respectively. Three as-cast specimen samples failed even before testing at 200 and 300 F/T cycles. Therefore, the sample size is too small to draw any conclusion. Although the tensile bond strength used here is not a standard test method, the literature indicates that pull-off tensile bond strength tests report highly variable results with significantly high COV, such as 39% (Bonaldo et al., 2005), 40% (Ramos et al., 2012; Robins & Austin, 1995), and 67% (Valipour & Khayat, 2020), indicating a location dependency of the pull-off test. One of the main reasons for such scattering could be the non-negligible bending moments caused by misalignments of specimens and the load axis (Li, 1997). Some differences could have resulted from location-specific material variations, such as the size and strength of aggregates at the testing location. Additionally, coring induces torque at the interface bond, damaging and interfering with various specimen interface adhesive qualities, contributing to strength variations. However, since waterjet was used to extract samples in this study, the complications from coring are not a concern.

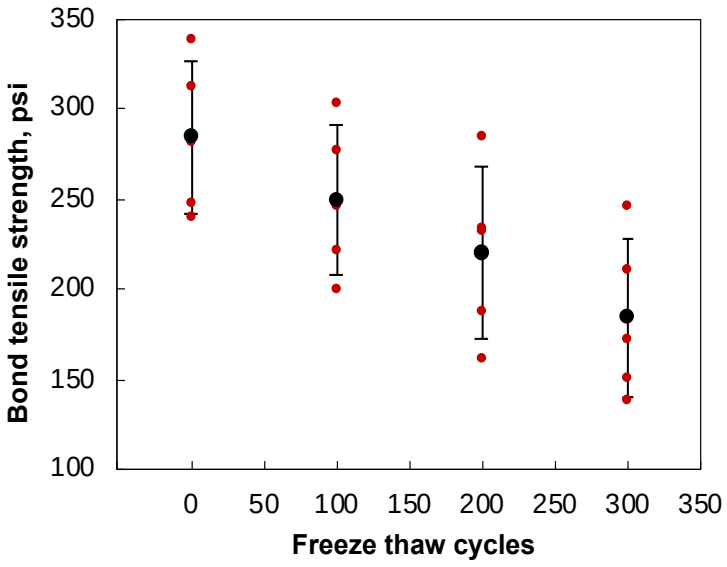

Figure 4.27 Dispersion of the tensile bond strength of chipped samples for different freeze-thaw cycles

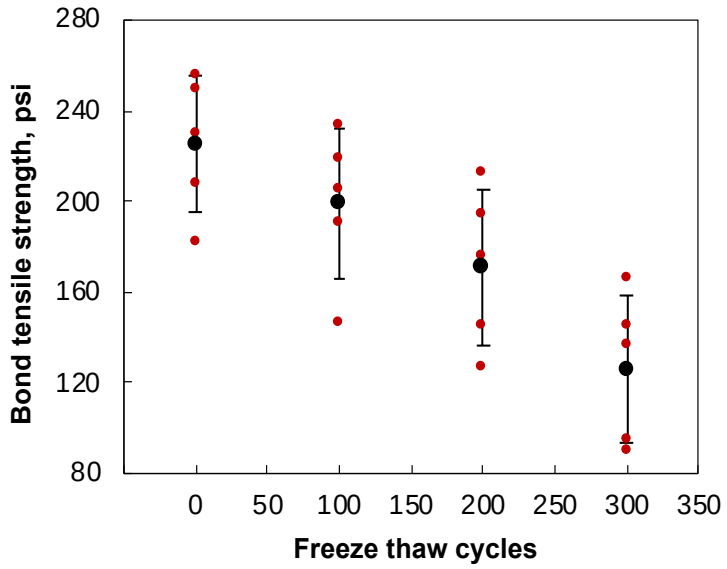

Figure 4.28 Dispersion of the tensile bond strength of pressure-washed samples for

different freeze-thaw cycles

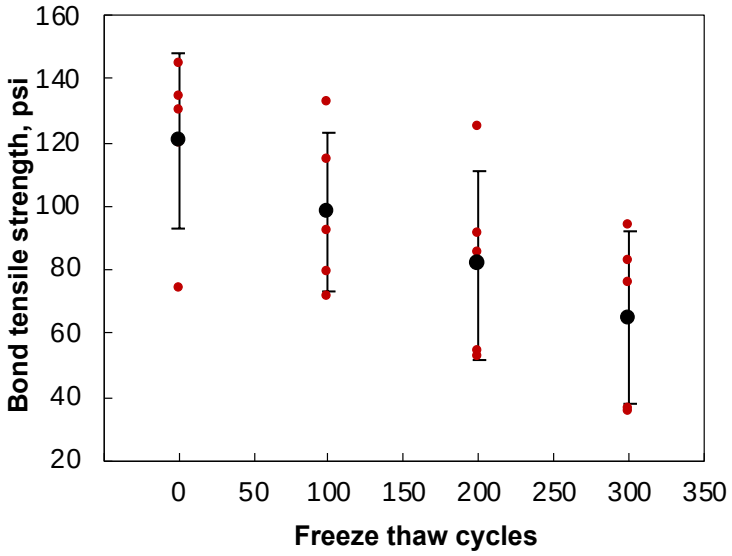

Figure 4.29 Dispersion of the tensile bond strength of sandblasted samples for different freeze-thaw cycles

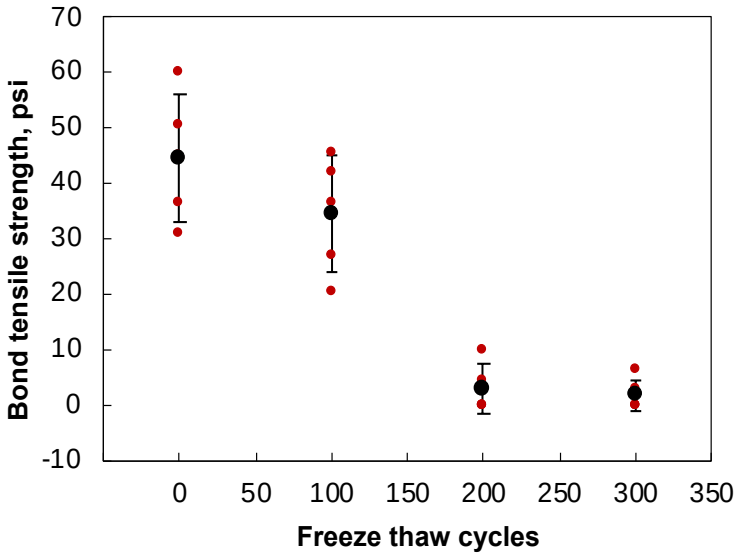

Figure 4.30 Dispersion of the tensile bond strength of as-cast samples for different freeze-thaw cycles

4.3 Mode-II fracture behavior of F/T conditioned samples.

Table 4.13 indicates the fracture energies for individual butterfly mode-II test specimens. Figure 4.31 indicates the mode-II fracture behavior subjected to rapid freezing-thawing conditioning cycles. The mode-II fracture energy has decreased by 8.6%, 58.4%, 53.5%, and 93.41% respectively for the chipped, pressure-washed, sandblasted, and as-cast substrate surface preparation techniques. The RDFs of the respective substrate surfaces are 0.914, 0.416, 0.465, and 0.0659 for the chipped, pressure-washed, sandblasted, and as-cast substrate surface preparation techniques, respectively. ASTM C666 mentions a relative dynamic modulus limit of 60% at 300 freeze-thaw cycles. Relative dynamic modulus (RDM) is a non-destructive test. The Phase II study indicated that the relative fracture energy (RFE) is more sensitive to freezing and thawing than the RDM. Hence these limits may not be applicable in here. Note that, the variation of the individual data has increased with freezing and thawing.

Table 4.13 Mode-II fracture energy of F/T conditioned samples (lb.ft/ft^2)

Specimen	Frac. Energy	Specimen	Frac. Energy	Specimen	Frac. Energy	Specimen	Frac. Energy
M2-C1	350	M2-PW1	87	M2-SB1	244	M2-AC1	52
M2-C2	404	M2-PW2	94	M2-SB2	212	M2-AC2	64
M2-C3	354	M2-PW3	37	M2-SB3	316	M2-AC3	66
M2-C4	410	M2-PW4	39	M2-SB4	233	M2-AC4	53
M2-C5	269	M2-PW5	117	M2-SB5	271	M2-AC5	45
M2-C6	420	M2-PW6	121	M2-SB6	240	M2-AC6	44
300-M2-C1	457	300-M2-PW1	4	300-M2-SB1	161	300-M2-AC1	4

300-M2-C2	332	300-M2-PW2	67	300-M2-SB2	143	300-M2-AC2	7
300-M2-C3	225	300-M2-PW3	22	300-M2-SB3	56	300-M2-AC3	2
300-M2-C4	400	300-M2-PW4	18	300-M2-SB4	77	300-M2-AC4	0
300-M2-C5	349	300-M2-PW5	41	300-M2-SB5	202	300-M2-AC5	1
300-M2-C6	255	300-M2-PW6	52	300-M2-SB6	66	300-M2-AC6	8

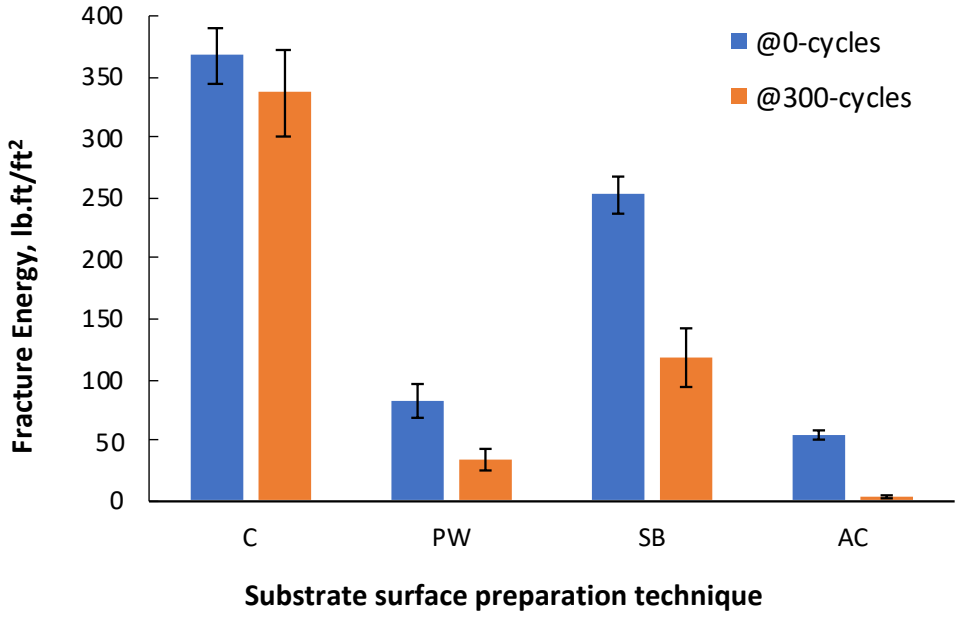

Figure 4.31 Mode-II fracture test results for F/T conditioned samples

4.4 Statistical damage analysis and service life prediction

4.4.1 Statistical regression analysis

Due to the scattering of data and variability in test results, a statistical analysis is necessary to interpret the data more accurately. Statistical analysis was conducted to establish a relationship between the tensile bond strength and the number of freeze-thaw cycles for each type of bond, depending on the surface preparation technique. The model predicts the remaining life of material after a specific time has passed. Regression analysis

indicates that the scattering and the variation of the relative durability factor (RDF) and the number of freeze-thaw cycles (N) are best fitted with a non-linear third-order polynomial function, as indicated in Figure 4.32 through 4.34. The coefficient of determination (R^2) value represents the scatter of data around the regression line. In general, the chipped, pressure-washed, and as-cast specimen categories displayed an R^2 value greater than 90%, indicating a good fit between the RDF and the number of F/T cycles. The sandblasted specimens have an R^2 of 72.4%, which means a high correlation, but a high scattering in individual test results influencing the precision of the prediction.

Figures 4.32 through 4.35 also depict the 95% confidence intervals (CI) and 95% prediction intervals (PI) for each surface preparation technique, which indicates the ranges in which the mean values of the test data and the individual test data points are likely to fall in the prediction, respectively. The estimated regression function for chipped, pressure-washed, and sandblasted specimens are expressed in Equations (3) to (5), respectively. Note that, the as-cast specimens failed by 200 cycles, and hence is not included in the prediction. In particular, when considering a linear relationship between 0-200 F/T cycles, the failure of as-cast specimens occurs at the 144th F/T cycles.

$$RDF = -6 \times 10^{-9}N^3 + 3 \times 10^{-6}N^2 - 0.0014N + 1 \quad (3)$$

$$RDF = -8 \times 10^{-8}N^3 + 3 \times 10^{-6}N^2 - 0.0014N + 1 \quad (4)$$

$$RDF = -4 \times 10^{-9}N^3 + 3 \times 10^{-6}N^2 - 0.002N + 1 \quad (5)$$

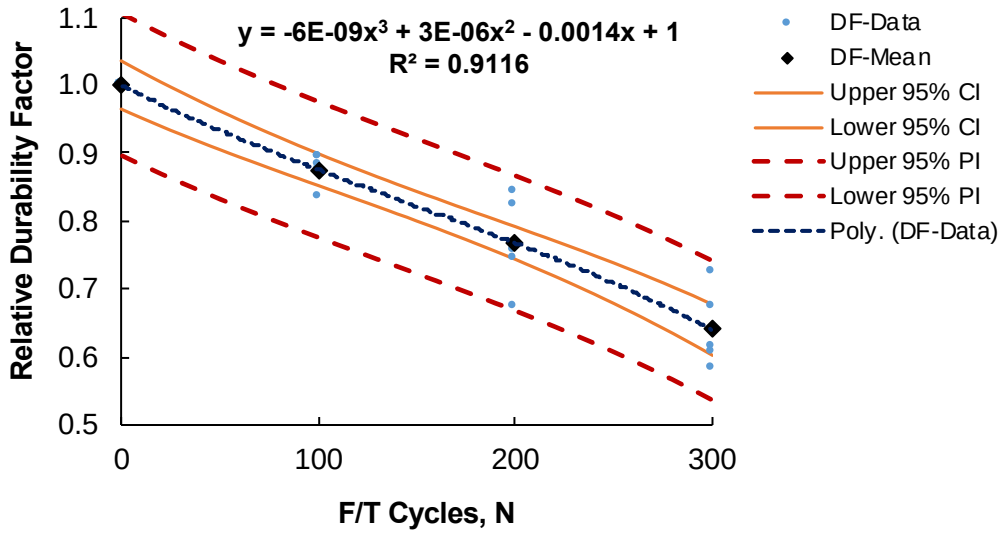

Figure 4.32 Regression analysis and scattering plot of the relative durability factor for chipped samples

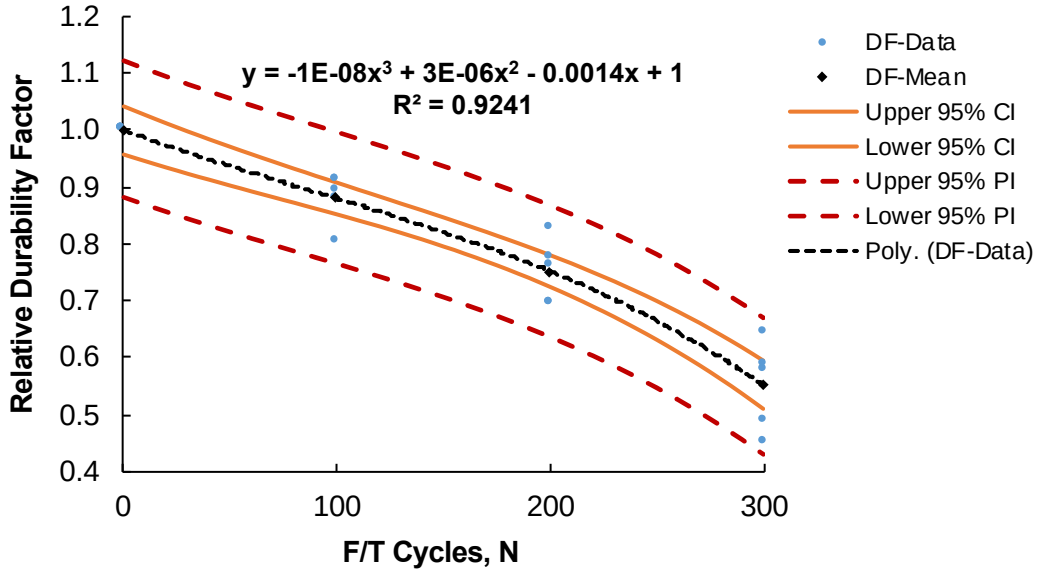

Figure 4.33 Regression analysis and scattering plot of the relative durability factor

for pressure-washed samples

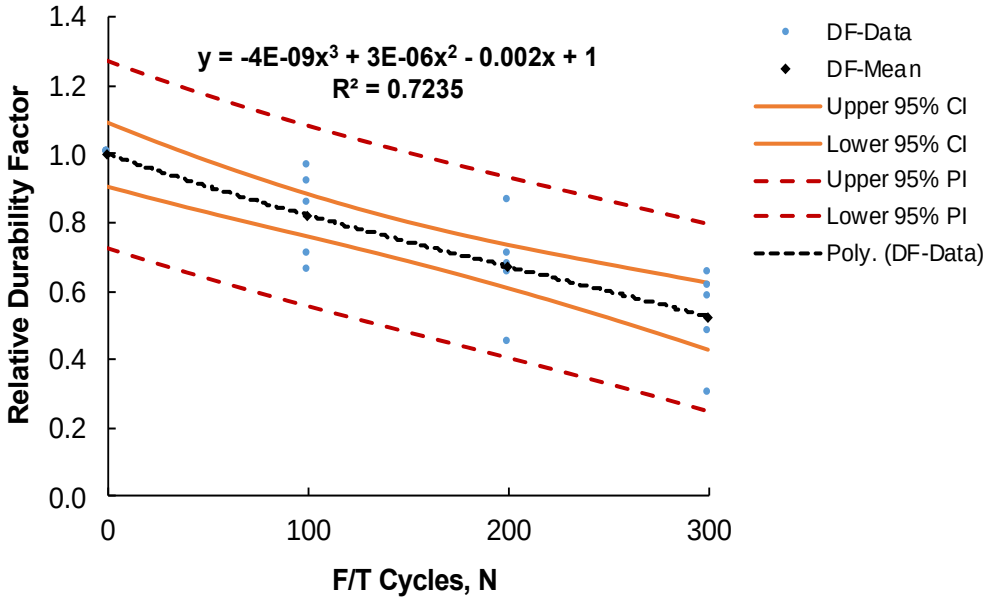

Figure 4.34 Regression analysis and scattering plot of the relative durability factor for sandblasted samples

4.4.2 Probabilistic damage model

This study uses a Weibull distribution to conduct probabilistic damage and life prediction analysis for the shotcrete-concrete interface bonds. The Weibull distribution can analyze failure trends, and it could be used in small data sets. This method has widely been used to predict mechanical properties and fatigue life in the composite materials (Naresh et al., 2018; Yang et al., 2010a, 2010b; Zhao & Liu, 2014). Unlike the normal distribution, the Weibull distribution is more flexible and can model skewed data. The theory of Weibull distribution is briefly introduced as follows. The freeze-thaw damage measurement is assumed to be the cumulative density function (CDF) of a three-parameter Weibull distribution. The probability density function (PDF) of the three-parameter Weibull distribution for the freeze-thaw cycles (N) is given by the Equation (6), as below (Kundu & Raqab, 2009).

$$f(N) = \frac{\beta}{\alpha}\left(\frac{N-\gamma}{\alpha}\right)^{\beta-1} exp\left[-\left(\frac{N-\gamma}{\alpha}\right)^{\beta}\right] \quad (6)$$

Here, $f(N) \geq 0, N \geq 0 \; or \; \gamma, \beta > 0, \alpha > 0, -\infty < \gamma < \infty$ and α is the scale parameter, β is the shape parameter (Weibull slope), and γ is the location parameter (or the minimum life). When γ is set to zero, the PDF reduces to a two-parameter Weibull distribution.

The CDF is the probability of failure or the cumulative damage parameter, which can be calculated by integrating the PDF and is given by Equation (7).

$$F(N) = \int_0^N f(s)ds = 1 - exp\left[-\left(\frac{N-\gamma}{\alpha}\right)^{\beta}\right] \quad (7)$$

Equation (7) can be written as a linear equation of the type a $y = Ax + B$ by taking the natural logarithm of both sides as,

$$\ln\left(ln\left(\frac{1}{1-F(N)}\right)\right) = \beta \ln(N-\gamma) - \beta ln\alpha \quad (8)$$

where $A=\beta$ and $B = -\beta ln\alpha$. There are different methods to express CDF in Equation (8). In this study F(N) is expressed using the median rank formula as given in equation (10).

$$F(N) = \frac{i-0.3}{n+0.4} \quad (9)$$

where i and n are the current and total test numbers in each series, respectively. The Equation (8) is then solved numerically by initially assuming the three parameters (α, β, and γ) and using the least square method (LSM) due to the limited number of samples tested.

Similarly, the Weibull reliability function R(N) or the survival function is defined as the probability that the material/structure remains in its designated state without failure from the operating time zero to the freeze-thaw life N and is indicated by Equation (10).

$$R(N) = 1 - F(N) = exp\left[-\left(\frac{N-\gamma}{\alpha}\right)^{\beta}\right] \tag{10}$$

The failure rate function, L(N) is the frequency with which the material or structure fails. It is also known as the hazard function which is denoted as the number of failures per unit of time as given in Equation (11).

$$L(N) = \frac{f(N)}{R(N)} = \frac{\beta}{\alpha}\left(\frac{N-\gamma}{\alpha}\right)^{\beta-1} \tag{11}$$

In the following discussion the probabilistic damage variable of the shotcrete-concrete interface bond (D) due to freezing and thawing is defined mathematically as given in Equation (12) based on one-dimensional continuum damage mechanics (Chaboche, 1988; Lemaitre, 1985).

$$D(N) = 1 - \frac{TS(N)}{TS_0} = 1 - RDF(N) \tag{12}$$

Here, TS(N) and TS_0 are the tensile strength of the shotcrete-concrete interface bonds (at the N^{th} cycle) and virgin sample (at 0 cycles), respectively.

4.4.3 Analysis results

Based on the test data of the tensile strength of the shotcrete-concrete interface bonds, the numbers of freeze-thaw cycles needed are obtained at different damage levels, as indicated in Table 4.14 through 4.16 for chipped, pressure-washed, and sandblasted specimen categories, respectively. Ten different damage levels are considered as D=0.05, 0.1,0.15…,0.5, which correspond to 95%, 90%, 85%….,50% of the original RDF,

respectively. Only five different levels are indicated in the tables, and graphs for clarity, and the obtained freeze-thaw cycles are sorted in ascending order ($N_1<N_2<N_3<N_4<N_5$). The data is insufficient to create a probability assessment for the as-cast samples because three of the specimens at every 200 and 300 cycles failed even before the tests. Therefore, the probability analysis was only conducted for the chipped, pressure-washed, and sandblasted samples.

Table 4.14 Freeze-thaw cycles at different damage levels for chipped samples

Damage (D)	Freeze-thaw cycles (N)				
	N_1	N_2	N_3	N_4	N_5
0.05	30	40	42	46	48
0.10	61	80	84	93	95
0.20	122	160	166	211	236
0.30	184	237	258	264	334
0.50	363	377	411	442	535

Table 4.15 Freeze-thaw cycles at different damage levels for pressure-washed samples

Damage (D)	Freeze-thaw cycles (N)				
	N_1	N_2	N_3	N_4	N_5
0.05	25	40	45	55	55
0.10	50	80	92	105	115
0.20	102	152	170	175	217
0.30	198	200	235	238	269
0.50	280	294	342	346	374

Table 4.16 Freeze-thaw cycles at different damage levels for sandblasted samples

Damage (D)	Freeze-thaw cycles (N)				
	N_1	N_2	N_3	N_4	N_5
0.05	15	17	35	60	105
0.10	29	34	70	125	133
0.20	59	68	130	164	230
0.30	88	115	187	204	276
0.50	176	291	339	366	367

For each set of sorted data from Table 4.14 to Table 4.16, the α, β, and γ are computed using the method described in Section 4.4.2. Figure 4.35 graphically represents the chipped samples' complete Weibull description at a damage level of D=0.05. Table

4.17 to Table 4.19 indicates the summary of the Weibull parameters for each specimen category. For clarity, only five damage levels are shown here. Note that the $\beta=0$ values are very small and indicated with only two decimal places.

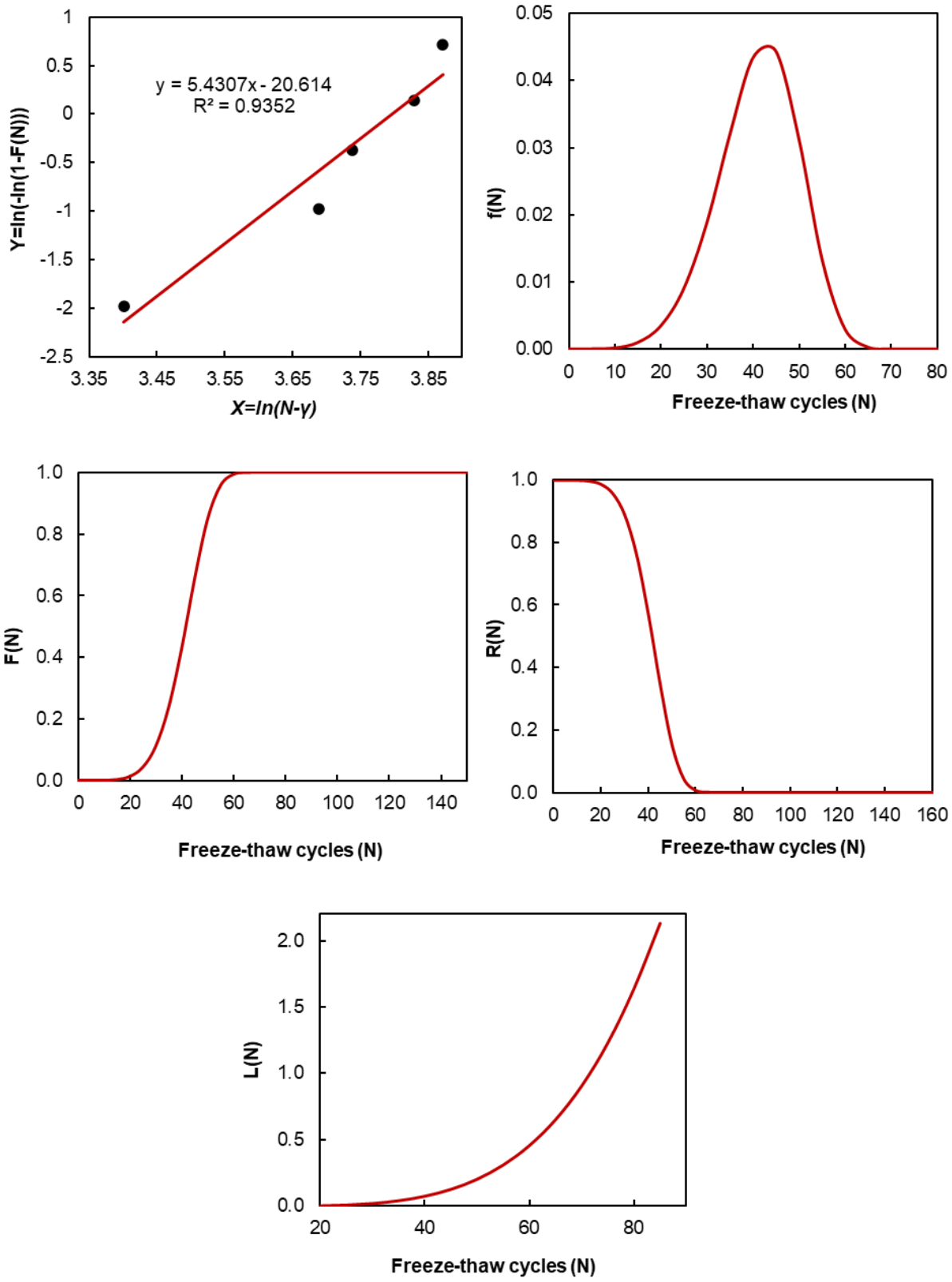

Figure 4.35 Complete Weibull description of the chipped samples at D=0.05

Table 4.17 Weibull parameters of chipped samples at different damage levels

Damage	α	β	γ	R^2
0.05	0	5.43	45	0.9352
0.10	0	5.64	89	0.9316
0.20	60	2.51	136	0.9708
0.30	85	3.03	192	0.9520
0.40	273	0.81	85	0.9572
0.50	357	0.80	75	0.9956

Table 4.18 Weibull parameters of pressure-washed samples at different damage levels

Damage	α	β	γ	R^2
0.05	0	3.08	50	0.9289
0.10	0	3.10	100	0.9537
0.20	0	3.63	181	0.9490
0.30	171	1.74	67	0.8850
0.40	234	0.81	52	0.9421
0.50	261	1.34	79	0.9395

Table 4.19 Weibull parameters of sandblasted samples at different damage levels

Damage	α	β	γ	R^2
0.05	15	0.45	28	0.9745
0.10	28	0.51	51	0.9448
0.20	56	0.60	79	0.9555
0.30	53	1.37	143	0.9710
0.40	0	2.59	292	0.8646
0.50	0	3.13	348	0.8659

The results indicate that except for a few damage levels for each sandblasted and as-cast specimen, the correlation coefficient (R^2) is more significant than 0.92, indicating that the Weibull distribution is a good fit for the RDF-based freeze-thaw life determination. As discussed before, the lowest values of R^2 are still greater than 0.7, indicating a good correlation between the two significant parameters. However, in the case of the lower R^2 more variability in the test results can be observed with scattering. Using the Weibull parameters, a complete Weibull description is established by determining the probability density function (PDF), the cumulative density function (CDF), the reliability function, and the failure rate function using the Equations (7), (8), (11), and (12), respectively. Note that the scale parameter α varies from 0 to 357, the shape parameter β varies from 0 to 5.64, and the location parameter varies from 0 to 348. To better understand the behavior of the PDF to the changes in the Weibull parameters, the following discussion is included.

Figure 4.36 describes the effect of the scale parameter (α) on the Weibull distribution when the location parameter (γ) and the shape parameter (β) are constant at 0 and 3, respectively. The scale parameter denotes the 63.2nd percentile in the distribution and is related to the variability of the PDF. The higher the α, the more the distribution will stretch; hence, the area under the PDF curve is a constant, reducing the peak value.

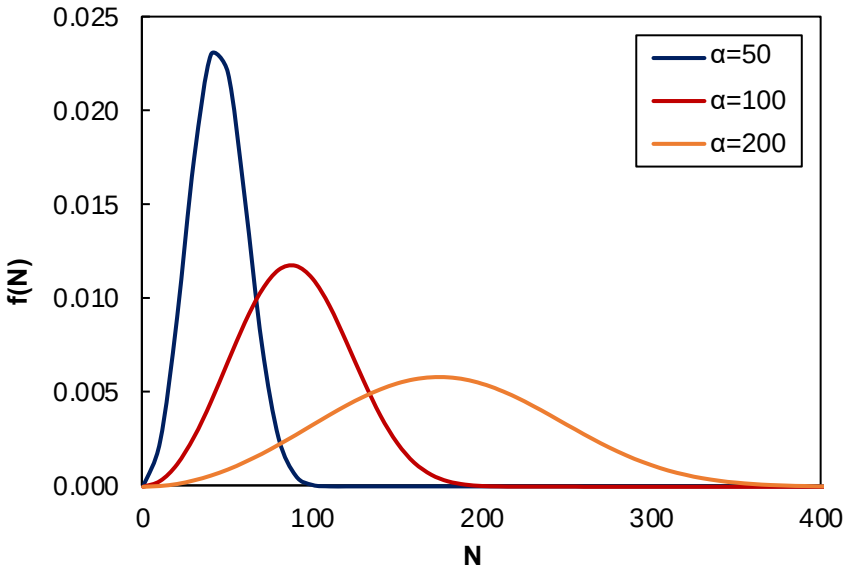

Figure 4.36 Weibull PDF for varying scale parameters (α)

Figure 4.37 indicates the influence of the Weibull shape parameter (β) on the PDF. It is also known as the Weibull slope and determines the shape of the distribution. When β<1, the PDF is steadily decreasing. At β=1, the Weibull distribution becomes a two-parameter exponential distribution, and at β=3, it approximates a normal distribution. Unlike the normal distribution, the Weibull distribution can model skewness in the probability distribution as indicated when β=1.5. These PDFs were observed in the detailed analysis of each specimen category for each damage level. The β value varied between 0 and 6 for all specimen categories at different damage levels.

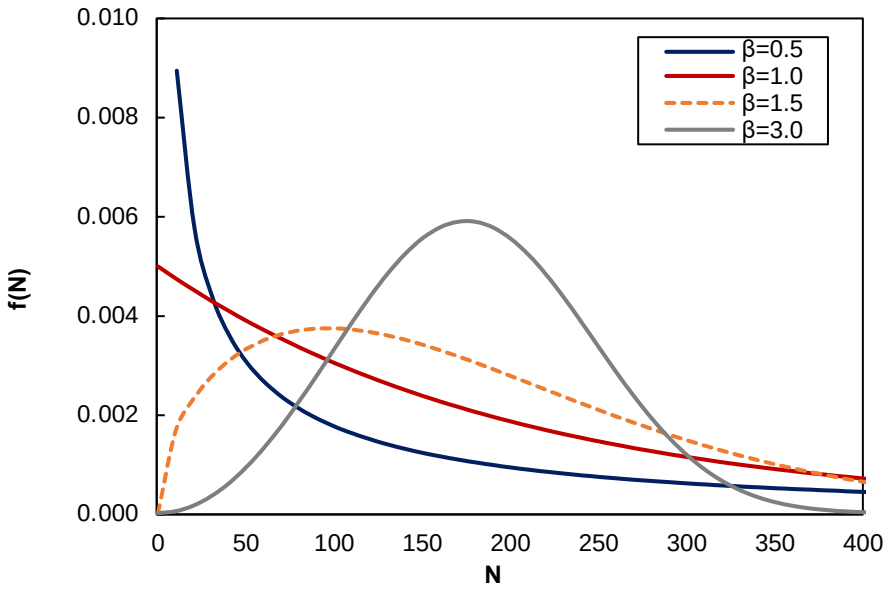

Figure 4.37 Weibull PDF for varying shape parameters (0<β<1, β=1, β>1)

The shape parameter also influences the failure rate function, as indicated in Figure 4.38. Generally, if β<1, the failure rate decreases over time. When β=1 or closer to one the Weibull distribution has a constant failure rate, and when β>1, the failure rate increases with time. Intuitively, the decreasing failure rate with the increasing number of freeze-thaw cycles fails to represent the actual behavior of the tensile bond strength. However, in the classic Weibull bathtub curve, these regions are associated with early-life failures, as indicated in Table 4.19. Then, gradually the failure rate becomes constant over time and finally reaches a failure rate that increases with time, also known as a wear-out failure. The classical bathtub curve has been observed with the non-destructive dynamic elastic dynamic modulus tests (Chen & Qiao, 2015). Although this behavior is kept in the sandblasted specimens (Table 4.19), the chipped and pressure-washed specimen categories do not follow the same pattern. Note that the tensile bond strength test is destructive, and the data considered for the Weibull analysis from the same specimen was from different specimens. This assumption may have influenced the failure rate of each assumed sample.

Another observation is that the bond failure gradually shifted from more cohesive to adhesive failure, which the Weibull model fails to capture, which might have also affected the failure rate function.

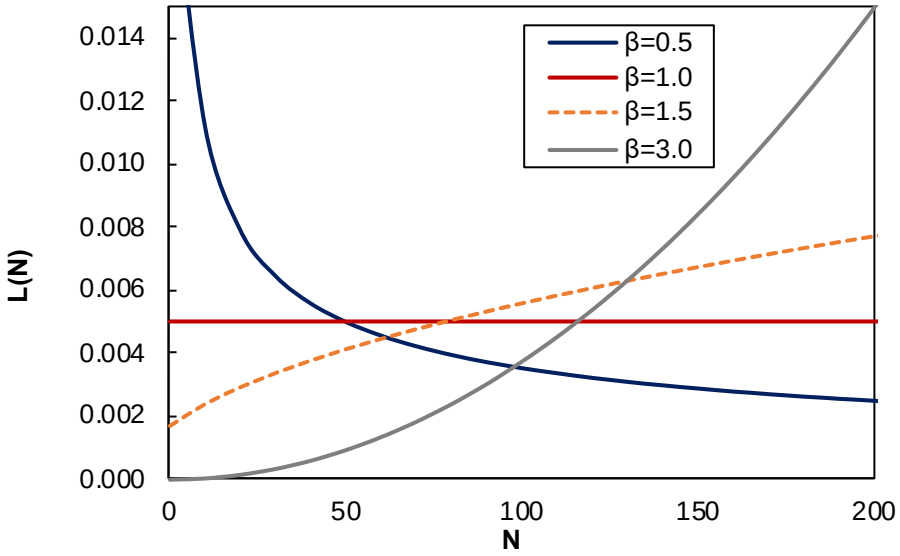

Figure 4.38 Weibull failure rate function for different shape parameters (0<β<1, β=1, β>1)

In contrast to α and β, the location parameter (γ), also known as the threshold does not influence the shape or the scale of the PDF. Instead, it shifts the PDF along the x-axis depending on its value. For all the specimen categories at all damage, γ was a positive value. Using the reliability function for each specimen category, the number of freeze-thaw cycles for a given damage is selected, as indicated in Table 4.20 to Table 4.22. Three different reliability levels are considered as 95%, 50%, and 10% for the chipped, pressure-washed, and sandblasted specimens. Using the tables, the relationship between the damage level and the freeze-thaw cycles are established as indicated in Figure 4.39 to Figure 4.41 and Equation (13) to (24). Any reliability level below 50% is considered unacceptable. The relationships are assumed to be third-order polynomials.

Table 4.20 F/T cycles for different damage levels under different reliabilities for the chipped samples

Reliability (%)	Damage (D)					
	0.05	0.1	0.2	0.3	0.4	0.5
95% Reliability	30	55	105	160	275	365
90% Reliability	35	65	120	180	280	370
50% Reliability	45	85	180	260	330	405
10% Reliability	55	105	250	340	510	575

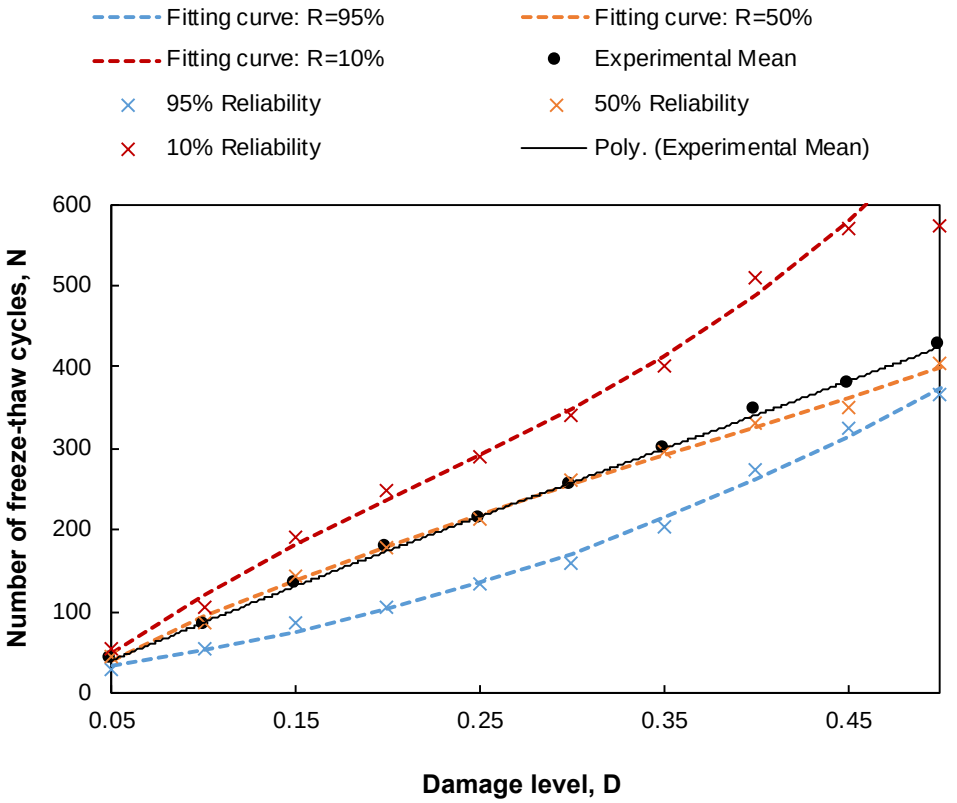

Figure 4.39 Probabilistic relationship between the life (F/T cycles) and the damage parameter for chipped samples

$$N = 5622.9D^3 - 3673.9D^2 + 1878.4D - 35.794 \quad (13)$$

$$N = 1289.8D^3 - 1412.6D^2 + 1214D - 15.667 \quad (14)$$

$$N = 349.65D^3 + 537.3D^2 + 363.87D + 20 \quad (15)$$

$$N = 372.96D^3 + 692.31D^2 + 270.05D + 19 \quad (16)$$

Table 4.21 F/T cycles for different damage levels under different reliabilities for the pressure-washed samples.

Reliability (%)	Damage (D)					
	0.05	**0.1**	**0.2**	**0.3**	**0.4**	**0.5**
95% Reliability	30	55	105	160	275	365
90% Reliability	35	65	120	180	280	370
50% Reliability	45	85	180	260	330	405
10% Reliability	55	105	250	340	510	575

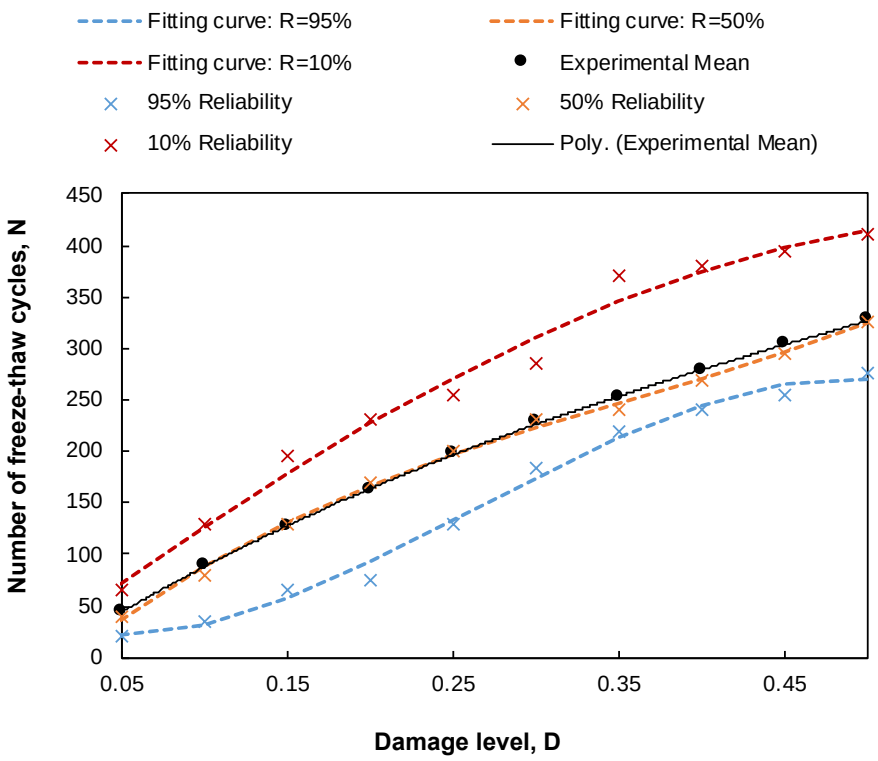

Figure 4.40 Probabilistic relationship between the life (F/T cycles) and the damage parameter for pressure-washed samples

$$N = -613.83D^3 - 455.71D^2 + 1180.3D + 14 \quad (17)$$

$$N = 2377.6D^3 - 2582.8D^2 + 1401.3D - 28.667 \quad (18)$$

$$N = -3869.5D^3 + 2889.3D^2 + 42.016D + 16.167 \quad (19)$$

$$N = -5672.1D^3 + 4528D^2 - 365.48D + 29.167 \quad (20)$$

Table 4.22 F/T cycles for different damage levels under different reliabilities for the sandblasted samples

Reliability (%)	Damage (D)					
	0.05	**0.1**	**0.2**	**0.3**	**0.4**	**0.5**
95% Reliability	20	35	60	70	90	140
90% Reliability	20	35	60	85	125	175
50% Reliability	25	55	105	165	225	315
10% Reliability	195	285	320	365	405	455

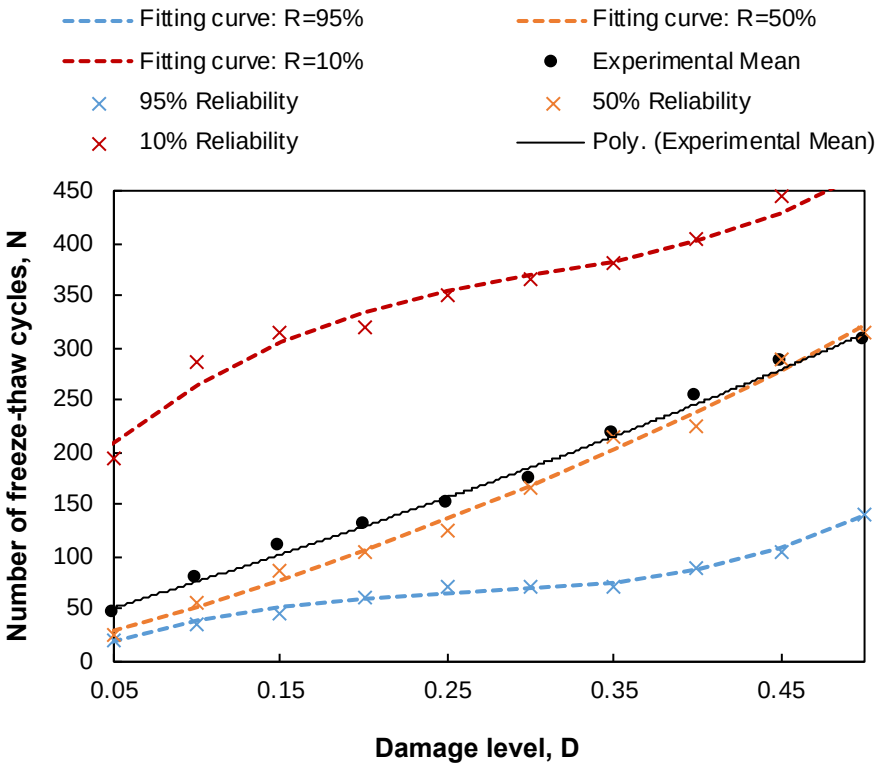

Figure 4.41 Probabilistic relationship between the life (F/T cycles) and the damage parameter for sandblasted samples

$$N = 5423.5D^3 - 4959.2D^2 + 1796.1D + 129.83 \quad (21)$$

$$N = 155.4D^3 + 326.34D^2 + 425.02D + 6.3333 \quad (22)$$

$$N = 1802.6D^3 - 1138.7D^2 + 471.89D - 0.8333 \quad (23)$$

$$N = 3380D^3 - 2553.6D^2 + 735.08D - 13.667 \quad (24)$$

It is evident that all the correlation coefficients are above 90% and show a good correlation. The remaining service life of the shotcrete-concrete interface bond under freezing and thawing can be predicted using these relationships. In other words, the probabilistic damage model can predict the service life of existing or newly developed shotcrete materials subjected to severe frost damage in cold climates. It is also evident that the actual distributions are closer to the 50% reliability-based damage prediction.

4.4.4 Service life prediction

ASTM C666 considers a sample to fail when the RDF reaches 60% (or D=0.4). Therefore, the probabilistic model is used to determine the F/T cycles at failure (RDF=60%), and Table 4.23 indicate these results. Nevertheless, note that this 60% RDF value is based on the dynamic modulus of elasticity obtained from a non-destructive test. However, destructive tests such as the pull-off direct tension test may inherently give a lower RDF (i.e., higher damage, D, at a given cycle) than the non-destructive dynamic modulus test.

Table 4.23 Comparison of service life prediction based on probabilistic damage model-based equations with D=0.4

	Probabilistic damage model with 50% probability			Probabilistic damage model with 90% probability		
	C	**PW**	**SB**	**C**	**PW**	**SB**
F-T cycles (N_{lab})	275.9	247.6	121.1	326.5	275.8	238.5

These results are based on laboratory F/T conditions, which might differ from the field F/T cycles. Therefore, it is necessary to determine the equivalent F/T cycles to predict the service life of a shotcrete-concrete bond in the field. However, only a limited number of studies correlate the laboratory data to field conditions. The difficulties arise due to the non-uniformity of freezing temperatures, frequency, and duration of F/T cycles in different parts of the country, over the years, because frost damage is related to the number of cold days and the lowest temperature. One of the standard methods to overcome this issue is to use the mean equivalent number of F/T cycles per year, which is 39.5 for Pullman, WA, and 2.5 for SeaTac, WA, based on weather data in 1998 and 1999 (Masad & James, 2001). In this study, the authors have characterized an F/T cycle with a drop below 28.94°F (-1.7°C) to an increase above 35.06°F (1.7°C). The data has been collected from two locations in Pullman, WA (elevation 736 m, 46.73° N, 117.17° W), and SeaTac, WA (elevation 80 m, 47.44° N, 122.3° W). Although both these locations are from Washington, the weather in the two regions is very different. Pullman (Eastern Washington) is characterized by its warmer summers and colder winters than SeaTac (Western Washington). The topography, elevation, and the presence of the ocean (in SeaTac) all

contribute to these differences. Hence, the annual equivalent number of F/T cycles in Pullman, WA, is relatively high compared to SeaTac, WA.

In the Phase II study of this project, temperature histories obtained for the years 2017 and 2018 from Weather Underground (wunerground.com) indicate that there were 94 and 111 frost days corresponding to 35 and 52 equivalent F/T cycles in Pullman. In contrast, for SeaTac, this has been 15 and 19 frost days with just 11 and 6 F/T cycles in the two years. The minimum temperatures recorded for the two years (2017 and 2018) have been -7.06°F (-21.7°C) and 1.94°F (-16.7°C) for Pullman, whereas, in SeaTac, it has been 24.4°F (-4.2°C) and 19.4°F (-7°C). Due to the high variability of the parameters, this study assumed the mean equivalent number of F/T cycles as 42.17 and 6.5 for Pullman and SeaTac, respectively, averaging the values above. Note that this value could vary significantly depending on the year and the climate changes. By comparing the equivalent number of F/T cycles per year (N_{eq}) with the laboratory failure life (N_{lab}), the service life (equivalent years, T) could be approximated in years as,

$$T = N_{lab}/N_{eq} \tag{25}$$

Table 4.24 indicates that the equivalent service life of a given shotcrete-concrete interface bond in years. Note that the following results depend significantly on the mean equivalent number of F/T cycles. Nevertheless, the results indicate the importance of taking additional measures contributing to bond strength and surface preparation in colder regions. For example, a shotcrete-concrete bond made of a chipped surface that would last 42.4 years in SeaTac, WA, would only have a life of 6.5 years in Pullman, WA. Although F/T seems to be of least concern to the shotcrete repairs in SeaTac, WA, it might be interesting to study the influence of drying-wetting cycles on the shotcrete-concrete bonds.

In addition, the as-cast specimens failed after 144 F/T cycle, which translated to 3.4 and 22.2 years in Pullman and SeaTac, respectively, indicating the need for proper surface preparation. However it is noted that these predicted lives are worst scenarios, actual frost penetration also depends on the thickness of shotcrete overlay thickness. Also, even in Eastern Washington, the number of F/T cycles can vary, depending on the specific locations, e.g. Tri-Cities or Mountain passes. For the regions in which durability of bond is a concern, shotcrete may need to be anchored to the substrate.

Table 4.24 Equivalent service life of shotcrete-concrete interface bonds

	Probabilistic damage model with 50% probability			**Probabilistic damage model with 90% probability**		
	C	**PW**	**SB**	**C**	**PW**	**SB**
Eastern Washington (Pullman)	6.5	5.9	2.9	7.7	6.5	5.7
Western Washington (SeaTac)	42.4	38.1	18.6	50.2	42.4	36.7

Chapter 5. CONCLUSIONS AND RECOMMENDATIONS

5.1 Summary

This Phase III project aimed to develop test methods and specifications to address the debonding issues in shotcrete-concrete bonds, especially applicable to wall fascia, slope stabilization, and concrete repairs. Shotcrete applications depend on the quality of the interface bonds. Therefore, this Phase III study investigated the influence of substrate surface preparation, surface texture, and test methods on the bond performance and frost resistance of shotcrete-concrete interface bonds. The following findings and conclusions can be drawn from the study:

(1) Literature review and industry survey: Based on the literature review and the industry survey, four types of substrate surface preparation techniques, namely, chipped, pressure-washed, sandblasted, and as-cast, were identified for this study. Two types of established test methods, shear and tensile bond strengths were identified to characterize these surfaces. Additionally, a fracture mechanics-based test was designed and developed for the interface characterization of the structures. Freeze-thaw durability of the shotcrete-concrete interface bonds was also identified as an essential aspect.

(2) Short-term tensile bond strength: The tensile bond strength values are correlated with the surface preparation technique. These techniques can be sorted from the largest to smallest interface tensile bond strengths as chipped, pressure-washed sandblasted, and as-cast. For comparison purposes, the chipped, pressure-washed, and sandblasted specimens were reported to have 6.4, 5, and 2.7 times more resistance to tensile bond failure than the unprepared surfaces. The advisable limit for a good bond mentioned in ACI 506-R16 is 145 psi (1 MPa). Only the chipped and sandblasted samples achieved this bond quality. An

estimated texture depth (ETD) of 0.294 mm is needed to achieve a good quality at the overlay to substrate interface bond.

(3) Short-term shear bond strength: The shear bond strength values were obtained using a guillotine-type direct shear test and reported values in descending order as chipped, sandblasted, pressure-washed, and as-cast specimens. Specifically, the shear bond strength specimens with chipped, sandblasted, and pressure-washed surface preparation were 5.7, 2.9, and 1.6, times more resistant to shear bond failure than that of specimens with as-cast surfaces. In contrast to tensile bond strength, the sandblasted specimens recorded a superior shear bond strength compared to pressure-washed specimens. Based on ACI 546.3R-14, only samples with chipped or sandblasted surface preparations can meet the minimum of 300 psi shear bond strength.

(4) Short-term fracture tests: Mode-II (in-plane shear) was used to compute the bond fracture resistance of all four substrate preparation techniques. The chipped samples reported the highest mode-II fracture energy with 368 $lb.ft/ft^2$ (498 J/m^2), followed by sandblasted and pressure-washed samples. Specifically, the fracture energies of specimens with chipped, sandblasted and pressure-washed surface preparation were 6.81, 4.68, and 1.53 times more resistant to mode-II fracture failure than the unprepared surfaces. The corresponding surface texture depths for shear specimens correlate with the shear bond strengths of the shotcrete-concrete interface bonds.

(5) Comparison of test methods: The data for the chipped samples shows the highest bond strengths and fracture energy of all test categories, while the as-cast specimens showed the lowest values. The surface preparation technique influences the tensile bond strength values. The shear bond strength to tensile bond strength ratios of chipped,

pressure-washed, sandblasted, and as-cast samples are 2.09, 0.73, 2.49, and 2.35. In contrast, the fracture energy correlates with the shear strength behavior across different surface preparation techniques.

(6) Long-term F/T durability of shotcrete-concrete interface bonds: In general, the bond durability has decreased with the number of freeze-thaw cycles tested (0, 100, 200, and 300). The chipped samples indicated the highest durability, followed by pressure-washed, sandblasted, and as-cast samples. Specifically, the retained tensile bond strength after 300 cycles were 64.7%, 55.8%, 53.7% and 4.0% of strength at 0 cycle, for the chipped, pressure-washed, sandblasted and as-cast specimens, respectively. In contrast, the mode-II fracture-based durability tests indicated retained fracture energy of 91.4%, 41.6%, 46.5%, and 6.59% at 300 cycles, for the chipped, pressure-washed, sandblasted and as-cast specimens, respectively. The sandblasted and pressure-washed specimens have comparable freeze-thaw durability in the same range, while the chipped samples have superior durability. In both tensile and fracture tests, the as-cast interface bonds have reduced their performance by over 90%, indicating surface preparation's importance in cold regions. The ASTM C666 mentions an allowable retained dynamic modulus of 60% or more at 300 cycles to qualify an individual material as durable. Based on that, only chipped surface preparation can pass this criterion. However, note that the dynamic modulus is a non-destructive test that indicates lower durability reductions than destructive tests.

(7) Probabilistic damage model: The relative durability factor of shotcrete-concrete interface bonds for freeze-thaw cycles were assessed using the three-parameter Weibull distribution model. It is observed that the predicted results based on the exponential probabilistic damage model at 50% reliability are more consistent with the experimental

mean, which provides a more conservative and safer prediction. This model was used to predict the field service life of shotcrete-concrete interface bonds. It was found that the service life of shotcrete-concrete bond in Eastern Washington (e.g. Pullman) can be less than ten years while those in Western Washington can be up to 50 years, depending on the surface preparation methods.

5.2 Recommendations for shotcrete specifications

Based on above findings, it is recommended to include the following in the shotcrete specifications, if applicable:

(1) Tensile bond strength should be is determined when shotcrete is applied to overhead structure and shear bond strength for the slope stabilization. The bond strength should meet the ACI's recommendations of minimum 145 psi for tensile bond strength in accordance with ASTM C1583 and minimum 300 psi for shear bond strength in accordance with AASHTO T323.

(2) Chipped surface preparation should be applied whenever possible. Otherwise, pressure washing can be applied for the overhead structure application of shotcrete and sandblasting for slope stabilization. After chipping or sandblasting, the substrate surface should be washed to remove dust or debris for better bond performance. Unprepared substrate concrete surface is not recommended to use.

(3) A minimum estimated texture depth (ETD) of 0.294 mm of substrate concrete which can be determined using a laser texture scanner (ASTM E2157) or a digital concrete profile gauge (ASTM D8271) is needed to achieve a good quality of the shotcrete overlay to substrate interface bond.

Alternatively, an International Concrete Repair Institute (ICRI)'s Concrete Surface Profile (CSP) No. 4 or higher can be specified as an alternative to ETD.

(4) Caution should be exercised when the shotcrete is applied to a structure in regions which are subject to frequent freeze-thaw cycles, due to concern on the long-term durability of the interface bond. For the regions in which durability of bond is a concern, anchors in substrate may need to be placed in substrate prior to the shotcrete application.

Note that the above recommendations are based on the assumptions that shotcrete is applied to sound substrate concrete.

5.3 Recommendations for further studies

Based on the experimental program conducted in the Phase III study, the following suggestions are provided for future study so that the performance of shotcrete can be better understood:

(1) Test methods for tensile and shear bond strength: ASTM C1583 can be used to determine the direct tensile bond strength. However, ASTM C1583 is designed for *in situ* tensile bond strength, instead of laboratory samples. AASHTO T323 can be used to determine the direct shear bond strength. However, modifications of these tests are needed for shotcrete application.

(2) Multilayering shotcrete application: This study focused on single shotcrete layer on hardened concrete substrate. More studies are needed to verify the applicability of the findings to multilayer shotcrete application.

(3) Shotcrete mix designs: Only one shotcrete mix design was used in this study. More studies are needed to verify the applicability of the recommendations in this study to other shotcrete mix designs.

(4) Bond enhancement techniques: Based on the four surface preparation techniques, the bond strength of specimens with unprepared substrate concrete surface does not meet the ACI specifications. The techniques of chipping, pressure-washing, or sandblasting can be impractical or cost-prohibitive in some cases. The techniques to enhance bond performance of the shotcrete-concrete interface bonds should be investigated, such as surface pre-wetting, inclusion of steel fiber and/or silica fume in shotcrete, and use of anchors, etc.

(5) Durability enhancement techniques: The techniques to enhance bond durability performance of the shotcrete-concrete interface bonds should be investigated, especially for applications in regions with frequent freeze-thaw cycles.

(6) Chloride ion penetration: Existing flaws at the interface region due to construction and life loadings could lead to chloride penetration which may negative affect the long-term durability of the interface bond. It might be an area of interest to explore.

References

Abo Sabah, S. H., Hassan, M. H., Muhamad Bunnori, N., & Megat Johari, M. A. (2019). Bond strength of the interface between normal concrete substrate and GUSMRC repair material overlay. *Construction and Building Materials*, *216*, 261–271. https://doi.org/10.1016/j.conbuildmat.2019.04.270

Abu-Tair, A. I., Rigden, S. R., & Burley, E. (1996). Testing the Bond between Repair Materials and Concrete Substrate. *Materials Journal*, *93*(6), 553–558. https://doi.org/10.14359/9861

ACI Committee 506. (1994). *Guide for the evaluation of shotcrete*. American Concrete Institute; WorldCat.org.

ACI Committee 506. (2014). *Specification for shotcrete: An ACI standard*. American Concrete Institute; WorldCat.org.

ACI Committee 506. (2019). *ACI. 506.4R-19. Guide for the evaluation of shotcrete*. American Concrete Institute; WorldCat.org.

ACI Committee 506-R. (2016). *Guide to Shotcrete*. American Concrete Institute; WorldCat.org.

American Concrete Institute. (2014). *Guide to materials selection for concrete repair*. American Concrete Institute; WorldCat.org.

Arioglu, N., Girgin, Z., & Arioglu, E. (2006). Evaluation of ratio between splitting tensile strength and compressive strength for concretes up to 120 MPa and its application in strength criterion. *ACI Materials Journal*, *103*(1), 18–24. https://doi.org/10.14359/15123

ASTM International. (2005). *Standard Test Method for Bond Strength of Epoxy-Resin Systems Used With Concrete By Slant Shear*. ASTM International; WorldCat.org. https://doi.org/10.1520/C0882-05

ASTM International. (2008). *Standard test method for resistance of concrete to rapid freezing and thawing* (Vol. 1–1 electronic text (6 pages) : PDF). ASTM International; WorldCat.org.

ASTM International. (2010a). *Standard Test Method for Air Content of Freshly Mixed Concrete by the Pressure Method*. ASTM International; WorldCat.org. https://doi.org/10.1520/C0231_C0231M-10

ASTM International. (2010b). *Standard Test Method for Microscopical Determination of Parameters of the Air-Void System in Hardened Concrete*. ASTM International; WorldCat.org. https://doi.org/10.1520/C0457_C0457M-10A

ASTM International. (2011). *Standard test method for splitting tensile strength of cylindrical concrete specimens.* ASTM International; WorldCat.org.

ASTM International. (2013a). *Standard Test Method for Strength Properties of Adhesive Bonds in Shear by Compression Loading*.

ASTM International. (2013b). *Standard test method for tensile strength of concrete surfaces and the bond strength or tensile strength of concrete repair and overlay materials by direct tension (pull-off method): Designation C1583/C1583M-13*. ASTM International; WorldCat.org.

ASTM International. (2015). *Standard Practice for Calculating Pavement Macrotexture Mean Profile Depth*. ASTM International; WorldCat.org. https://doi.org/10.1520/E1845-09

Austin, S., & Robins, P. J. (1993). Development of patch test to study behavior of shallow concrete patch repairs. *Magazine of Concrete Research*, *45*(164), 221–229. https://doi.org/10.1680/macr.1993.45.164.221

Austin, S., Robins, P., & Pan, Y. (1995). Tensile bond testing of concrete repairs. *Materials and Structures*, *28*(5), 249–259. https://doi.org/10.1007/BF02473259

Austin, S., Robins, P., & Pan, Y. (1999). Shear bond testing of concrete repairs. *Cement and Concrete Research*, *29*(7), 1067–1076. https://doi.org/10.1016/S0008-8846(99)00088-5

Bahraq, A. A., Al-Osta, M. A., Khan, M. I., & Ahmad, S. (2021). Numerical and analytical modeling of seismic behavior of beam-column joints retrofitted with ultra-high performance fiber reinforced concrete. *Structures*, *32*, 1986–2003. https://doi.org/10.1016/j.istruc.2021.04.004

Bažant, Z. P., & Pfeiffer, P. A. (1986). Shear fracture tests of concrete. *Materials and Structures*, *19*(2), 111. https://doi.org/10.1007/BF02481755

Beaupre, D. (1994). *Rheology of High-Performance Shotcrete* [Ph.D. Dissertation]. University of British Columbia.

Beaupre, D. (1999, May). Bond Strength of Shotcrete Repair. *Shotcrete Magazine*. https://shotcrete.org/wp-content/uploads/2020/01/1999Spr_Beaupre.pdf

Bentz, D. P., De la Varga, I., Muñoz, J. F., Spragg, R. P., Graybeal, B. A., Hussey, D. S., Jacobson, D. L., Jones, S. Z., & LaManna, J. M. (2018). Influence of substrate moisture state and roughness on interface microstructure and bond strength: Slant shear vs. pull-off testing. *Cement and Concrete Composites*, *87*, 63–72. https://doi.org/10.1016/j.cemconcomp.2017.12.005

Benzarti, K., Chataigner, S., Quiertant, M., Marty, C., & Aubagnac, C. (2011). Accelerated ageing behavior of the adhesive bond between concrete specimens and CFRP overlays. *Construction and Building Materials*, *25*(2), 523–538. https://doi.org/10.1016/j.conbuildmat.2010.08.003

Beushausen, H. (2010). The influence of concrete substrate preparation on overlay bond strength. *Magazine of Concrete Research*, *62*(11), 845–852.

Beushausen, H., Höhlig, B., & Talotti, M. (2017). The influence of substrate moisture preparation on bond strength of concrete overlays and the microstructure of the OTZ. *Cement and Concrete Research*, *92*, 84–91. https://doi.org/10.1016/j.cemconres.2016.11.017

Bissonnette, B., Vaysburd, A. M., & von Fay, K. F. (2012). *Best Practices for Preparing Concrete Surfaces Prior to Repairs and Overlays* (MERL 12-17). https://trid.trb.org/view/1290821

Bonaldo, E., Barros, J. A. O., & Lourenço, P. B. (2005). Bond characterization between concrete substrate and repairing SFRC using pull-off testing. *International Journal of Adhesion and Adhesives*, *25*(6), 463–474. https://doi.org/10.1016/j.ijadhadh.2005.01.002

British Standards Institution. (1999). *Products and systems for the protection and repair of concrete structures. Test methods. Measurement of bond strength by pull-off*. (Vol. 1–1 online resource (10 pages)). British Standards Institution; WorldCat.org.

Bryne, L. E., Ansell, A., & Holmgren, J. (2014). Laboratory testing of early age bond strength of shotcrete on hard rock. *Tunnelling and Underground Space Technology*, *41*, 113–119. https://doi.org/10.1016/j.tust.2013.12.002

BSI British Standards. (1984). *Testing of resin and polymer/cement compositions for use in construction Method for measurement of bond strength (slant shear method)*. BSI British Standards; WorldCat.org. https://doi.org/10.3403/00042770

Chaboche, J.-L. (1988). *Continuum damage mechanics: Part I—General concepts*.

Chbani, H., Saadouki, B., Boudlal, M., & Barakat, M. (2019). A Determination of fracture toughness in plain concrete specimens by R curve. *Frattura Ed Integrità Strutturale*, *13*(49), 763–774. https://doi.org/10.3221/IGF-ESIS.49.68

Chen, F., & Qiao, P. (2015). Probabilistic damage modeling and service-life prediction of concrete under freeze–thaw action. *Materials and Structures*, *48*(8), 2697–2711. https://doi.org/10.1617/s11527-014-0347-y

Chen, J., Zhao, X., Luo, Y., Deng, X., & Liu, Q. (2014). Investigating freeze-proof durability of C25 shotcrete. *Construction and Building Materials*, *61*, 33–40. https://doi.org/10.1016/j.conbuildmat.2014.02.077

ChiaHwan, Y., & Wei, L. (2014). Application of Interfacial Propagation and Kinking Crack Concept to ECC/Concrete Overlay Repair System. *Advances in Materials Science and Engineering*, *2014*, e623467. https://doi.org/10.1155/2014/623467

Choi, P., Yeon, J. H., & Yun, K.-K. (2016). Air-void structure, strength, and permeability of wet-mix shotcrete before and after shotcreting operation: The influences of silica fume and air-entraining agent. *Cement & Concrete Composites*, *70*, 69–77. https://doi.org/10.1016/j.cemconcomp.2016.03.012

Cifuentes, H., Lozano, M., Holušová, T., Medina, F., Seitl, S., & Fernández-Canteli, A. (2017). Modified Disk-Shaped Compact Tension Test for Measuring Concrete

Fracture Properties. *International Journal of Concrete Structures and Materials*, *11*(2), 215–228. https://doi.org/10.1007/s40069-017-0189-4

Clímaco, J. C. T. S., & Regan, P. E. (2001). Evaluation of bond strength between old and new concrete in structural repairs. *Magazine of Concrete Research*, *53*(6), 377–390. https://doi.org/10.1680/macr.2001.53.6.377

Courard, L., Piotrowski, T., & Garbacz, A. (2014). Near-to-surface properties affecting bond strength in concrete repair. *Cement and Concrete Composites*, *46*, 73–80. https://doi.org/10.1016/j.cemconcomp.2013.11.005

Davalos, J. F., Kodkani, S. S., & Ray, I. (2006). Fracture Mechanics Method for Mode-I Interface Evaluation of FRP Bonded to Concrete Substrates. *Journal of Materials in Civil Engineering*, *18*(5), 732–742. https://doi.org/10.1061/(ASCE)0899-1561(2006)18:5(732)

Delatte, N., Williamson, M., & Fowler, D. (2000). Bond strength development with maturity of high-early-strength bonded concrete overlays. *ACI Materials Journal*, *97*(2), 201–207.

Dhir, M. P. (1984). A study on the effect of temperature variations on the bonding of concrete overlays. *Journal of the American Concrete Institute.* WorldCat.org.

Diab, A. M., Abd Elmoaty, A. E. M., & Tag Eldin, M. R. (2017). Slant shear bond strength between self-compacting concrete and old concrete. *Construction and Building Materials*, *130*, 73–82. https://doi.org/10.1016/j.conbuildmat.2016.11.023

Ding, Z., Wen, J., Li, X., & Yang, X. (2019). Permeability of the bonding interface between strain-hardening cementitious composite and normal concrete. *AIP Advances*, *9*(5), 055107. https://doi.org/10.1063/1.5086915

Dzugan, J., Konopik, P., & Rund, M. (2018). Fracture Toughness Determination with the Use of Miniaturized Specimens. *Contact and Fracture Mechanics*. https://doi.org/10.5772/intechopen.73093

Emmons, P. H. (1994). Part Three: Surface Repair, Section 6: Bonding Repair Materials to Existing Concrete. In *Concrete Repair and Maintenance* (pp. 154–163). R.S. Means Company.

Erhard, DR., & Chorinsky, GF. (1986). Repair of Concrete Floors with Polymer Modified Cement Mortars. In H. R. Sasse (Ed.), *Adhesion between polymers and concrete / Adhésion entre polymères et béton: Bonding · Protection · Repair / Revêtement · Protection · Réparation* (pp. 230–234). Springer US. https://doi.org/10.1007/978-1-4899-3454-3_25

Espeche, A. D., & León, J. (2011). Estimation of bond strength envelopes for old-to-new concrete interfaces based on a cylinder splitting test. *Construction and Building Materials*, *25*(3), 1222–1235. https://doi.org/10.1016/j.conbuildmat.2010.09.032

Farahani, B. V., Tavares, P. J., Belinha, J., & Moreira, P. M. G. P. (2017). A Fracture Mechanics Study of a Compact Tension Specimen: Digital Image Correlation, Finite Element and Meshless Methods. *Procedia Structural Integrity*, *5*, 920–927. https://doi.org/10.1016/j.prostr.2017.07.113

Farzad, M., Shafieifar, M., & Azizinamini, A. (2019). Experimental and numerical study on bond strength between conventional concrete and Ultra High-Performance Concrete (UHPC). *Engineering Structures*, *186*, 297–305. https://doi.org/10.1016/j.engstruct.2019.02.030

Geissert, D. G., Li, S. (Eric), Franz, G. C., & Stephens, J. E. (1999). Splitting Prism Test Method to Evaluate Concrete-to-Concrete Bond Strength. *Materials Journal*, *96*(3), 359–366. https://doi.org/10.14359/634

Gendy, A. E., & Shalaby, A. (2007). Mean Profile Depth of Pavement Surface Macrotexture Using Photometric Stereo Techniques. *Journal of Transportation Engineering*, *133*(7), 433–440. https://doi.org/10.1061/(ASCE)0733-947X(2007)133:7(433)

Haber, Z. B., Munoz, J. F., De la Varga, I., & Graybeal, B. A. (2018). Bond characterization of UHPC overlays for concrete bridge decks: Laboratory and field testing. *Construction and Building Materials*, *190*, 1056–1068. https://doi.org/10.1016/j.conbuildmat.2018.09.167

Hanjari, K. Z., Utgenannt, P., & Lundgren, K. (2011). Experimental study of the material and bond properties of frost-damaged concrete. *Cement and Concrete Research*, *41*(3), 244–254. https://doi.org/10.1016/j.cemconres.2010.11.007

Harris, D. K., Sarkar, J., & Ahlborn, T. (Tess) M. (2011). Characterization of Interface Bond of Ultra-High-Performance Concrete Bridge Deck Overlays. *Transportation Research Record*, *2240*(1), 40–49. https://doi.org/10.3141/2240-07

Iosipescu, N., & Negoita, A. (1969). A new method for determining the pure shearing strength of concrete. *Concrete (London)*.

Jacobsen, S., Sellevold, E. J., & Matala, S. (1996). Frost durability of high strength concrete: Effect of internal cracking on ice formation. *Cement and Concrete Research*, *26*(6), 919–931. https://doi.org/10.1016/0008-8846(96)00066-X

Jolin, M., Beaupré, D., Pigeon, M., & Lamontagne, A. (1997). Use of Set Accelerating Admixtures in Dry-Mix Shotcrete. *Journal of Materials in Civil Engineering*, *9*(4), 180–184. https://doi.org/10.1061/(ASCE)0899-1561(1997)9:4(180)

Julio, E., Branco, E., & Silva, V. (2005). Concrete-to-concrete bond strength: Influence of an epoxy-based bonding agent on a roughened substrate surface. *Magazine of Concrete Research*, *57*(8), 463–468. https://doi.org/10.1680/macr.2005.57.8.463

Júlio, E. N. B. S., Branco, F. A. B., & Silva, V. D. (2004). Concrete-to-concrete bond strength. Influence of the roughness of the substrate surface. *Construction and Building Materials*, *18*(9), 675–681.

Júlio, E. N. B. S., Branco, F. A. B., & Silva, V. D. (2005). Concrete-to-concrete bond strength: Influence of an epoxy-based bonding agent on a roughened substrate surface. *Magazine of Concrete Research*, *57*(8), 463–468. https://doi.org/10.1680/macr.2005.57.8.463

Kamada, T., & Li, V. C. (2000). The effects of surface preparation on the fracture behavior of ECC/concrete repair system. *Cement and Concrete Composites*, *22*(6), 423–431. https://doi.org/10.1016/S0958-9465(00)00042-1

Kanellopoulos, A., Farhat, F. A., Nicolaides, D., & Karihaloo, B. L. (2009). Mechanical and fracture properties of cement-based bi-materials after thermal cycling. *Cement and Concrete Research*, *39*(11), 1087–1094. https://doi.org/10.1016/j.cemconres.2009.07.008

Kim, M. O., & Bordelon, A. (2016). Fiber Effect on Interfacial Bond Between Concrete and Fiber-Reinforced Mortar. *Transportation Research Record*, *2591*(1), 11–18. https://doi.org/10.3141/2591-02

Knab, L., & Spring, C. (1989). Evaluation of Test Methods for Measuring the Bond Strength of Portland Cement Based Repair Materials to Concrete. *Cement, Concrete and Aggregates*, *11*(1), 3–14. https://doi.org/10.1520/CCA10096J

Kundu, D., & Raqab, M. Z. (2009). Estimation of R = P (Y < X) for three-parameter Weibull distribution. *Statistics & Probability Letters*, *79*(17), 1839–1846. https://doi.org/10.1016/j.spl.2009.05.026

Lamontagne, A., Pigeon, M., Pleau, R., & Beaupre, D. (1996). Use of air-entraining admixtures in dry-mix shotcrete. *ACI Materials Journal*, *93*(1), 69–74. https://doi.org/10.14359/9798

Lemaitre, J. (1985). A Continuous Damage Mechanics Model for Ductile Fracture. *Journal of Engineering Materials and Technology*, *107*(1), 83–89. https://doi.org/10.1115/1.3225775

Li, S. (1997). Durability and bond of high-performance concrete and repaired Portland cement concrete. *Doctoral Dissertations*, 1–232.

Li, S., Geissert, D., Frantz, G., & Stephans, J. (1999). Freeze-thaw bond durability of rapid-setting concrete repair materials. *ACI Materials Journal*, *96*(2), 242–249.

Li, S. (1997). *Durability and bond of high-performance concrete and repaired Portland cement concrete: Final report* (Vol. 1–xvi, 232 pages : illustrations ; 28 cm). Connecticut Transportation Institute, School of Engineering, University of Connecticut; WorldCat.org. https://cslib.contentdm.oclc.org/digital/collection/p128501coll2/search/searchterm/38158638/field/dmoclcno/mode/all/conn/all/order/pdidat/ad/desc

Li, V. C., Lim, Y. M., & Foremsky, D. J. (1995). Interfacial fracture toughness of concrete repair materials. *Proceedings of Fracture Mechanics of Concrete Structures II, Aedificatio Publishers, Freiburg*, 1329–1344.

Lim, Y. M., Kim, M. K., Shin, S. K., & Li, V. C. (2001). *Numerical simulation for quasi-brittle interface fracture in cementitious bi-material system*.

Long, A. E., & Murray, A. M. (1984). The "Pull-Off" Partially Destructive Test for Concrete. *Special Publication*, *82*, 327–350. https://doi.org/10.14359/6562

López-Carreño, R.-D., Pujadas, P., Cavalaro, S. H. P., & Aguado, A. (2017). Bond strength of white toppings and bonded overlays constructed with self-compacting high-performance concrete. *Construction and Building Materials*, *153*, 835–845. https://doi.org/10.1016/j.conbuildmat.2017.07.136

Ma, Z., Zhao, T., & Yang, J. (2017). Fracture Behavior of Concrete Exposed to the Freeze-Thaw Environment. *Journal of Materials in Civil Engineering*, *29*(8), 04017071. https://doi.org/10.1061/(ASCE)MT.1943-5533.0001901

Mainali, G., Dineva, S., & Nordlund, E. (2015). Experimental study on debonding of shotcrete with acoustic emission during freezing and thawing cycle. *Cold Regions Science and Technology*, *111*, 1–12. https://doi.org/10.1016/j.coldregions.2014.11.014

Martin, L. A., Clark, C. C., Seymour, J. B., Stepan, M. A., & National Institute for Occupational Safety and Health. (2015). *Shotcrete design and installation compliance testing: Early strength, load capacity, toughness, adhesion strength, and applied quality.* Dept. of Health and Human Services, Centers for Disease

Control and Prevention, National Institute for Occupational Safety and Health; WorldCat.org.

Marzouk, H., & Jiang, K. (1995). Effects of Freezing and Thawing on the Tension Properties of High-Strength Concrete. *Materials Journal, 91*(6), 577–586. https://doi.org/10.14359/1378

Masad, E. A., & James, E. A. (2001). *Implementation of High-Performance Concrete in Washington State* (WA-RD 530.1). https://rosap.ntl.bts.gov/view/dot/42022

Miarka, P., Pan, L., Bilek, V., Cifuentes, H., & Seitl, S. (2019). *Fracture behavior of alkali activated concrete measured from three-point bending test with chevron notch*. 10th International Conference on Fracture Mechanics and Concrete Structures.

Mohamad, M. E., Ibrahim, I. S., Abdullah, R., Abd. Rahman, A. B., Kueh, A. B. H., & Usman, J. (2015). Friction and cohesion coefficients of composite concrete-to-concrete bond. *Cement and Concrete Composites*, *56*, 1–14. https://doi.org/10.1016/j.cemconcomp.2014.10.003

Momayez, A., Ehsani, M. R., Ramezanianpour, A. A., & Rajaie, H. (2005). Comparison of methods for evaluating bond strength between concrete substrate and repair materials. *Cement and Concrete Research*, *35*(4), 748–757. https://doi.org/10.1016/j.cemconres.2004.05.027

Momayez, A., Eshani, M. R., Ramezanianpour, A. A., & Rajaie, H. (2005). Comparison of methods for evaluating bond strength between concrete substrate and repair materials. *Cement and Concrete Research*, *35*(4), 748–757.

Momayez, A., Ramezanianpour, A., Rajaie, H., & Ehsani, M. (2004). Bi-surface shear test for evaluating bond between existing and new concrete. *ACI Materials Journal*, *101*(2), 99–106.

Morgan, D. (1989). Freeze-thaw durability of shotcrete. *Concrete International : Design and Construction Aug.1989*, *11*(8), 86–93. WorldCat.org.

Morgan, D., & Totten, L. (2014). Guide specification for structural shotcrete walls. *Shotcrete Magazine*, *10*(1), 18–27. WorldCat.org.

Naresh, K., Shankar, K., & Velmurugan, R. (2018). Reliability analysis of tensile strengths using Weibull distribution in glass/epoxy and carbon/epoxy composites. *Composites Part B: Engineering*, *133*, 129–144. https://doi.org/10.1016/j.compositesb.2017.09.002

Powers, T. C. (1945). A Working Hypothesis for Further Studies of Frost Resistance of Concrete. *Journal Proceedings*, *41*(1), 245–272. https://doi.org/10.14359/8684

Powers, T. C. (1955). Basic Considerations Pertaining to Freezing- And-Thawing Tests. *ASTM Proceedings*. https://trid.trb.org/view/102313

Qian, J., You, C., Wang, Q., Wang, H., & Jia, X. (2014). A method for assessing bond performance of cement-based repair materials. *Construction and Building Materials*, *68*, 307–313. https://doi.org/10.1016/j.conbuildmat.2014.06.048

Qian, P., & Xu, Q. (2018). Experimental investigation on properties of interface between concrete layers. *Construction and Building Materials*, *174*, 120–129. https://doi.org/10.1016/j.conbuildmat.2018.04.114

Ramey, G. E., Strickland, A. M. 1951-, United States. Federal Highway Administration., Auburn University. Department of Civil Engineering., & Alabama. State Highway

Department. Bureau of Materials and Tests. (1984). *An experimental evaluation of rapid-setting patching materials used in the repair of concrete bridges and pavements*. State of Alabama Highway Dept.; WorldCat.org.

Ramos, N. M. M., Simões, M. L., Delgado, J. M. P. Q., & de Freitas, V. P. (2012). Reliability of the pull-off test for in situ evaluation of adhesion strength. *Construction and Building Materials*, *31*, 86–93. https://doi.org/10.1016/j.conbuildmat.2011.12.097

Rashid, K., Ahmad, M., Ueda, T., Deng, J., Aslam, K., Nazir, I., & Azam Sarwar, M. (2020). Experimental investigation of the bond strength between new to old concrete using different adhesive layers. *Construction and Building Materials*, *249*, 118798. https://doi.org/10.1016/j.conbuildmat.2020.118798

Ray, I., Davalos, J. F., & Luo, S. (2005). Interface evaluations of overlay-concrete bi-layer composites by a direct shear test method. *Cement and Concrete Composites*, *27*(3), 339–347. https://doi.org/10.1016/j.cemconcomp.2004.02.048

Rith, M., Kim, Y. K., Lee, S. W., Park, J. Y., & Han, S. H. (2016). Analysis of in situ bond strength of bonded concrete overlay. *Construction and Building Materials*, *111*, 111–118. https://doi.org/10.1016/j.conbuildmat.2016.02.062

Robins, P., & Austin, S. (1995). A unified failure envelope from the evaluation of concrete repair bond tests. *Magazine of Concrete Research*, *47*(170), 57–68. https://doi.org/10.1680/macr.1995.47.170.57

Rosen, C. J. (2016). *Shear strength at the interface of bonded concrete overlays*. WorldCat.org.

Roy, M., Ray, I., & Davalos, J. F. (2014). High-Performance Fiber-Reinforced Concrete: Development and Evaluation as a Repairing Material. *Journal of Materials in Civil Engineering*, *26*(10), 04014074. https://doi.org/10.1061/(ASCE)MT.1943-5533.0000980

Sadrmomtazi, A., & Khoshkbijari, R. K. (2017). Bonding durability of polymer-modified concrete repair overlays under freeze–thaw conditions. *Magazine of Concrete Research*, *69*(24), 1268–1275. https://doi.org/10.1680/jmacr.17.00014

Sadrmomtazi, A., & Khoshkbijari, R. K. (2019). Determination and Prediction of Bonding Strength of Polymer Modified Concrete (PMC) as the Repair Overlay on the Conventional Concrete Substrate. *KSCE Journal of Civil Engineering*, *23*(3), 1141–1149. https://doi.org/10.1007/s12205-019-0113-3

Saldanha, R., Júlio, E., Dias-da-Costa, D., & Santos, P. (2013). A modified slant shear test designed to enforce adhesive failure. *Construction and Building Materials*, *41*, 673–680. https://doi.org/10.1016/j.conbuildmat.2012.12.053

Santos, D. S., Santos, P. M. D., & Dias-da-Costa, D. (2012). Effect of surface preparation and bonding agent on the concrete-to-concrete interface strength. *Construction and Building Materials*, *37*, 102–110. https://doi.org/10.1016/j.conbuildmat.2012.07.028

Santos, P. M. D., Júlio, E. N. B. S., & Silva, V. D. (2007). Correlation between concrete-to-concrete bond strength and the roughness of the substrate surface. *Construction and Building Materials*, *21*(8), 1688–1695. https://doi.org/10.1016/j.conbuildmat.2006.05.044

Saucier, F., Bastien, J., Pigeon, M., & Fafard, M. (1991). A Combined Shear-Compression Device to Measure Concrete-to-Concrete Bonding. *Experimental Techniques (Westport, Conn.)*, *15*(5), 50–55.

Seymour, J. B., Martin, L. A., Clark, C. C., Stepan, M. A., Jacksha, R. D., Pakalnis, R. T., Roworth, M., & Caceres, C. (2010). *A Practical Method of Measuring Shotcrete Adhesion Strength*. 1–9. https://www.cdc.gov/niosh/mining/works/coversheet1456.html

Shah, S. G., & Chandra Kishen, J. M. (2011). Fracture Properties of Concrete–Concrete Interfaces Using Digital Image Correlation. *Experimental Mechanics*, *51*(3), 303–313. https://doi.org/10.1007/s11340-010-9358-y

Shah, S. P., Swartz, S. E., & Ouyang, Chengsheng. (1995). *Fracture mechanics of concrete: Applications of fracture mechanics to concrete, rock and other quasi-brittle materials*. Wiley; WorldCat.org. http://catdir.loc.gov/catdir/toc/onix01/95024676.html

Shahrooz, B. M., Gillum, A. J., Cole, J., & Turer, A. (2000). Bond Characteristics of Overlays Placed over Bridge Decks Sealed with High-Molecular-Weight Methacrylate. *Transportation Research Record*, *1697*(1), 24–30. https://doi.org/10.3141/1697-05

Silfwerbrand, J. (1990). Improving concrete bond in repaired bridge decks. *Concrete International : Design and Construction*, *12*(9), 61–66. WorldCat.org.

Silfwerbrand, J. (2003). Shear bond strength in repaired concrete structures. *Materials and Structures*, *36*(6), 419–424. https://doi.org/10.1007/BF02481068

Silfwerbrand, J., & Beushausen, H. (2005). Bonded Concrete Overlays: Bond Strength Issues. *International Conference on Concrete Repair, Rehabilitation and Retrofitting. Cape Town, South Africa, November 21-23*, 19–21.

Soares, S., Sena-Cruz, J., Cruz, J. R., & Fernandes, P. (2019). Influence of Surface Preparation Method on the Bond Behavior of Externally Bonded CFRP Reinforcements in Concrete. *Materials (1996-1944)*, *12*(3), 414. https://doi.org/10.3390/ma12030414

Swartz, S. E., Lu, L. W., Tang, L. D., & Refai, T. M. E. (1988). Mode II fracture-parameter estimates for concrete from beam specimens. *Experimental Mechanics*, *28*(2), 146–153. https://doi.org/10.1007/BF02317565

Talbot, C., Pigeon, M., & Beaupre, D. (1994). Influence of surface preparation on long-term bonding of shotcrete. *ACI Materials Journal Nov/Dec*, *91*(6), 560–566. WorldCat.org.

Talukdar, S., & Heere, R. (2019). The effects of pumping on the air content and void structure of air-entrained, wet mix fiber reinforced shotcrete. *Case Studies in Construction Materials*, *11*, e00288. https://doi.org/10.1016/j.cscm.2019.e00288

Tang, Y., Xu, G., Lian, J., Su, H., & Qu, C. (2016). Effect of temperature and humidity on the adhesion strength and damage mechanism of shotcrete-surrounded rock. *Construction & Building Materials*, *124*, 1109–1119. https://doi.org/10.1016/j.conbuildmat.2016.08.126

Tayeh, B. A., Abu Bakar, B. H., & Megat Johari, M. A. (2013). Characterization of the interfacial bond between old concrete substrate and ultra-high performance fiber

concrete repair composite. *Materials and Structures*, *46*(5), 743–753. https://doi.org/10.1617/s11527-012-9931-1

Tayeh, B. A., Abu Bakar, B. H., Megat Johari, M. A., & Voo, Y. L. (2012). Mechanical and permeability properties of the interface between normal concrete substrate and ultra-high performance fiber concrete overlay. *Construction and Building Materials*, *36*, 538–548. https://doi.org/10.1016/j.conbuildmat.2012.06.013

Tayeh, B. A., Bakar, B. H. A., Johari, M. A. M., & Ratnam, M. M. (2013). The relationship between substrate roughness parameters and bond strength of ultra-high-performance fiber concrete. *Journal of Adhesion Science & Technology*, *27*(16), 1790–1810. https://doi.org/10.1080/01694243.2012.761543

Tschegg, E. K., Elser, M., & Stanzl-Tschegg, S. E. (1995). Biaxial fracture tests on concrete—Development and experience. *Cement and Concrete Composites*, *17*(1), 57–75. https://doi.org/10.1016/0958-9465(95)95760-W

Tschegg, E. K., Ingruber, M., Surberg, C. H., & Munger, F. (2000). Factors influencing fracture behavior of old-new concrete bonds. *ACI Materials Journal*, *97*(4), 447–453. https://doi.org/10.14359/7409

Tschegg, E. K., Rotter, H. M., Roelfstra, P. E., Bourgund, U., & Jussel, P. (1995). Fracture Mechanical Behavior of Aggregate–Cement Matrix Interfaces. *Journal of Materials in Civil Engineering*, *7*(4), 199–203. https://doi.org/10.1061/(ASCE)0899-1561(1995)7:4(199)

Tschegg, E. K., & Stanzl, S. E. (1991). Adhesive power measurements of bonds between old and new concrete. *Journal of Materials Science*, *26*(19), 5189–5194. https://doi.org/10.1007/BF01143212

Valipour, M., & Khayat, K. H. (2020). Debonding test method to evaluate bond strength between UHPC and concrete substrate. *Materials and Structures*, *53*(1), 15. https://doi.org/10.1617/s11527-020-1446-6

Wall, J. S., & Shrive, N. G. (1988). Factors Affecting Bond Between New and Old Concrete. *Materials Journal*, *85*(2), 117–125. https://doi.org/10.14359/2329

Wang, J., Niu, D., Wang, Y., & Wang, B. (2018). Durability performance of brine-exposed shotcrete in salt lake environment. *Construction & Building Materials*, *188*, 520–536. https://doi.org/10.1016/j.conbuildmat.2018.08.139

Whitney, D. P., Texas. Department of Transportation., & University of Texas at Austin. Center for Transportation Research. (1992). *An Investigation of various factors affecting bond in bonded concrete overlays*. Center for Transportation Research, University of Texas ; WorldCat.org.

WSDOT. (2022). *Standard Specifications for Road, Bridge, and Municipal Construction | Manuals | WSDOT*. https://wsdot.wa.gov/engineering-standards/all-manuals-and-standards/manuals/standard-specifications-road-bridge-and-municipal-construction

Xiong, G., Liu, J., Li, G., & Xie, H. (2002). A way for improving interfacial transition zone between concrete substrate and repair materials. *Cement and Concrete Research*, *32*(12), 1877–1881. https://doi.org/10.1016/S0008-8846(02)00840-2

Yang, H.-S., Qiao, P., & Wolcott, M. P. (2010a). Fatigue characterization and reliability analysis of wood flour filled polypropylene composites. *Polymer Composites*, *31*(4), 553–560. https://doi.org/10.1002/pc.20848

Yang, H.-S., Qiao, P., & Wolcott, M. P. (2010b). Flexural Fatigue and Reliability Analysis of Wood Flour/High-density Polyethylene Composites. *Journal of Reinforced Plastics and Composites*, *29*(9), 1295–1310. https://doi.org/10.1177/0731684409102753

Youm, H.-S., Lim, W.-Y., Hong, S.-G., & Joh, C. (2021). Interface Shear Strength between Ultra-High-Performance Concrete and Normal-Strength Concrete. *Structural Journal*, *118*(2), 287–298. https://doi.org/10.14359/51729350

Yun, K.-K., Kim, S.-H., Jeong, W.-K., & Kim, K. W. (2004). In Situ Criteria of Pull-Off Test for Measuring Bond Strength of Latex-Modified Concrete Overlay. *Transportation Research Record*, *1893*(1), 37–45. https://doi.org/10.3141/1893-05

Zanotti, C., Banthia, N., & Plizzari, G. (2014). A study of some factors affecting bond in cementitious fiber reinforced repairs. *Cement and Concrete Research*, *63*, 117–126. https://doi.org/10.1016/j.cemconres.2014.05.008

Zanotti, C., & Randl, N. (2019). Are concrete-concrete bond tests comparable? *Cement and Concrete Composites*, *99*, 80–88. https://doi.org/10.1016/j.cemconcomp.2019.02.012

Zhang, L. (2014). Variability of Compressive Strength of Shotcrete in a Tunnel-Lining Project. *Shotcrete Magazine*.

Zhang, X., Zhang, S., Luo, Y., & Wang, L. (2020). Effects of Interface Orientations on Bond Strength between Old Conventional Concrete and New Self-Consolidating Concrete. *ACI Structural Journal*, *117*(5), 191–201.

Zhang Xuhui, Zhang Wei, Luo Yuming, Wang Lei, Peng Jianxin, & Zhang Jianren. (2020). Interface Shear Strength between Self-Compacting Concrete and Carbonated

Concrete. *Journal of Materials in Civil Engineering*, *32*(6), 04020113. https://doi.org/10.1061/(ASCE)MT.1943-5533.0003229

Zhang, Y., Zhu, P., Liao, Z., & Wang, L. (2020). Interfacial bond properties between normal strength concrete substrate and ultra-high-performance concrete as a repair material. *Construction and Building Materials*, *235*, 117431. https://doi.org/10.1016/j.conbuildmat.2019.117431

Zhao, Y. X., & Liu, H. B. (2014). Weibull modeling of the probabilistic S–N curves for rolling contact fatigue. *International Journal of Fatigue*, *66*, 47–54. https://doi.org/10.1016/j.ijfatigue.2014.03.008

Zhou, Z., & Qiao, P. (2019). Durability of air-entrained shotcrete exposed to cyclic freezing and thawing effect. *Cold Regions Science and Technology*, *164*, 102778. https://doi.org/10.1016/j.coldregions.2019.05.004

Zuo, S., Xiao, J., & Yuan, Q. (2020). Comparative study on the new-old mortar interface deterioration after wet-dry cycles and heat-cool cycles. *Construction and Building Materials*, *244*, 118374. https://doi.org/10.1016/j.conbuildmat.2020.118374

Appendix

Appendix 1: Bond strength test results from previous studies (psi)

Reference	Specimen	Pull-off Tension (PO)	Splitting Prism (SP)	Splitting Cylinder (SC)	Guillotine Shear (GS)	Bi-surface shear (BSS)	Jacking Shear (JS)	Torsion Test (TT)	Slant Shear (SS)
Momayez et al. (2005)	0% SF L	171	173			348			1178
	5% SF L	181	184			386			1331
	7% SF L	199	200			432			1497
	10% SF L	200	202			435			1474
	K100 L	264	283			495			1681
	SBR L	345	390			554			1768
	0% SF H	191	197			1614			435
	5% SF H	200	209			1726			477
	7% SF H	218	235			1915			526
	10% SF H	222	238			1888			531
	K100 H	283	310			1967			554
	SBR H	363	421			1962			603
Sabah et al. (2016)	Grooved	335		962					3466
	Sandblasted	373		1214					5105
Rosen (2016)	1	281			496		96		2205
	2	180			228		104		1465
	3	284			457		157		2147
	4	186			400		116		1537
	5	151			294		241		1537
	6	132			271		142		1030
Pultorak (2019)	1A	113			334		162		4828
	1B	165			448		172		5940
	2A	165			423		231		5791
	2B	42			173		139		5078
	3A	185			385		219		4543
	3B	177			416		223		4825
Silfwerband (2003)	Sandblasted	251						570	